ISSN 1105-4999

ΦΑΡΜΑΚΕΥΤΙΚΗ
PHARMAKEFTIKI

ΤΡΙΜΗΝΙΑΙΑ ΕΚΔΟΣΗ ΜΕ ΘΕΜΑΤΑ ΦΑΡΜΑΚΕΥΤΙΚΩΝ ΕΠΙΣΤΗΜΩΝ
A QUARTERLY EDITION ON PHARMACEUTICAL SCIENCES' TOPICS

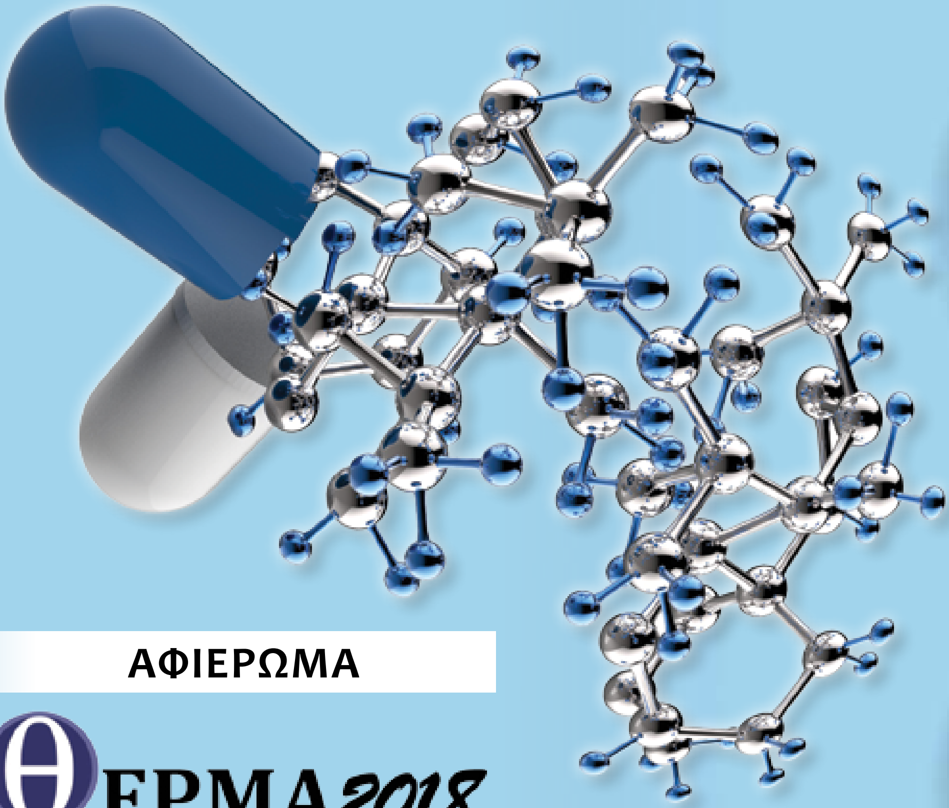

ΑΦΙΕΡΩΜΑ

ΘΕΡΜΑ2018

ΑΘΗΝΑ, 12 - 13 Οκτωβρίου 2018

ΤΟΜΟΣ
VOLUME 30 • ΤΕΥΧΟΣ
ISSUE IV

ΟΚΤΩΒΡΙΟΣ - ΔΕΚΕΜΒΡΙΟΣ
OCTOBER - DECEMBER 2018

ΦΑΡΜΑΚΕΥΤΙΚΗ

ΤΡΙΜΗΝΙΑΙΑ ΕΚΔΟΣΗ ΜΕ ΘΕΜΑΤΑ
ΦΑΡΜΑΚΕΥΤΙΚΩΝ ΕΠΙΣΤΗΜΩΝ
ΤΟΜΟΣ 30, ΤΕΥΧΟΣ Ι,
ΙΑΝΟΥΑΡΙΟΣ - ΜΑΡΤΙΟΣ 2018

ΔΙΕΥΘΥΝΤΗΣ ΣΥΝΤΑΞΗΣ
Α. Τσαντίλη
Ομοτ. Καθηγήτρια, Εθνικό και Καποδιστριακό
Πανεπιστήμιο Αθηνών (ΕΚΠΑ)
tsantili@pharm.uoa.gr

ΑΡΧΙΣΥΝΤΑΚΤΗΣ
Γ.Α. Καρίκας
Ομότιμος καθηγητής, Πανεπιστήμιο
Δυτικής Αττικής, karikasg@uniwa.gr

ΣΥΝΤΑΚΤΙΚΗ ΕΠΙΤΡΟΠΗ
Κ. Δεμέτζος
Καθηγητής, ΕΚΠΑ
Β. Δημόπουλος
Καθηγητής, Πανεπιστήμιο Θεσσαλονίκης, ΑΠΘ
Ν. Κόλμαν
Galenica SA
Χ. Κοντογιώργης
PhD, Πανεπιστήμιο Θεσσαλονίκης, ΑΠΘ
Π. Κουρουνάκης
Ομοτ. Καθηγητής,
Πανεπιστήμιο Θεσσαλονίκης, ΑΠΘ
Π. Μαχαίρας
Ομοτ. Καθηγητής, ΕΚΠΑ
Σ. Νικολαρόπουλος
Αναπλ. Καθηγητής, Πανεπιστήμιο Πατρών
Γ. Πάιρας
Αναπλ. Καθηγητής, Πανεπιστήμιο Πατρών
Ε. Παντερή
Καθηγήτρια, ΕΚΠΑ
Δ. Ρέκκας
Αναπλ. Καθηγητής, ΕΚΠΑ

E-mail για υποβολή εργασιών:
tsantili@pharm.uoa.gr, karikasg@teiath.gr

**Για την ηλεκτρονική έκδοση της «Φαρμακευτικής»
και οδηγίες προς συγγραφείς
επισκεφτείτε την διεύθυνση: www.hsmc.gr**

***Τα άρθρα που δημοσιεύονται
στην «Φαρμακευτική» καταχωρούνται
στα Chemicals Abstracts, EMBASE,
SCOPUS και EBSCO***

PHARMAKEFTIKI

A QUARTERLY EDITION
ON PHARMACEUTICAL SCIENCES' TOPICS
VOLUME 30, ISSUE I,
JANUARY - MARCH 2018

EDITOR
A. Tsantili
Emeritus Professor, National and Kapodistrian
University of Athens (NKUA)
tsantili@pharm.uoa.gr

CO EDITOR
G.A. Karikas
Emeritus professor, University of West Attica,
Greece, karikasg@uniwa.gr

EDITORIAL BOARD
C. Demetzos
Professor, NKUA
V.J. Demopoulos
Professor, University of Thessaloniki, AUTh
N. Kolman
Galenica SA
Ch. Kontogiorgis
PhD, University of Thessaloniki, AUTh
P. Kourounakis
Emeritus Professor,
University of Thessaloniki, AUTh
P. Macheras
Emeritus Professor, NKUA
S. Nikolaropoulos
Associate Professor, University of Patras
G. Pairas
Associate Professor, University of Patras
I. Panderi
Professor, NKUA
D. Rekkas
Associate Professor, NKUA

E-mail for manuscript submission:
tsantili@pharm.uoa.gr, karikasg@teiath.gr

**For "Pharmakeftiki" electronic edition
and instructions to authors
please visit www.hsmc.gr**

***Articles published in "Pharmakeftiki"
are indexed in Chemical Abstracts,
EMBASE, SCOPUS and EBSCO***

ΠΕΡΙΕΧΟΜΕΝΑ / CONTENTS

ΠΕΡΙΕΧΟΜΕΝΑ / CONTENTS

ΦΑΡΜΑΚΕΥΤΙΚΗ

ΤΡΙΜΗΝΙΑΙΑ ΕΚΔΟΣΗ
ΤΗΣ ΕΛΛΗΝΙΚΗΣ ΕΤΑΙΡΕΙΑΣ ΦΑΡΜΑΚΟΧΗΜΕΙΑΣ
& ΤΗΣ ΕΛΛΗΝΙΚΗΣ ΦΑΡΜΑΚΕΥΤΙΚΗΣ ΕΤΑΙΡΕΙΑΣ

PHARMAKEFTIKI

A QUARTERLY JOINT EDITION OF
THE HELLENIC SOCIETY OF
MEDICINAL CHEMISTRY &
THE HELLENIC PHARMACEUTICAL SOCIETY

ZITA MEDICAL MANAGEMENT

ZITA MEDICAL MANAGEMENT, Ομήρου 29, Πέτα Σαρωνικού, Ελλάδα
Τηλ.: + 30 22994 40962, E-mail: g.kouloumpis@zitamanagement .com

Ελληνική Εταιρεία Θερμικής Ανάλυσης (Ε.Ε.Θ.Α.)

Η Ελληνική Εταιρεία Θερμικής Ανάλυσης (Ε.Ε.Θ.Α.) ιδρύθηκε το 1994 από μια ομάδα Ελλήνων επιστημόνων που δραστηριοποιούνταν στο χώρο της θερμικής ανάλυσης και σε συναφείς με αυτήν τεχνικές.

Σκοπός της προσπάθειας αυτής είναι η ανάδειξη του επιστημονικού έργου των Ελλήνων ερευνητών που ασχολούνται με τον παραπάνω τομέα, η αναζήτηση συνεργασιών με άλλους επιστήμονες του εξωτερικού και η ανάπτυξη και βελτίωση των τεχνικών της θερμικής ανάλυσης.

Μέσα από συναντήσεις, συμμετοχή σε συνέδρια και δημοσιεύσεις επιστημονικών εργασιών σε σχετικά περιοδικά πιστεύουμε ότι δίνεται η ευκαιρία για μια πιο ουσιαστική και εποικοδομητική συμβολή των Ελλήνων επιστημόνων στην περιοχή της Θερμικής Ανάλυσης.

Μετά την ολοκλήρωση των τυπικών ενεργειών και τη συγκρότηση του πρώτου διοικητικού της συμβουλίου, η Ε.Ε.Θ.Α. έγινε δεκτή ως ισότιμο μέλος της International Confederation for Thermal Analysis and Calorimetry (I.C.T.A.C) που αριθμεί πάνω από 6,000 μέλη.

Με βάση τα παραπάνω καθίσταται σαφές ότι οι δραστηριότητες της ΕΕΘΑ στοχεύουν όχι μόνο στην προώθηση της σχετικής έρευνας στα Ακαδημαϊκά Ιδρύματα και Ερευνητικά Κέντρα της χώρας μας, αλλά επιπλέον στην ποιοτική αναβάθμιση των βιομηχανικών προϊόντων. Αυτό γίνεται εφικτό με την παροχή συμβουλευτικού έργου στην ελληνική βιομηχανία ως προς την εισαγωγή της αντίστοιχης τεχνολογίας θερμικής ανάλυσης, όπως απαιτεί το ανταγωνιστικό διεθνές περιβάλλον.

Η Ε.Ε.Θ.Α διοργανώνει κάθε δύο χρόνια το Πανελλήνιο συνέδριο ΘΕΡΜΑ. Στις 12 και 13 Οκτώβριου 2018 διοργανώθηκε στην Αθήνα το 8ο Συνέδριο ΘΕΡΜΑ2018.

ΟΡΓΑΝΩΤΙΚΗ ΕΠΙΤΡΟΠΗ

- Μουζάκης Δ.Ε., Αναπληρωτής Καθηγητής
- Στρατιωτική Σχολή Ευελπίδων- Εργ. Μηχανικής
- Κοντού Ε., Καθηγήτρια
- Σ.Ε.Μ.Φ.Ε., Ε.Μ.Π.
- Δεμέτζος Κ., Καθηγητής
- Τμήμα Φαρμακευτικής, Ε.Κ.Π.Α.
- Δρ Πίππα Νατάσσα
- Τμήμα Φαρμακευτικής, Ε.Κ.Π.Α.

ΕΠΙΣΤΗΜΟΝΙΚΗ ΕΠΙΤΡΟΠΗ

- Αχιλιάς Δημήτριος
- Δεμέτζος Κων/νος
- Ζαούτσος Στέφανος
- Κοντού Εύη
- Μαρία Λάλια-Καντούρη
- Μπάρκουλα Νεκταρία-Μαριάνθη
- Μουζάκης Διονύσιος
- Μπικιάρης Δημήτριος
- Πίππα Αναστασία-Γεωργία
- Παπαγεωργίου Γεώργιος
- Παπανικολάου Γεώργιος
- Χρυσάφης Κωνσταντίνος

ΘΕΡΜΑ2018

Α Θ Η Ν Α, 12 - 13 Οκτωβρίου 2018

ΠΡΟΓΡΑΜΜΑ ΣΥΝΕΔΡΙΟΥ

Παρασκευή 12/10

ΠΡΟΕΔΡΕΙΟ:	Ε. ΚΟΝΤΟΥ, Κ. ΔΕΜΕΤΖΟΣ
9:30 - 9:45	Χαιρετισμός Προέδρου ΕΕΘΑ
9:45 - 10:30	Προσκεκλημένη Ομιλία: **Dimitrios Fessas** **Universita degli Studi, Milano** *Food Calorimetry: classical and novel applications*
10:30-10:50	**E. Vouvoudi**, D. Achilias *Catalytic pyrolysis of polymeric materials used as packaging via TGA and Py-GC/MS*
10:50-11:10	**Dimitris S. Achilias**, Ioannis Tsagkalias *Contribution of the Differential Scanning Calorimetry to the investigation of complex polymerization kinetics*
11:10-11:30	Διάλειμμα– Καφές
11:30-11:50	Προσκεκλημένη Ομιλία: **ThomasM. Mavromoustakos** Kapodistrian University of Athens, Chemistry Department, Laboratory of Organic Chemistry *DSC: A valuable tool to study drug: membrane interactions using Differential Scanning Calorimetry*
11:50-12:10	**TatiaPaka** and D.E. Mouzakis *Role of transient receptor potential in thermal detection*
12:10-12:30	**Nikolaos Naziris**, Maria Chountoulesi, SzymonSekowski, Maria Zamaraeva, Nodira Abdulladjanova, Costas Demetzos

Thermotropic Effect of RhustyphinaTannin on Model Membranes

12:30-13:00 ΠροσκεκλημένηΟμιλία: **Apostolos Kyritsis**
Department of Physics, National Technical University of Athens
DSC studies on the nature of freezing and nonfreezing water in polymer-water mixtures

13:00-14:30 Γεύμα – Μπουφές

ΠΡΟΕΔΡΕΙΟ: Ν.ΠΙΠΠΑ, Δ.Ε. ΜΟΥΖΑΚΗΣ

14:30-14:45 **Ομιλία Χορηγού MALVA SA**
Γ. Ζαχαρίδης: *Quick overview of Thermal Analysis Techniques, Instruments and Applications, Ranging from Biomaterials to Proteins and Polymers to Metals*

14:45-15:05 **Theodore Sentoukas**, Despoina Giaouzi, Stergios Pispas
Thermal Characterization of Novel Block Copolymer Systems

15:05-15:25 **A. Stimoniaris** and C. Delides
Synergy effects of carbon based fillers in polymer nanocomposites studied by thermomechanical techniques

15:25-16:25 ***e-PostersSession***

16:25-16:45 Διάλειμμα – Καφές

16:45-17:30 Γενική Συνέλευση ΕΕΘΑ-Εκλογές νέου Δ.Σ.

20:30 Επίσημο Δείπνο Συνεδρίου ΕΕΘΑ2018

Σάββατο 13/10

ΠΡΟΕΔΡΕΙΟ: Δ. ΑΧΙΛΛΙΑΣ, Ν. ΜΠΑΡΚΟΥΛΑ

09:30 - 10:00 Προσκεκλημένη Ομιλία: **Νικόλαος Μπουρόπουλος**,
Τμήμα Επιστήμης Υλικών, Πανεπιστήμιο Πατρών
Synthesis, characterization and thermal properties of Calcium phosphates for biomedical applications

10:00 – 10:20 **Natassa Pippa,** Diego Romano Perinelli, StergiosPispas, Giulia Bonacucina, Costas Demetzos
Materials' properties of chimeric liposomes using thermal analysis techniques

10:20 -10:40 **Christos Ganos**, Nikolaos Naziris, Maria Chountoulesi, Konstantia Graikou, Costas Demetzos
Thermal analysis on the effect of quercetin-3-rutinoside-7-rhamnoside and flavonoids on model phospholipid membranes

10:40-11:00	**Maria Chountoulesi,** Athina Konstantinidi, Nikolaos Naziris, Dimitris Kolokouris, Antonios Kolocouris, Costas Demetzos, Thomas Mavromoustakos *Kinetic study of the thermodynamic behavior of lipid bilayers in the presence of aminoadamantane drugs*
11:00-11:20	**Nikolaos Naziris,** Athanasios Skandalis, Stergios Pispas, Costas Demetzos *Linear Thermodynamic Behavior in Complex Chimeric Nanosystems*
11:20-11:40	Διάλειμμα – Καφές
ΠΡΟΕΔΡΕΙΟ:	Ν. ΜΠΟΥΡΟΠΟΥΛΟΣ, K. CHRISSAFIS
11:40-12:10	ΠροσκεκλημένηΟμιλία: **ΝεκταρίαΜπάρκουλα,** Τμήμα Μηχανικών Επιστήμης Υλικών, Πανεπιστήμιο Ιωαννίνων *Study of the environmental degradation of polymers, composites and nanocomposites using Dynamic Mechanical Analysis*
12:10-12:30	**EvangeliaTarani,** Zoe Terzopoulou, Theodora Kyratsi, Thomas Kehagias, Dimitrios N. Bikiaris, George Vourlias, Konstantinos Chrissafis Significant enhancement of thermal and mechanical properties of high-density polyethylene using large diameter size graphene nanoplatelets: A review
12:30-12:50	**Dionysios E. Mouzakis**, Aggelos Koutsomichalis, Thomas Kalampoukas Thermomechanical Response &Time- Temperature Superposition Analysis using two different approaches in Antiballistic Hybrid Kevlar/Aluminum and Vectran/Aluminum Composites
12:50-13:10	**A. Kollia**, G.C. Papanicolaou, S.P. Zaoutsos *Influence of Thermal Shock on the Dynamic Mechanical Properties of Flax Fiber Reinforced Epoxy Polymer Composites*
13:10-13:30	**D. Kourtidou**, E. Tarani, D. N. Bikiaris, G. Vourlias, K. Chrissafis Synthesis, characterization and thermal analysis of PE-RT/graphene nanocomposites
13:30-13:50	**Zoi Terzopoulou**, George Z. Papageorgiou, Dimitrios Bikiaris Current challenges in furan based polyesters from renewable resources
13:50-14:00	Απονομή Βραβείων ΕΕΘΑ
14:00	Λήξη Συνεδρίου Θερμά 2018

e-Posters session (5' / poster or 5 slides/poster)

P1. A. Rousi, **E. Vouvoudi**, D. Achilias
Products obtained from the catalytic pyrolysis of polymeric materials found in WEEE.

P2. Nejib Kasmi, **Niki Poulopoulou**, Zoi Terzopoulou, Dimitrios G. Papageorgiou, Dimitrios N. Bikiaris, George Z. Papageorgiou
Sustainable Thermoplastics from Renewable Resources: Thermal behavior of Poly(1,4-cyclohexane dimethylene 2,5-furandicarboxylate)

P3. **Niki Poulopoulou**, Dimitra Smyrnioti, Maria Siambani, Polyxeni Kalisperati, George Z. Papageorgiou, Maria Kapnisti
Miscibility and crystallization behavior of poly(alkylene terephthalate) blends. DSC study

P4. **Lazaros Papadopoulos**, Dimitra Patsiaoura, Kostantinos Chrissafis and Dimitrios Bikiaris
Synthesis and characterization of novel cross-linked polyester resins (UPRs) based on succinic acid

P5. Φειδίας**Μπαϊράμης**, Ιωάννης Κωνσταντίνου, Τιβέριος Βαϊμάκης
Σύνθεση Γραφιτικού Νιτριδίου g-C3N4 από Ουρία. Μελέτη με Θερμική Ανάλυση

P6. **IoulianaChrysafi**, Lamprini Malletzidou, Pavlos Beinas, Vassiliki Touli, Konstantinos M. Paraskevopoulos, Eleni Pavlidou, George Vourlias
Monastery of the Ascension, Elassona, Mount Olympus: Complementary analysis of the Catholicon wall paintings

P7. **A. Vasileiadou,** S. Zoras, A. Dimoudi, A. Iordanidis, A. Asvesta, V. Evagelopoulos
Determination of the combustion parameters of municipal solid waste samples and their blends with lignite with the help of Thermogravimetry (TG/DTG)

P8. **ZoiTerzopoulou,** Arsenios Tziolas, Apostolos Avgeropoulos, Dimitrios Bikiaris
Effect of nanofillers on the thermal properties of poly(lactic acid)

P9. **I. Charitos**, G. Georgousis, E. Kontou
Thermal and rheological behavior of linear low density polyethylene nanocomposites

P10. Electra Papadopoulou, Dimitra Patsiaoura, Dimitra Kourtidou, Iouliana Chrysafi, **EvangeliaTarani**
Thermal properties of Phenol Formaldehyde composites reinforced with textile Waste.

P11. **A. Sanida**, S. G. Stavropoulos, G. C. Psarras
Thermal and dielectric characterization of polymer nanocomposites

www.hsmc.gr/en/pharmakeftiki-journal/

ΦΑΡΜΑΚΕΥΤΙΚΗ, 30, 4 (2018) ΕΡΕΥΝΗΤΙΚΗ ΕΡΓΑΣΙΑ

PHARMAKEFTIKI, 30, 4 (2018) RESEARCH ARTICLE

DSC studies on the nature of freezing and nonfreezing water in polymer-water mixtures

Apostolos Kyritsis

Department of Physics, National Technical University of Athens, Zografou Campus, 15780, Athens, Greece

KEY WORDS:
hydrogels, hydration properties, plasticization, nonfreezing water

***Correspondent author:**
akyrits@central.ntua.gr

Introduction

The interaction of water with natural and synthetic polymers has been the subject of continued interest because hydration phenomena of polymers can modulate the physicochemical properties of such systems. Indeed, hydration of biomolecules such as proteins and enzymes is particularly important for the stability of the structure as well as proper functionality. On the other hand, hydrogels based on synthetic or natural polymers have become especially attractive not only for their use in biomedical applications but also for applications in other diverse fields, such as ion-conducting membranes, water retention in agriculture and sensors and actuators[1]. A detailed description of the water–macromolecule interactions and of their role in determining the structural, dynamic, and functional properties is a necessary prerequisite to optimize hydrogel characteristics for specific applications. It is known that water molecules in close proximity to biomolecules exhibit properties different than bulk water molecules and in order to describe these peculiar properties of water next to biomolecules the concept of a hydration shell has been employed. In a qualitative picture, the hydration shell consists of the first water layer or sometimes the first few water layers surrounding the biomolecule and interacting with it or at least noticeably influenced by it[2]. A variety of complex macromolecular structures can be formed depending on hydration and, therefore, on the degree of water – macromolecule association. Water may act also as a "plasticizer" affecting, thus, not only the conformation but also the dynamical properties at a molecular level[1].

Different conceptual frameworks have been used to describe the water–polymer associations in a range of hydrophilic polymers[1]. Terms such as ''free, loosely bound, and tightly bound'' or "freezable, bound freezable and non-freezable" help to describe the distribution of physical and chemical environments that water experiences in a hydrophilic polymer network leading thus to a classification of absorbed water into different states (classes). Alternatively, hydration properties have been discussed in terms of phase diagrams and of kinetic factors that inhibit the water crystallization. One method that is often used to distinguish between "free" or "bulk-like" and "bound" or "hydration" water is based on monitoring the thermodynamics of dehydration of the polymers. The desiccating force commonly used to distinguish between types of water is the freezing of water by employing differential scanning calorimetry (DSC) at subzero temperatures. In calorimetric experiments, the enthalpy of ice melting is monitored and recalculated to the mass of water that undergoes the melting transition. If this mass is lower than the total mass of water in the system, the difference in the masses constitutes the amount of nonfreezing (or non-freezable) water. Many experimental and theoretical works have focused on the investigation of the nature of nonfreez-

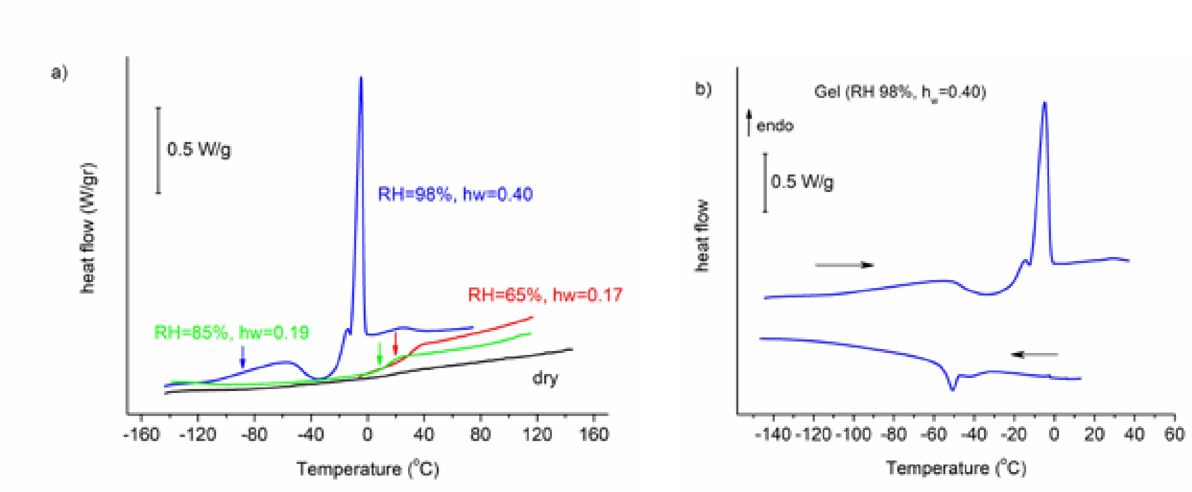

***Figure 1**. (a) DSC heating curves obtained on Gel hydrogels at various hydration levels indicated on the plot. The glass transition temperatures are marked by an arrow. (b) DSC cooling and heating curves of Gel hydrogel with h_w = 0.40. The heating rate was 10 °C/min.*

ing water. Different states of water, physically binding to polymer chains, have been proposed, among them hydrogen-bond bound water, water trapped in "nanocavities" in the polymer or simply water molecules that are not able to diffuse due to the vitrification of the amorphous polymer matrix.

The main objective of this work is to study the thermodynamics of water phases in polymer-water mixtures and to reveal the role of hydrogen bond networks existed in the biomolecules, as a function of added water molecules. To that end, we employ DSC method for monitoring the plasticization of the matrix and for studying the thermodynamics of the separate water phase (ice) formed at subzero temperatures, by gradual tuning the hydration level (from almost dry polymer up to highly concentrated solutions).

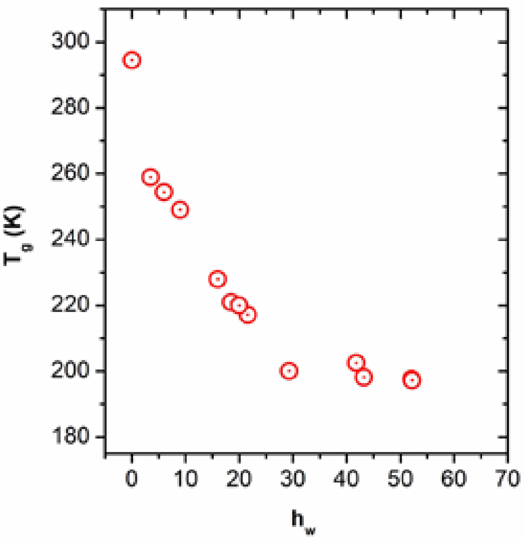

***Figure 2**. Glass transition temperature, Tg, measured by DSC, against water fraction h_w in neat PHEA hydrogels.*

Material and methods

In the present work we focus on the hydration properties of synthetic hydrogels based on poly(hydroxyethyl acrylate) (PHEA). In particular, we focus mostly on using PHEA copolymers, as well as PHEA/silica and copolymer/silica nanocomposites, as hydrogel matrices (xerogels)[1]. In addition, we investigate the hydration properties of a family of injectable natural hydrogels that mimic the composition of the extracellular matrix, with a homogeneous distribution of gelatin (Gel) and hyaluronic acid (HA) chains by enzymatic gelation of aqueous solutions of different mixtures of both polymers. Protein (Gel) and polysaccharide (HA) have been combined in an injectable crosslinked hydrogel with controlled Gel–HA ratio[3].

The hydration of the hydrogels was achieved by equilibration of the samples over certain salt solutions, i.e. within environments with varied relative humidity (RH). The hydration level is expressed in terms of water fraction, h_w (=m_{water}/m_{total}). Thermal transitions of the materials were investigated in high purity helium (99.9995 %) atmosphere in the temperature range from −150 to 150 ^{o}C using a TA Q200 series DSC instrument, calibrated with indium (for temperature and enthalpy) and sapphire (for heat capacity).

Results and Discussion

Figure 1 show DSC heating curves obtained on Gel hydrogels at various hydration levels indicated in the plot. We observe the strong plasticization of the gelatin matrix. For the highest water fraction studied, $h_w = 0.40$ for Gel, we observe in **Figure 1b** that during cooling the thermogram shows a weak exothermic peak that corresponds to water crystallization (with strong super-cooling). During heating the thermogram shows strong cold crystallization process and subsequent (rather complex) melting of ice crystals formed during both, cooling and heating. The analysis of the spectrum reveals that the fraction of nonfreezing water in Gel is about 0.24. It is worth to notice that HA do not shows water crystallization at the hydration level of 0.40. Water crystallizes during cooling only for $h_w \geq 0.60$, whereas the analysis reveals that in that case the non-freezing water is again about 0.23. These results, on the one hand, highlight the, well known, property of HA to absorb large amount of water at elevated RH values, on the other, reveal that the nonfreezing fraction of absorbed water is similar in Gel and HA hydrogels, irrespectively of the total water fraction absorbed.

In **Figure 2** we can see the strong plasticization action of water molecules being absorbed in neat PHEA hydrogels. In the range $0 < h_w < 30\%$ (or 0.30) water does not phase separate at subzero temperatures, i.e. no ice crystals are formed, implying that water molecules are molecularly distributed, forming eventually water clusters, and affect strongly the molecular mobility and chain conformations of the PHEA macromolecules. For higher water fractions, ice is formed during cooling and the plasticization action of water stops. Interestingly, the Tg of PHEA is not affected by the formation of the ice phase.

Conclusions

DSC is a powerful tool for studying hydration properties of hydrogels. The method provide information regarding both, the molecular mobility of the hosting macromolecules and the thermodynamic properties of the separate ice phase formed at subzero temperatures. ☐

Acknowledgment

The author is indebted to Prof. P. Pissis for fruitful collaboration and many helpful discussions.

REFERENCES

1. Pissis P., Kyritsis A. Hydration Studies in Polymer Hydrogels, *J. Polym. Sci., Part B: Polymer Physics* 51, 159 – 175, 2013.
2. Laage D., Elsaesser T., Hynes J.T. Water Dynamics in the Hydration Shells of Biomolecules, *Chem. Rev.* 117, 10694–10725, 2017.
3. Poveda-Reyes S., Moulisova V., Sanmartín-Masiá E., Quintanilla-Sierra L., Salmerón-Sánchez M., Gallego Ferrer G. *Macromol. Biosci*. 16, 1311–1324, 2016.

ΕΡΕΥΝΗΤΙΚΗ ΕΡΓΑΣΙΑ

RESEARCH ARTICLE

Ιερά Μονή Αναλήψεως του Σωτήρος, Ελασσόνα: Φυσικοχημικός χαρακτηρισμός των τοιχογραφιών του Καθολικού

Ιουλιάνα Χρυσάφη[1*], Λαμπρινή Μαλλετζίδου[1], Παύλος Μπεινάς[2], Βασιλική Τούλη[3], Κωνσταντίνος Μ. Παρασκευόπουλος[1], Ελένη Παυλίδου[1], Γιώργος Βουρλιάς[1]

[1]Εργαστήριο ακτίνων Χ, Οπτικού χαρακτηρισμού και Θερμικής ανάλυσης, Τμήμα Φυσικής, Αριστοτέλειο Πανεπιστήμιο Θεσσαλονίκης, 54124 Θεσσαλονίκη, Ελλάδα

[2]Συντηρητής έργων τέχνης, Εργαστήριο Συντήρησης Έργων «Εσαίτεχνον», 60100 Κατερίνη, Ελλάδα

[3]Εφορεία Αρχαιοτήτων Λάρισας, 41500 Λάρισα, Ελλάδα

ΛΕΞΕΙΣ ΚΛΕΙΔΙΑ:
TG, FTIR, SEM-EDS, XRD, νωπογραφία

***Correspondent author:**
iochrysa@physics.auth.gr

ΠΕΡΙΛΗΨΗ

Το Καθολικό της Ιεράς Μονής Αναλήψεως του Σωτήρος αποτελεί τον κύριο ναό του μοναστηριού που βρίσκεται στην ευρύτερη περιοχή της Ελασσόνας, στον Όλυμπο. Το μοναστήρι κατασκευάστηκε στα μέσα του 16ου αιώνα. Η παρούσα εργασία αφορά τη μελέτη των υποστρωμάτων των τοιχογραφιών του Καθολικού, οι οποίες χρονολογούνται στα μέσα του 17ου αιώνα. Μέσω της μελέτης προσδιορίζονται τα υλικά που χρησιμοποιήθηκαν στα υποστρώματα των τοιχογραφιών, με σκοπό τον προσδιορισμό της μεθόδου κατασκευής αυτών. Η ανάλυση των υποστρωμάτων πραγματοποιήθηκε μέσω θερμικής ανάλυσης, φασματοσκοπίας υπερύθρου, περιθλασιομετρίας Ακτίνων-Χ και ηλεκτρονικής μικροσκοπίας σάρωσης. Ταυτοποιήθηκε η χρήση ασβεστίτη με μικρή ποσότητα χαλαζία, ενώ υπάρχουν ισχυρές ενδείξεις της κατασκευής των τοιχογραφιών με την τεχνική της νωπογραφίας (*fresco*).

1. Θεωρητική Εισαγωγή

Η Μονή βρίσκεται δυτικά της Συκέας Ελασσόνας, χρονολογείται στο 1650 με ιδρυτές τους μοναχούς Ιωακείμ και Ιωάννη, και τον ιερομόναχο Διονύσιο. Το Καθολικό καθώς και οι υπόλοιποι χώροι του μοναστηριού έχουν ανακαινισθεί πλήρως[1,2].

Το Καθολικό βρίσκεται στο κέντρο της εσωτερικής αυλής με την αρχιτεκτονική του να είναι σταυροειδής εγγεγραμμένος με πλαγίους χορούς. Οι τοιχογραφίες έχουν επικαλυφθεί με κονίαμα στο μεγαλύτερό τους μέρος και έχουν υποστεί αρκετές φθορές. Η αγιογράφηση πραγματοποιήθηκε το 1650 με παραστάσεις Αγίων στο βόρειο και νότιο τμήμα του Ναού, ενώ στο τυφλό θόλο απεικονίζεται ο Παντοκράτωρ. Οι εικόνες που κοσμούν το τέμπλο κατασκευάστηκαν το 1778, δια χειρός Αστερίου εκ Καλαρρυτών Ιωαννίνων[1,2].

Η παρούσα εργασία έχει σκοπό να χαρακτηρίσει πλήρως τα υποστρώματα των τοιχογραφιών του Κα-

Σχήμα 1. *Η προς εξέταση τοιχογραφία. Τα σημεία δειγματοληψίας υποδεικνύονται αριθμητικά.*

θολικού της Ιεράς Μονής Αναλήψεως του Σωτήρος, ώστε να εξασφαλιστεί πλήρης προσδιορισμός των υλικών που χρησιμοποιήθηκαν αλλά και την τεχνική κατασκευής του υποστρώματος. Η βασική μελέτη πραγματοποιήθηκε μέσω θερμικής ανάλυσης, ενώ περαιτέρω ανάλυση για σύγκριση αποτελεσμάτων έγινε μέσω φασματοσκοπίας FTIR, περιθλασιομετρίας ακτίνων X-XRD ΚΑΙ ηλεκτρονικής μικροσκοπίας SEM-EDS[3,4].

2. Πειραματικό μέρος

Τα δείγματα συλλέχθηκαν από την ομάδα συντήρησης κατά τη διάρκεια αναστύλωσης της μονής και επιλέχθηκαν για μελέτη τόσο του υποστρώματος όσο και των χρωστικών (τμήμα άλλης μελέτης).

Η ανάλυση υπερύθρου μετασχηματισμού Fourier (FTIR) πραγματοποιήθηκε με φασματοσκόπιο Perkin Elmer, Spectrum 1000. Λήφθηκαν 32 σαρώσεις για

Σχήμα 2. *Φωτογράφιση στο ορατό του δείγματος el01, ως αντιπροσωπευτικό.*

κάθε φάσμα διαπερατότητας με διακριτική ικανότητα 4 cm^{-1} στην περιοχή του μέσου υπερύθρου (4000-400cm^{-1}). Για τη λήψη φασμάτων παρασκευάστηκαν δισκία βρωμιούχου καλίου (KBr) βάρους περίπου 200 mg με προσθήκη δείγματος 1.8 mg. Οι μετρήσεις εφαρμόστηκαν πριν και μετά την θερμική ανάλυση.

Η ηλεκτρονική μικροσκοπία σάρωσης (SEM-EDS) πραγματοποιήθηκε με ηλεκτρονικό μικροσκόπιο σάρωσης της Jeol (μοντέλο JSM 840A) με προσαρτημένο το αναλυτικό σύστημα OXFORD ISIS 300. Για την προετοιμασία του δείγματος, κόκκοι στερεώθηκαν απευθείας σε μεταλλικό δειγματοφορέα. Οι μετρήσεις έγιναν υπό λειτουργία χαμηλού κενού.

Για τη θερμική ανάλυση (TG) των δειγμάτων χρησιμοποιήθηκε το όργανο SETARAM Setsys 16/18. Η μέτρηση πραγματοποιήθηκε σε δυναμικές συνθήκες, στη θερμοκρασιακή περιοχή των 25-1000 °C, με ρυθμό θέρμανσης 20 °C/min σε ατμόσφαιρα αζώτου. Χρησιμοποιήθηκε δείγμα βάρους 8.4 mg το οποίο κονιορτοποιήθηκε και τοποθετήθηκε σε κυλινδρικό δειγματοφορέα από αλουμίνα.

Η περιθλασιομετρία ακτίνων Χ (XRD) πραγματοποιήθηκε με τη χρήση περιθλασίμετρου ακτίνων Χ κόνεως Rigaku Ultima+ δύο κύκλων, σε γεωμετρία Bragg-Brentano και ακτινοβολία λυχνίας CuK$_a$. Η ταυτοποίηση έγινε μέσω καρτελών περίθλασης του JCPDS-ICDD[5].

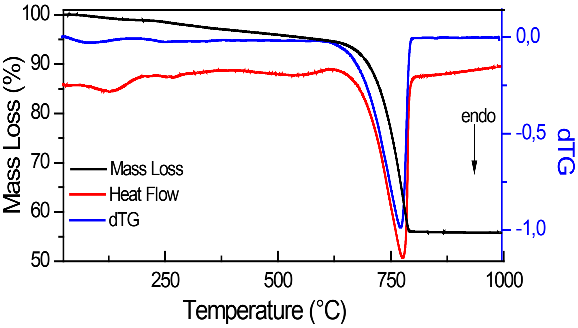

Σχήμα 3. *Καμπύλες θερμικής ανάλυσης*

3. Αποτελέσματα και συζήτηση

Σύμφωνα με τα αποτελέσματα της θερμικής ανάλυσης (**Σχήμα 3**) το δείγμα μας αποτελείται κυρίως από ασβεστίτη ($CaCO_3$) με μικρή συμμετοχή χαλαζία (SiO_2). Η απώλεια μάζας στη θερμοκρασιακή περιοχή μέχρι τους 120 °C οφείλεται στην απώλεια νερού (υγρασίας). Στους 550 °C παρατηρούμε μια μικρή και φαρδιά κορυφή η οποία αντιστοιχεί στο χαλαζία. Σε θερμοκρασίες μεγαλύτερες των 600 °C η απώλεια μάζας κατά την απομάκρυνση των ανθρακικών οφείλεται στην απομάκρυνση του διοξειδίου

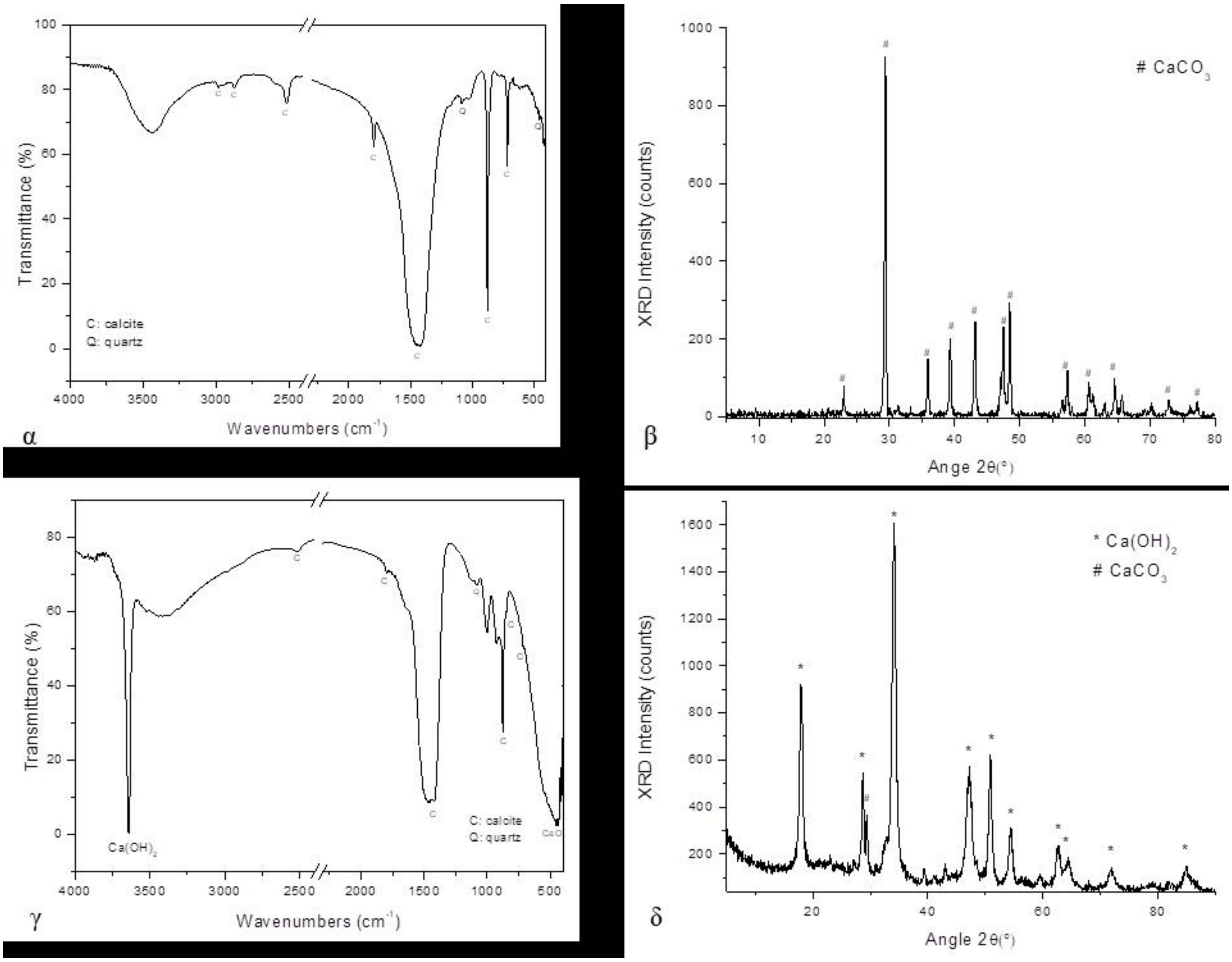

***Σχήμα 4.** Φάσματα FTIR και XRD πριν (α, β) και μετά (γ, δ) τη θερμική ανάλυση*

του άνθρακα[4,6]. Βρέθηκε ο λόγος CO_2/H_20 ο οποίος μπορεί να χρησιμοποιηθεί ώστε να προσδιοριστεί η υδραυλικότητα του κονιάματος. Ο λόγος βρέθηκε ίσος με 35,6 >10 πράγμα που ταυτοποιεί την ένδειξη αερικών κονιαμάτων[7].

Στο φάσμα ανάλυσης FTIR πριν τη θερμική ανάλυση (**Σχήμα 4α**) οι κύριες χαρακτηριστικές κορυφές του ασβεστίτη βρίσκονται στα 1796, 1419, 874, 713 cm^{-1} [8,9] ενώ του χαλαζία στα 1084 cm^{-1} [10]. Οι κορυφές που εμφανίζονται στη περιοχή 1100-900 cm^{-1} μπορούν να αποδοθούν επίσης σε αργυλοπυριτικές φάσεις. Στο φάσμα ανάλυσης FTIR μετά τη θερμική ανάλυση (**Σχήμα 4γ**) παρατηρούνται επίσης οι χαρακτηριστικές κορυφές του ασβεστίτη και του χαλαζία. Επίσης παρατηρείται η ύπαρξη CaO και $Ca(OH)_2$, τα οποία προήλθαν από τη διάσπαση του ασβεστίτη.

Τα περιθλασιογραφήματα XRD πριν (**Σχήμα 4β**) και μετά την εφαρμογή της θερμικής ανάλυσης (**Σχήμα 4δ**) συμφωνούν με τις προηγούμενες αναλύσεις (calcite hexagonal #47-1743, calcium hydroxide hexagonal #44-1481).

Πίνακας 1. Ανάλυση στοιχείων EDS

Spectrum	O	Al	Si	S	Cl	Ca
Spectrum 1	84.92	-	<1	<1	<1	14.91
Spectrum 2	85.12	<1	<1	-	-	14.31
Spectrum 3	81.06	<1	<1	<1	<1	17.75
Spectrum 4	82.50	<1	<1	<1	<1	15.88

Η στοιχειακή ανάλυση που πραγματοποιήθηκε μέσω SEM-EDS (**Πίνακας 1**) επιβεβαίωσε τη συμμετοχή ασβεστίτη. Επιπλέον, παρατηρείται και μικρή συμμετοχή αργιλοπυριτικών.

4. Συμπεράσματα

Η παρούσα εργασία στοχεύει στο στη μελέτη του υποστρώματος των τοιχογραφιών του Καθολικού της Ιεράς Μονής Αναλήψεως του Σωτήρος. Οι τεχνικές που εφαρμόστηκαν ήταν αυτές της θερμικής ανάλυσης, της φασματοσκοπίας FTIR, της περιθλασιομετρίας ακτίνων Χ και της ηλεκτρονικής μικροσκοπίας σάρωσης SEM-EDS. Η βασική μελέτη πραγματοποιήθηκε μέσω της θερμικής ανάλυσης και μας έδωσε ακριβή αποτελέσματα τα οποία επιβεβαιώθηκαν και μέσω των άλλων φυσικοχημικών μεθόδων. Κύριο συστατικό του κονιάματος βρέθηκε ο ασβεστίτης, ενώ εμφανίστηκε κι ένα μικρό ποσοστό χαλαζία που αποδίδεται στην ύπαρξη κόκκων άμμου -παραδοσιακά συστατικά κατασκευής υποστρωμάτων. Υπάρχουν ισχυρές ενδείξεις της εφαρμογής της τεχνικής της νωπογραφίας για την κατασκευή των τοιχογραφιών. Σε επόμενο στάδιο θα ακολουθήσει η μικρο-στρωματογραφική μελέτη των τοιχογραφιών για την επιβεβαίωση της τεχνικής της νωπογραφίας[11,12]. □

Ευχαριστίες

Η Υπ. Διδ. Λ. Μαλλετζίδου ευχαριστεί τη Γενική Γραμματεία Έρευνας και Τεχνολογίας και το Ελληνικό Ίδρυμα Έρευνας και Καινοτομίας (ΓΓΕΤ-ΕΛΙΔΕΚ) για την οικονομική υποστήριξη για τη συμμετοχή κατά την προετοιμασία της παρούσας εργασίας, στο πλαίσιο της χρηματοδότησης του διδακτορικού της (Κωδ.: 95546).

www.hsmc.gr/en/pharmakeftiki-journal/

ΦΑΡΜΑΚΕΥΤΙΚΗ, 30, 4 (2018) ΕΡΕΥΝΗΤΙΚΗ ΕΡΓΑΣΙΑ

PHARMAKEFTIKI, 30, 4 (2018) RESEARCH ARTICLE

Monastery of the Ascension, Elassona, Mount Olympus: Complementary analysis of the Catholicon wall paintings

Iouliana Chrysafi[1], L. Malletzidou[1], P. Beinas[2], V. Touli[3], K. M. Paraskevopoulos[1], E. Pavlidou[1], G. Vourlias[1]

[1] *X-Rays, Optical Characterization and Thermal Analysis Laboratory, School of Physics, Aristotle University Of Thessaloniki, GR-54124 Thessaloniki, Greece*

[2] Private *Conservator, 'Esaeitechnon' Artwork Conservation Laboratory, GR-60100 Katerini, Greece*

[3] *Ephorate of Antiquities of Larissa, GR-41500 Larissa, Greece*

KEYWORDS:
TG, FTIR, SEM-EDS, XRD, νωπογραφία

ABSTRACT

The Monastery of the Ascension (mid-16th century) is located near the village of Elassona, Mount Olympus. The interior of its catholicon (the main church) is decorated with wall paintings, which were constructed in the mid-17th century. In the framework of the present work, the wall paintings' plaster layers are examined. Through this study, the materials which were used in the substrates of the murals are identified, in order to obtain insights regarding the applied construction technique. The analysis was performed by Thermal Analysis, Fourier Transform Infrared Spectroscopy, X-Ray Diffractometry and Scanning Electron Microscopy. The use of calcite with a small amount of quartz was identified. In addition, there are strong indications of the use of the fresco technique.

ΒΙΒΛΙΟΓΡΑΦΙΑ

1. Αρχιμανδίτης Χαρίτων Τούμπας. Η ιερά Μητρόπολις Ελασσώνος- Οι Ενορίες, οι Ιερές Μονές και τα κειμήλιά τους, Ασπροβάλτα, Θεσσαλονικη: Ιερά Μητροπόλεως Ελασσώνος, 2007, pp. 215–219.
2. Αναζήτηση διαρκούς καταλόγου κηρυγμένων αρχαιολογικών χώρων και μνημείων-Χαρακτηρισμός της Ιεράς Μονής Αναλήψεως του Σωτήρος στην Κοινότητα Συκέα Ελασσώνας ως ιστορικού διατηρητέου μνημείου. [Online http://listedmonuments.culture.gr/fek_print.php?ID_FEKYA=6024].
3. Malletzidou L., et al., Unraveling the materials and techniques of post-Byzantine wall paintings: Is there a sole pictorial phase at the catholicon of Stomion, Central Greece? *Spectrochim. Acta - Part A* 206, 328–339, 2019.
4. Anastasiou M., Hasapis T., Zorba T., Pavlidou E., Chrissafis K., Paraskevopoulos K. M., TG-DTA and FTIR analyses of plasters from byzantine monuments in Balkan region: Comparative study. *J. Therm. Anal. Calorim*. 84, 27–32, 2006.
5. PC Powder Diffraction Files, (2003) JCPDS-ICDD.
6. Földvári M. (2013) Handbook of the thermogravimetric system of minerals and its use in geological practice. vol. 56, no. 4.
7. Moropoulou A., Bakolas A., Bisbikou K., Investigation of the technology of historic mortars. *J. Cult. Herit*. 1. 45–58, 2000.
8. White W.B., The Carbonate Minerals, in The Infrared Spectra of Minerals, London: Mineralogical Society of Great Britain and Ireland. (V.C. Farmer Editor) pp. 227–284, 1974.
9. Gunasekaran S., Anbalagan G., Pandi S., Raman and infrared spectra of carbonates of calcite structure. *J. Raman Spectrosc*. 37, 892–899, 2006.
10. Moenke H.W., Silica, the Three-dimensional Silicates, Borosilicates and Beryllium Silicates, in The Infrared Spectra of Minerals, London: Mineralogical Society of Great Britain and Ireland., (V.C. Farmer, editor) pp. 365–382, 1974.
11. Regazzoni L., Cavallo G., Biondelli D., Gilardi J., Microscopic Analysis of Wall Painting Techniques: Laboratory Replicas and Romanesque Case Studies in Southern Switzerland, *Stud. Conserv*. 63, 326-341, 2018.
12. Piovesan R., Mazzoli C., Maritan L., Cornale P., Fresco and lime-paint: An experimental study and objective criteria for distinguishing between these painting techniques. *Archaeometry*. 54, 723-736, 2012

ΦΑΡΜΑΚΕΥΤΙΚΗ, 30, 4 (2018)
ΕΡΕΥΝΗΤΙΚΗ ΕΡΓΑΣΙΑ

PHARMAKEFTIKI, 30, 4 (2018)
RESEARCH ARTICLE

Contribution of Differential Scanning Calorimetry to the Investigation of Polymerization Kinetics

Dimitris S. Achilias*, Ioannis Tsagkalias

Laboratory of Polymer and Dyes Chemistry and Technology, Department of Chemistry, Aristotle University of Thessaloniki, 54124 Thessaloniki, Greece.

KEYWORDS: Polymerization kinetics; DSC; PHEMA; PEGMA; PEGMEMA

***Corresponding author**
Dimitris S. Achilias, e-mail: axilias@chem.auth.gr

Introduction

Free radical polymerization is extensively employed to produce several polymers, ranging from the commodity polyethylene, polystyrene, etc. to specialty biopolymers, such as poly(2-hydroxylethyl methacrylate), PHEMA, etc. The latter, is a polymer hydrogel that has been widely used in the biomedical field because of its nontoxicity, antigenicity and excellent compatibility with living organism tissue. In fact, hydrophilic polymers based on HEMA have been widely used in soft contact lenses, as well as in the field of tissue engineering as matrix for repairing and regenerating a wide variety of tissues and organs, in artificial skin manufacturing and burn dressings, as it ensures good wound-healing conditions[1,2]. Recently, new monomers have been employed in the preparation of "smart" biorelevant materials composed of a methacrylate moiety connected to a short poly(ethylene glycol) (PEG) chain[3]. These materials form polymeric hydrogels with several applications as biosensors, artificial tissues, etc. Although their applications have been studied, their polymerization kinetics has not been explored so far in literature.

Differential Scanning Calorimetry (DSC) is a powerful technique usually used to measure thermal properties (such as melting or glass transition temperature) of several materials, including polymers. In this investigation its application in measuring complex polymerization kinetics is presented. Recently, this technique has been used in our lab to study the polymerization kinetics of several polymers[4-8]. DSC presents several advantages compared to other techniques, such as requirement of small monomer amounts, achievement of homogeneous reaction conditions and controlled temperature, as well as a continuous recording of the variation of polymerization rate with either time or temperature.

Radical polymerization of vinyl monomers is an exothermic reaction accompanied by a significant heat release (polymerization enthalpy) due to the addition reaction to the double bond. The amount of heat released during polymerization can be recorded via the DSC as a function of time (isothermal) or temperature (non-isothermal) variation[4]. Then the polymerization rate (*dx/dt*) can be estimated from the rate of heat released (*d(ΔH)/dt*) measured by the DSC, from the following equation:

$$\frac{dx}{dt} = \frac{1}{\Delta H_T} \frac{d(\Delta H)}{dt}$$

where ΔH_T is used to account for the total reaction enthalpy and *x* is monomer conversion.

The degree of monomer conversion (in terms of double bond) is calculated by integrating the area between the DSC thermograms and the baseline established by extrapolation from the trace produced after complete polymerization (no change in the heat produced during the reaction). It should be noticed that DSC measures consumption of double bonds. This is identical to monomer conversion only in mono-functional monomers, while it is not the same in di- or multi- functional monomers (i.e. dimethacrylates etc.).

Material and methods

The monomers used were methyl methacrylate (MMA) with a purity > 99% from Alfa Aesar, 2-hydroxyethyl methacrylate (HEMA), purity ≥ 97% from Sigma-Aldrich, poly(ethylene glycol) methacrylate (PEGMA) with average molecular weight 360 and poly(ethylene glycol) methyl ether methacrylate (PEGMEMA), with average molecular weight 300 (their chemical structure is shown below) both from Sigma-Aldrich. The free radical initiator used was benzoyl peroxide (BPO) with a purity >97 %, provided by Fluka and purified by fractional recrystallization twice from methanol (Merck). All other chemicals used were of reagent grade.

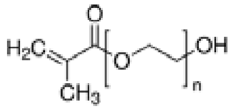

PEGMA

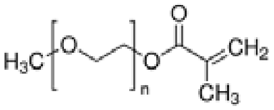

PEGMEMA

Polymerization was investigated using the DSC, Diamond (from Perkin-Elmer) equipped with the Pyris software for windows. Indium was used for the enthalpy and temperature calibration of the instrument. Polymerizations were carried out under both isothermal and non-isothermal conditions. Isothermal polymerizations were carried out at constant reaction temperatures ranging from 70 to 90 °C, whereas in non-isothermal experiments, constant heating rates were used varying between 2.5 and 20 °C min^{-1}.

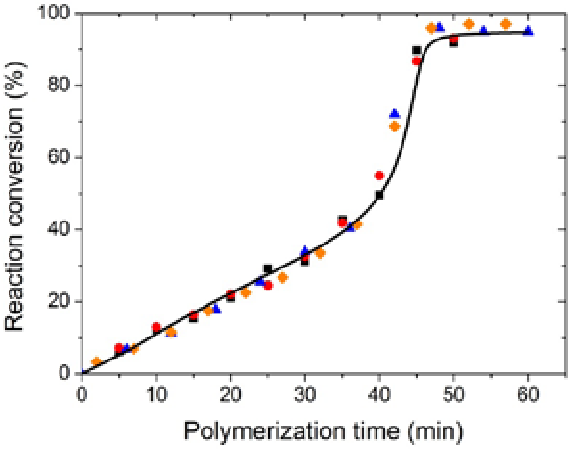

Figure 1: *Comparison of reaction conversion vs time experimental data obtained from DSC measurements (continuous line) to gravimetric measurements from four individual experiments (discrete points).*

Results and Discussion

The first step in order to check the accuracy of the DSC method in measuring the variation of monomer conversion with time is to compare results obtained from this technique to others. As such, gravimetry was employed since it provides absolute conversion data (i.e. without needing any calibration curve). Comparative experimental data are presented in **Figure 1**. It is clear that DSC data follow very well the corresponding gravimetric obtained from several repeated experiments.

Furthermore, several experiments were carried out under different experimental conditions and monomer types. It was found interesting to investigate the polymerization behavior of the new monomers, PEGMA and PEGMEMA and compare their polymerization profiles to corresponding of PHEMA and those of the model polymer, PMMA. A comparison of the dynamic evolution of polymerization rate and monomer conversion in isothermal experiments is presented in **Figure 2.** A totally different

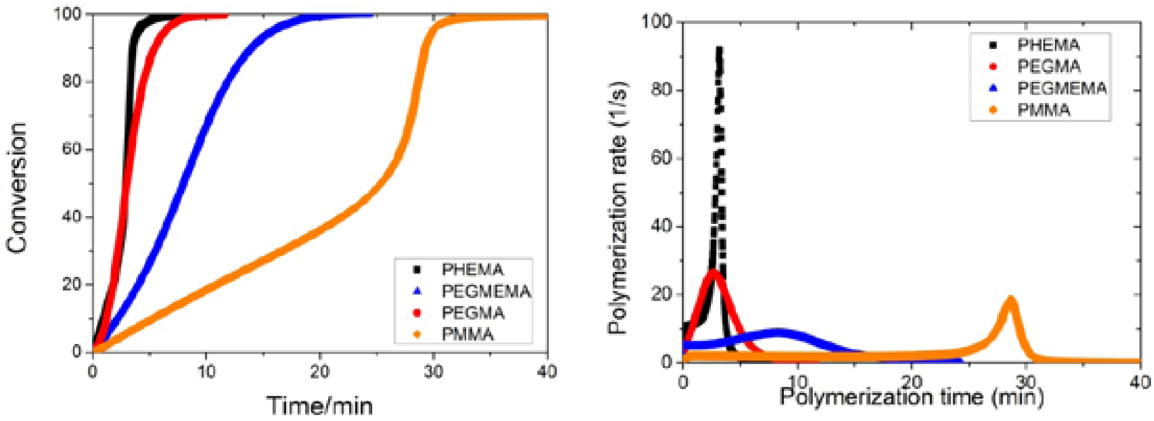

***Figure 2:** Variation of monomer conversion (as adapted from ref [5]) and reaction rate with time during polymerization of PHEMA, PEGMA, PEGMEMA and PMMA using benzoyl peroxide as initiator.*

behavior was observed from the four experiments. Initially, all three PHEMA, PEGMA and PEGMEMA result in much faster reaction rates compared to PMMA. PEGMA, having hydroxyl groups in its structure presents much faster reaction rate compared to PEGMEMA, which includes only methyl groups. The behavior of PEGMA is similar to that of PHEMA which also has hydroxyl groups. Therefore, it seems that such groups act as a catalyst promoting polymerization rate and resulting in higher monomer conversions. Moreover, PHEMA with smaller monomer molecules compared to PEGMA presents a very rapid polymerization completing in only a few minutes. Therefore, great care should be taken, since such high rates may result in increased temperature during polymerization, which may reach to more than 100 °C.

From the polymerization rate profiles the overall kinetic rate constant can be estimated from which the activation energy can be estimated. The initial activation energy from PMMA, PHEMA, PEGMA and PEGMEMA was estimated to be 84, 89, 82 and 100 kJ/mol, respectively[4-8].

Conclusions

DSC is a powerful tool in measuring radical polymerization kinetics and recording the phenomena taking place during the reaction. One should always have in mind the elementary chemical reactions taking place, as well as the effect of diffusion-controlled phenomena on the kinetic rate constants. Finally, functional groups in the monomer molecules always play an important role. ☐

REFERENCES

1. Zhang L., Zheng G.-J., Guo Y.-T., Zhou L., Du J., He H. Preparation of novel biodegradable PHEMA hydrogel for a tissue engineering scaffold by microwave-assisted polymerization. *Asian Pac. J. Trop. Med.* 7, 136–140, 2014.
2. Atzet S., Curtin S., Trinh P., Bryant S., Ratne B. Degradable poly(2-hydroxyethyl methacrylate)-co-polycaprolactone hydrogels for tissue engineering scaffolds. *Biomacromolecules* 9, 3370–3377, 2008.
3. Lutz J.-F. Polymerization of oligo(ethylene glycol) (meth)acrylates: Toward new generations of smart biocompatible materials. *J. Polym. Sci. A Polym. Chem*. 46, 3459–3470, 2008.
4. Achilias D.S., Verros G.D. Modeling of Diffusion Controlled Reactions in Free Radical Solution and Bulk Polymerization: Model Validation by DSC Experiments. *J. Appl. Polym. Sci.,* 116, 1842-1856, 2010.
5. Achilias D.S., Tsagkalias I. Investigation of radical polymerization kinetics of poly(ethylene glycol) methacrylate hydrogels via DSC and mechanistic or isoconversional models. *J. Therm. Anal. Calorim.* in press, 2018. DOI: 10.1007/s10973-018-7535-x
6. Achilias D.S., Siafaka P.I. Polymerization Kinetics of Poly(2-Hydroxyethyl Methacrylate) Hydrogels and Nanocomposite Materials. Processes 5, 21, 2017.
7. Siddiqui M.N., Redhwi H.H., Tsagkalias I., Softas C., Ioannidou M.D., Achilias D.S. Synthesis and characterization of poly(2-hydroxyethylmethacrylate)/silver hydrogel nanocomposites prepared via in situ radical polymerization. *Thermochim Acta* 643, 53–64, 2016.
8. Achilias D.S. Investigation of the radical polymerization kinetics using DSC and mechanistic or isoconversional methods. *J. Therm. Anal. Calorim.*, 116 (3), 1379-1386, 2014.

www.hsmc.gr/en/pharmakeftiki-journal/

ΦΑΡΜΑΚΕΥΤΙΚΗ, 30, 4 (2018) ΕΡΕΥΝΗΤΙΚΗ ΕΡΓΑΣΙΑ

PHARMAKEFTIKI, 30, 4 (2018) RESEARCH ARTICLE

Synthesis, characterization and thermal analysis of PE-RT/graphene nanocomposites

Dimitra Kourtidou[1*], Evangelia Tarani[1], Dimitrios N. Bikiaris[2], George Vourlias[1], Konstantinos Chrissafis[1]

[1] *X-ray, Optical Characterization and Thermal Analysis Laboratory, Physics Department, Aristotle University of Thessaloniki, GR 54124, Greece*

[2] *Laboratory of Polymer Chemistry and Technology, Department of Chemistry, Aristotle University of Thessaloniki, GR 54124, Greece*

KEYWORDS:
graphene nanoplatelets, nanocomposite, PE-RT, thermal stability

***Corresponding Author:**
Dimitra Kourtidou,
(+30) 2310998054,
dikourti@physics.auth.gr

ABSTRACT

Polyethylene of Raised Temperature resistance (PE-RT) nanocomposites with graphene nanoplatelets (GNPs) were prepared in order to investigate the effect of the nanofiller on the thermal stability of the polymer. PE-RT is a new type of polyethylene with improved mechanical and thermal properties and is commonly used as a piping material[1]. Various types of graphene are often used as a reinforcement filler material to improve electrical, thermal and mechanical properties of the polymeric matrix[2]. In the present work, PE-RT/GNPs nanocomposites were prepared by the melt mixing method using GNPs with 5μm diameter and 6nm thickness at different filler concentration (0.5, 1, 2.5% wt.). The characterization of neat PE-RT and the corresponding nanocomposites was achieved by X-Ray Diffraction (XRD). The effect of GNPs on the thermal properties of PE-RT nanocomposites was studied by using Differential Scanning Calorimetry (DSC) and Thermogravimetric Analysis (TGA). It was found that the presence of GNPs affected the crystalline structure of the PE-RT matrix. TGA results also showed that the nanocomposites exhibited better thermal stability than neat PE-RT. The nanocomposites with 2.5%wt. filler content exhibited the most improved thermal stability compared to the ones with lower filler content (0.5, 1%wt.).

1. Introduction

Polyethylene is one of the most commonly used polymers that has a wide range of applications. Because of this wide application range, many types of PE have been developed during the past years in order to achieve better suitability for each type of use. Polyethylene of Raised Temperature resistance (PE-RT) was developed for piping material due to its high thermal stability, excellent processability, and high impact strength[1].

Polymer/graphene nanocomposites have been produced to apply in commercial materials that demands high mechanical endurance and thermal stability such as piping. Graphene nanoplatelets (GNPs) are commonly used, at low loadings, as a nanofiller reinforcement of the polymeric matrix due to their excellent thermal and mechanical properties[2, 3, 4]. According to the literature, HDPE/GNPs composites with different diameters and filler's content were synthesized. It was found that HDPE nanocomposites show better thermal stability and conductivity than neat HDPE[5]. LDPE/GNP composites were also produced; the presence of GNPs into polymer matrix leads to higher thermal conductivity and increased Young's modulus compared to neat LDPE[6].

In this work, a series of PE-RT/GNP composites were prepared by melt mixing method with different filler content of GNPs having an average diameter of 5μm. X-Ray Diffraction was used to confirm the presence of the GNPs and to estimate the degree of crystallinity of nanocomposites. Differential Scanning Calorimetry was applied to study the melting and crystallization process of the PE-RT/GNP composites, while a more accurate crystallinity percentage was calculated from the peak area of the curves. Finally, the influence of the various concentrations of GNPs on the thermal stability of nanocomposites was studied using Thermogravimetric Analysis.

2. Materials and methods

Materials

PE-RT under the trade name DaelimPoly mLLDPE XP9000 was supplied by Daelim Industrial Petrochemical Division (Seoul, Korea). It has a melt flow index of 0.6 g/10 min and a density of 0.935 g/cm^3. The GNP filler with an average thickness of 7 nm were supplied by XG Sciences Inc., USA having average platelet diameter of 5 μm. This translates into an average particle surface area ranging of 120 to 150 m^2/g. The bulk density of the GNP filler is reported to be 2.2 g/cm^3.

Nanocomposites preparation

A series of PE-RT/graphene nanocomposites were prepared by the melt-mixing method. A certain mass-measured PE-RT and GNPs (content: 0, 0.5, 1 and 2.5 wt.%) were mixed in a Haake–Buchler Reomixer (model 600) with roller blades and a mixing head with a volumetric capacity of 69 cm^3 for 600 seconds at 180 ^{o}C with a torque speed of 30 rpm. The nanocomposite samples are referred to this work as x% wt. M5, where x is the GNPs content.

X-ray diffraction (XRD)

X-ray diffraction patterns were recorded at Bragg-Brentano geometry by a two-cycles Rigaku Ultima + powder X-ray diffractometer (Rigaku Corporation, Shibuya-Ku, Tokyo, Japan) using CuK$_a$ radiation, a step size of 0.05^o and a step time of 1.5 s, operating at 40 kV and 30 mA.

Differential scanning calorimetry (DSC)

Differential scanning calorimetry curves were obtained by using DSC 141, SETARAM instrument. 5.5 ± 0.2 mg of each sample was placed in crimped aluminium crucibles, while an empty one was used as a reference. Samples were heated from ambient temperature to 170 ^{o}C in a 50 ml/min flow of N_2 with a heating and cooling rate of 5 ^{o}C/min.

Thermogravimetric analysis (TGA)

The thermal stability of PE-RT/GNP nanocomposites was examined by TGA using a SETARAM SETSYS TG-DTA 16/18. Samples (5.5 ± 0.1 mg) were placed in alumina crucibles. An empty alumina crucible was used as a reference. The samples were heated from ambient temperature to 600 ^{o}C in a 50 ml/min flow of nitrogen, at a heating rate of 20 ^{o}C/min. Continuous recordings of sample temperature, sample weight, its first derivative and heat flow were performed.

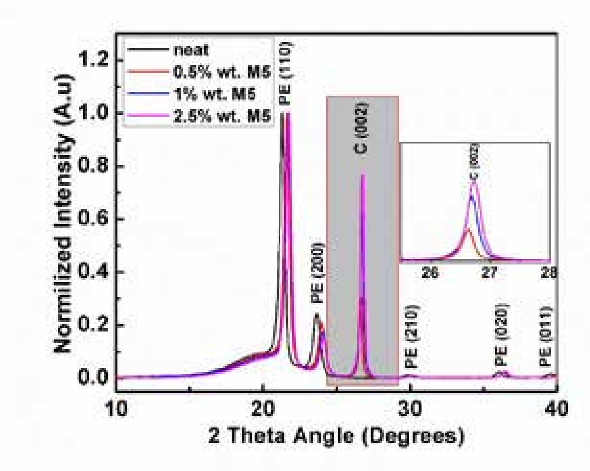

Figure 1. X-Ray Diffraction patterns of neat PE-RT and PE-RT/GNP composites

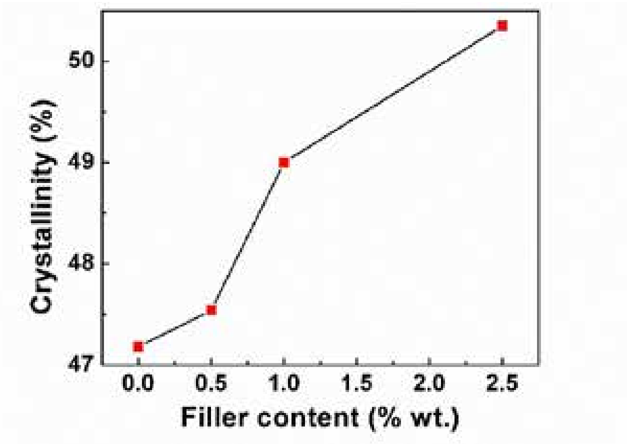

Figure 2. The degree of crystallinity as estimated from the XRD patterns for neat PE-RT and PE-RT/GNP composites at various filler's content

3. Results and Discussion.

XRD characterization

X-ray diffraction patterns of neat PE-RT and PE-RT/GNP composites are shown in **Figure 1**. Neat PE-RT and GNPs composites are characterized by five peaks, reflections (1 1 0), (2 0 0), (210), (0 2 0) and (0 1 1), corresponding to the orthorhombic phase (Pnam space group) of polyethylene[7]. The above-mentioned peaks for the neat polymer are individually located at 2θ values around 21.3**°,** **2**3.65**°,** 29.8° **and 36.**05**°, respectively**, while the peaks of all nanocomposites appear in slightly higher 2**θ** values (around 24.7°, 24.05°, 30.25° and 36.4°, respectively) indicating higher internal stress. GNP composites exhibit a sharp diffraction peak at 2θ≈26.7°**, which represents the diffraction of the (002) crystal plane of GNPs**[8]. As expected, the peak of the normalized intensity increases as the filler content increase in the polymeric matrix.

The degree of crystallinity was estimated using the Equation 1 where A_{cr} and A_{am} represent the relative area under the major crystalline components (the 110 and 200 reflections) and amorphous halo, respectively, **Figure 1**; K is a constant related to the scattering factors of crystalline and amorphous phases, here taken 1[9]. It was found that the degree of crystallinity of PE-RT/GNP composites is higher compared to neat PE-RT. Also, the crystallinity increases as the GNPs content increase in the polymeric matrix, **Figure 2**.

$$x_c = \frac{A_{cr}}{A_{cr}+K\cdot A_{am}}100\% \quad (1)$$

Melting and crystallization behavior of PE-RT/GNP composites

DSC melting and crystallization curves of neat PE-RT and its GNP composites are shown in **Figure 3a** and b, respectively. Table 1 lists the melting temperature (T_m), the crystallization temperature (T_c), as well as the melting (**ΔH_m**) and crystallization (ΔH_c) enthalpies for neat PE-RT and PE-RT/GNP composites. The melting temperature of all the nanocomposites were found to be around 125 ^{o}C close to the melting tem-

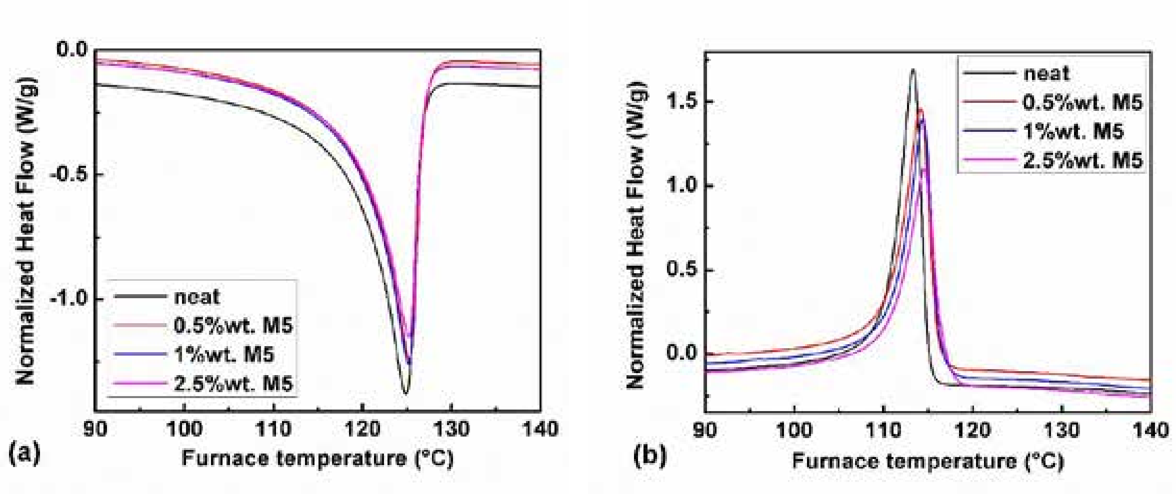

Figure 3. *a) DSC melting and b) crystallization curves of neat PE-RT and PE-RT/GNP composites*

Table 1: DSC melting and crystallization parameters of neat PE-RT and PE-RT/GNP composites

	Melting process		**Crystallization process**	
% Filler	**Tm (°C)**	**ΔH_m (J/gr)**	**Tc (°C)**	**ΔH_c (J/gr)**
neat	124.9	106.1	113.3	-121.5
0.5	125.3	106.3	114.2	-96.9
1	125.2	106.8	114.4	-94.7
2.5	125.2	111.5	114.6	-93.2

perature of the neat PE-RT. Also, the crystallization temperature of PE-RT/GNP composites increases with increasing filler content. This behavior was ascribed to the high thermal conductivity of the GNP filler that allows the latent heat to be transferred faster from the polymer to the surrounding medium. However, the more dominant effect is the crystal nucleation that can be formed at higher temperature due to the presence of GNPs which act as a foreign substance in the PE-RT matrix[10].

Figure 4 shows the crystallinity percentage of neat PE-RT and GNP composites versus GNP content calculated by using the Equation 2, where ΔH_m (in J/g) is the enthalpy of fusion of the samples, $\Delta H_m°$ is the heat of fusion of the completely crystalline PE (293 J/g)[11] and m is the polymer weight fraction of materials[12]. Higher crystallinity in the PE-RT/GNP composite samples attributed to the high surface area and the nucleation effect of the GNPs. GNPs act as heterogeneous nucleation sites, which can also be seen in the increase of crystallization peak temperature[13].

$$x_c = \frac{\Delta H_m}{(1-m)\Delta H_m^0} 100\% \quad (2)$$

Thermal stability of PE-RT/GNP composites

TGA curves of neat PE-RT and PE-RT/GNP composite with different filler content are shown in **Figure 5a** at a heating rate of 20 °C/min under the nitrogen atmosphere. The GNP composites present better thermal stability since no significant mass loss occurred until 444 °C. Mass loss temperature increases with increasing the content of GNPs. The residual amount of the nanocomposites raises with the content of GNPs; the additional residue is close to the added filler %wt. in

Table 2: Detailed data obtained from TGA tests for neat PE-RT and PE-RT/GNP composites

% Filler	$T_{2\%}$(^{o}C)	$T_{50\%}$(^{o}C)	T_{peak}(^{o}C)	Residual content (%)
neat	440.5	493.3	497.3	0.15
0.5	444.7	495.1	498.6	0.9
1	446.6	495	498.5	1.02
2.5	447.4	496.6	499.3	2.7

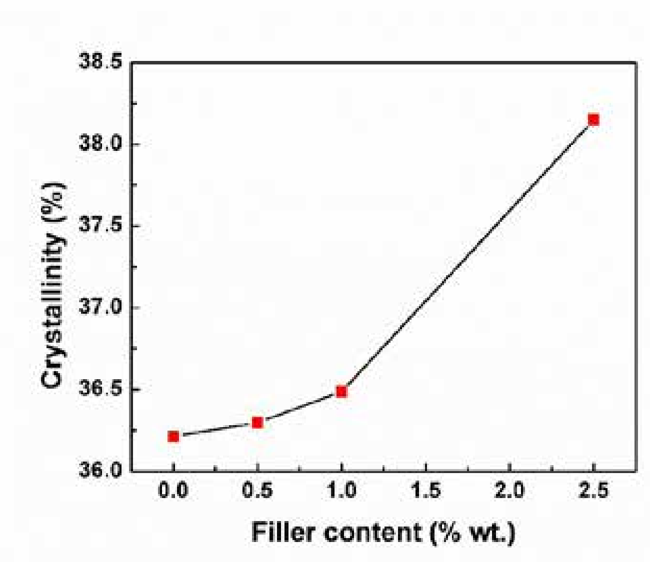

Figure 4. *Crystallinity as calculated by the DSC curves for neat PE-RT and PE-RT/GNP composites at various filler's content*

all the nanocomposites. The thermal decomposition of the PE-RT retards in the nanocomposites due to the decomposition of GNPs that have initial degradation temperature above 600 ^{o}C[14]. The derivative thermogravimetric curves (DTG), in **Figure 5b**, show the presence of one peak suggesting that the thermal degradation of neat PE-RT and PE-RT/GNP composites occurs at one stage until 497 ^{o}C.

The highest decomposition rate is around 497 and 499 ^{o}C, for neat PE-RT and PE-RT/GNP composite with 2.5% wt. GNP, respectively, as shown in **Table 2**. The increase at the highest decomposition rate temperature suggests that the incorporation of the GNPs increase the thermal stability of the PE-RT matrix. The temperature at which mass loss of neat PE-RT and its nanocomposites is 2%, versus the filler content, is given in **Table 1**. An enhancement of 4.2, 6.1, and 6.9 ^{o}C appeared for the nanocomposites containing 0.5, 1 and 2.5% wt. GNPs, respectively. The temperature at which mass loss of neat PE-RT and PE-RT/GNPs composites is 50% (**Table 2**) also shows an increase with increasing the filler content. The retarding of thermal stability may result from the restricted mobility of the polymeric chains due to the presence of the GNPs, leading to an increased activation energy of the nanocomposite PE-RT samples[15].

4. Conclusions

PE-RT/GNP composites were successfully prepared by the melt mixing method. XRD patterns revealed the main PE peaks of the orthorhombic phase of polyethylene. The presence of GNPs in the PE-RT nanocomposites was also confirmed. DSC study revealed a slight increase in the melting temperature of the PE-RT/GNP composites compared to neat polymer. Moreover, it was found that the crystallization temperature increases with increasing the filler content in the PE-RT matrix. According to the calculation of the crystallinity

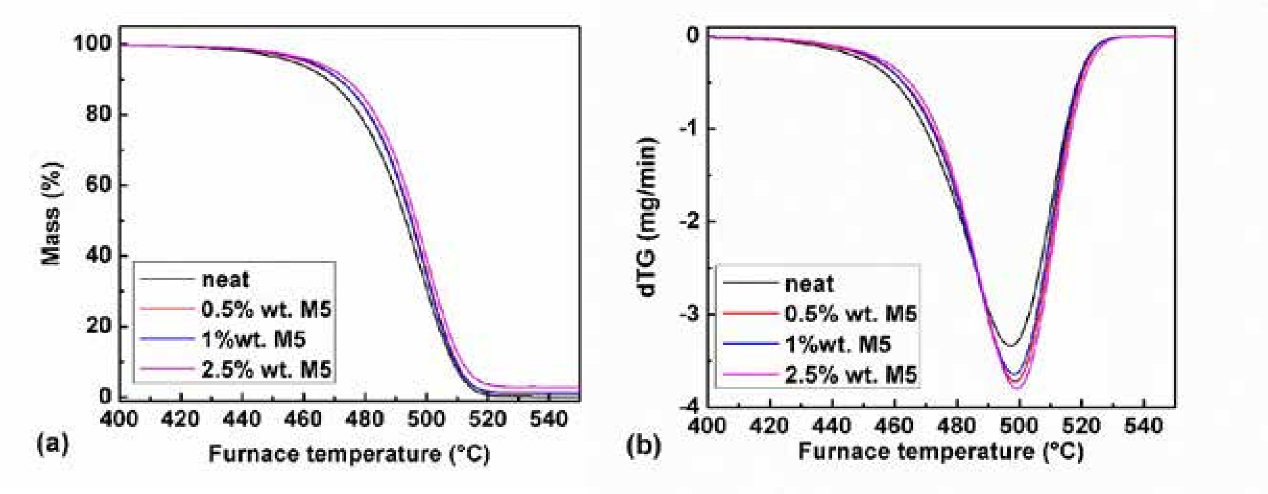

Figure 5. *a) Mass (%) and b) derivative of TGA curves for neat PE-RT and PE-RT/GNP composites at a heating rate of 20 oC/min under the nitrogen atmosphere*

from the XRD and DSC diagrams, GNPs serve as heterogeneous nucleation sites in PE-RT nanocomposites, leading to a higher percentage of crystallinity. Thermogravimetric measurements suggest higher thermal stability of the nanocomposites with increasing GNPs content compared to neat PE-RT. Summarizing, the PE-RT nanocomposite with 2.5% wt. GNP was found to be the most thermally stable sample.

Acknowledgements: This research has been co-financed by the European Union and Greek national funds through the Operational Program Competitiveness, Entrepreneurship and Innovation, under the call RESEARCH – CREATE – INNOVATE (project code: T1EDK- 02611).

Co-financed by Greece and the European Union

REFERENCES

1. Schramm D., Jeruzal M. PE-RT, A new class of polyethylene for industrial pipes, 2006, *Proceedings of the 24th International Conference on Offshore Mechanics and Arctic Engineering - OMAE*, Hamburg, Germany, 4-9 June 2006.
2. Kesong H., Dhaval D. K., Ikjun C., Vladimir V. T. Graphene-polymer nanocomposites for structural and functional applications, *Prog. Polym. Sci.* 39, 1934-1972, 2014.
3. Abdelrahman H., Byungki K. Graphene/polymer nanocomposites: The active role of the matrix in stiffening mechanics, *Compos. Struct.* 202, 170-181, 2018.
4. Singh K., Ohlan A., Dhawan S.K. (2012) Polymer-Graphene Nanocomposites: Preparation, Characterization, Properties, and Applications, In: Farzad Ebrahimi, eds: *Intechopen: Nanocomposites - New Trends and Developments*, Rijeka, Croatia, chapter 3.

5. Tarani E., Terzopoulou Z., Bikiaris D. N., Kyratsi Th., Chrissafis K., Vourlias G. Thermal conductivity and degradation behavior of HDPE/graphene nanocomposites, *J. Therm. Anal. Calorim.* 129, 1715–1726, 2017.

6. Yusof M. A., Rahman N. H. N., Sulaiman S. Z., Sofian A. H., Desa M. S. Z. M., Izirwan I. Development of low density polyethylene/graphene nanoplatelets with enhanced thermal properties, *2018 IEEE 9th International Conference on Mechanical and Intelligent Manufacturing Technologies (ICMIMT)*, Cape Town, 10-13 February 2018, pp. 6-9.

7. Rizzo P., Baione F., Guerra G., Martinotto L., Albizzati E. Polyethylene Unit Cell and Crystallinity Variations as a Consequence of Different Cross-Linking Processes, *Macromolecules*, 34, 5175-5179, 2001.

8. Um J. G., Jun Y. S., Alhumade H., Krithivasan H., Luia G., Yu A., Investigation of the size effect of graphene nano-platelets (GnPs) on the anti-corrosion performance of polyurethane/GnP composites, *RSC Adv.* 8, 17091-17100, 2018.

9. Matthews J. L., Peiser H. S., Richards R. B. The x-ray measurement of the amorphous content of polythene samples. *Acta Crystallogr.* 2, 85–90, 1949.

10. Steinmann W., Walter S., Beckers M., Seide G., Gries T. (2013) Thermal Analysis of Phase Transitions and Crystallization in polymeric Fibers, In: Amal Ali Elkordy, eds: *IntechOpen Applications of Calorimetry in a Wide Context*, Rijeka, Croatia, chapter 12.

11. Cormier C. M., Wunderlich B. Heat of Fusion of Polyethylene, *J. Polym. Sci., Part A: Polym. Chem.* 5, 987-988, 1967.

12. Wunderlich B., Jin Y., Boller A. Mathematical description of differential scanning calorimetry based on periodic temperature modulation. *Thermochim. Acta* 238, 277–293, 1994.

13. Mago G., Velasco-Santos C., Martínez-Hernández L., Kalyon, D. M., Frank F. T. (2008). Effect of Functionalization on the Crystallization Behavior of MWNT-PBT Nanocomposites. *Material Research Society Proceedings*, 1056, pp. 295-300, 2008.

14. Rybinski P., Anyszka R., Imiela M., Sicinski M., Gozdek T. Effect of modified graphene and carbon nanotubes on the thermal properties and flammability of elastomeric materials. *J. Therm. Anal. Calorim.* 127, 83–96, 2017.

15. Roumeli E., Markoulis A., Chrissafis K., Avgeropoulos A., Bikiaris D. N. Substantial enhancement of PP random copolymer's thermal stability due to the addition of MWCNTs and nanodiamonds: decomposition kinetics and mechanism study. *J. Anal. Appl. Pyrol.* 106, 71–80, 2014.

ΕΡΕΥΝΗΤΙΚΗ ΕΡΓΑΣΙΑ

RESEARCH ARTICLE

Effects of the Complex HP-β-CD with Irbesartan on Lipid Bilayers Containing Cholesterol

Georgios Leonis[1], Dimitrios Ntountaniotis[1], Eirini Christodoulou[2], Thomas Mavromoustakos[1*]

[1]National and Kapodistrian University of Athens, Department of Chemistry, Panepistimiopolis Zografou 15771, Athens, Greece.
[2]National and Kapodistrian University of Athens, Department of Pharmacy, Panepistimiopolis Zografou, 15771, Athens, Greece.

KEYWORDS: irbesartan, lipid bilayers, cholesterol, 2-hydroxypropyl-β-cyclodextrin, Differential Scanning Calorimetry.

***Corresponding author:** Thomas Mavromoustakos; National and Kapodistrian University of Athens, Department of Chemistry, Athens, Greece;
email: tmavrom@chem.uoa.gr

Introduction

Since AT1R antagonists are highly lipophilic molecules (**Table 1**), vehicles such as cyclodextrins are used to overcome low solubility and bioavailability barriers, and therefore to improve the pharmacological profile. In our previous study, we have examined the interactions of irbesartan (IRB) and irbesartan–2-hydroxypropyl-β-cyclodextrin (HP-β-CD) complex with dipalmitoyl phosphatidylcholine (DPPC) bilayers by utilizing an array of biophysical techniques, including Differential Scanning Calorimetry (DSC), Small angle X-ray Scattering (SAXS), ESI Mass-Spectrometry (ESI-MS), and solid state Nuclear Magnetic Resonance (ssNMR). Molecular Dynamics (MD) calculations have also been conducted to complement the experimental results and to provide insight into the molecular interactions of IRB and its complex in DPPC bilayers. Irbesartan was found to be embedded in the lipid membrane core and to perturb the phase transition properties of the DPPC bilayers. SAXS studies revealed that IRB alone does not display perfect solvation as some coexisting IRB crystallites were present. In its complexed form, IRB gets fully solvated in the membranes, showing that encapsulation of IRB in HP-β-CD may improve the ADME properties of this drug[1].

In the present work, we have used DSC along with SAXS experiments to study the effects of irbesartan–HP-β-CD in DPPC bilayers containing cholesterol.

Material and methods

Materials: IRB was kindly provided by Prof. M. Koupparis. DPPC and cholesterol were purchased from Avanti Polar Lipids Inc. (Alabaster, AL). HP-β-CD was purchased from Sigma Aldrich (St. Louis, MO).

Preparation of the IRB–HP-β-CD lyophilized complex: A freeze-drying procedure was applied for the preparation of IRB–HP-β-CD lyophilized product. For the preparation of IRB–HP-β-CD aqueous solutions for freeze-drying in a molar ratio of 1:2, the neutralization method was used[2]. More specifically, 0.060 g of irbersartan and 0.408 g of HP-β-CD were accurately weighed, transferred in a 100 mL beaker and suspended with 50 mL of water. Small amounts of ammonium hydroxide were then added under con-

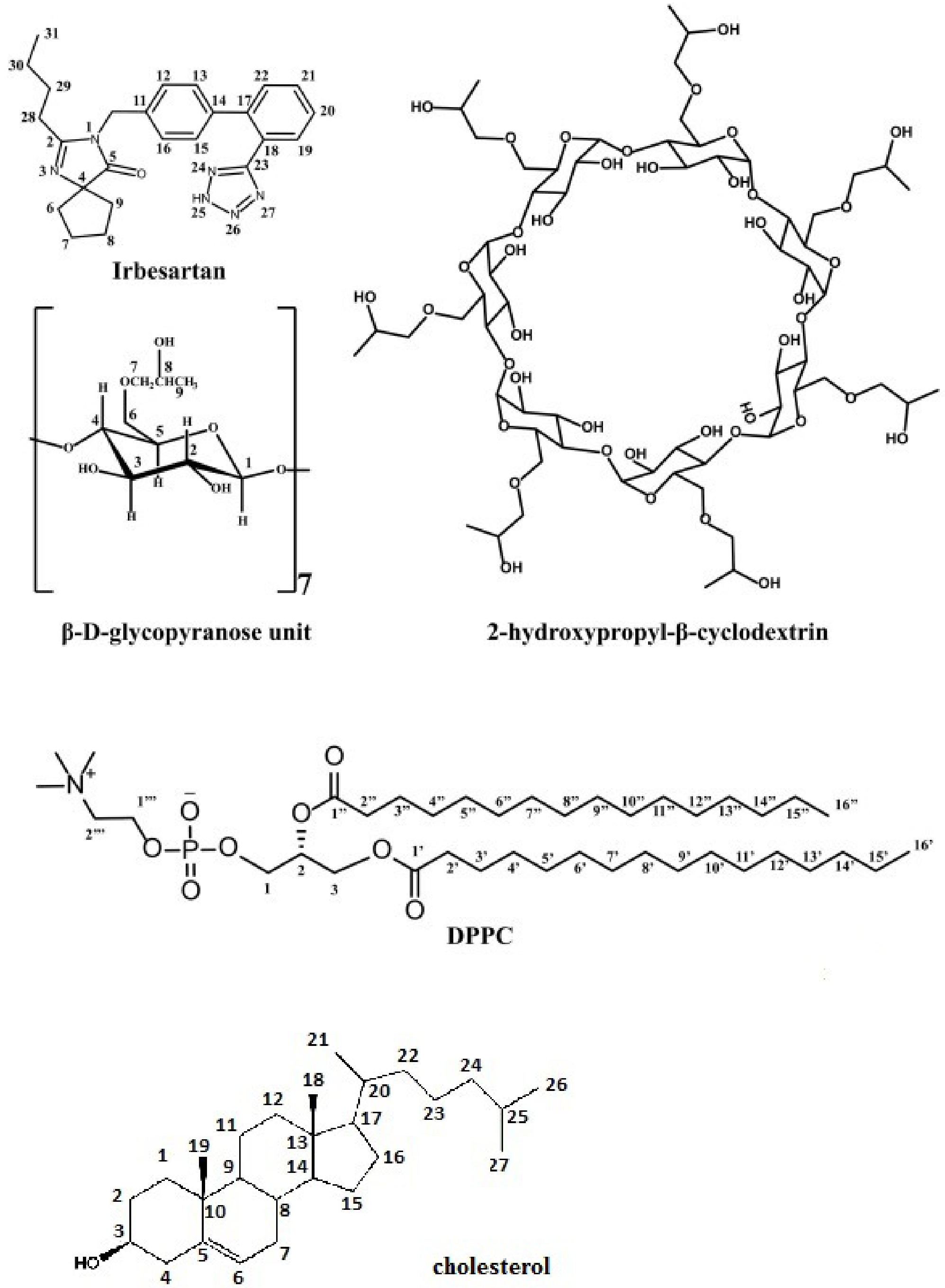

Figure 1: *Structures of irbesartan, 2-hydroxypropyl-β-cyclodextrin, DPPC, and cholesterol.*

Table 1: Predicted lipophilicity values (logP) of sartans.

Drug	Lipophilicity (logP)	Source
Azilsartan	6.03	DrugBank
Azilsartan Medoxomil	6.03	DrugBank
Candesartan	4.79*	J. Med. Chem., *2002, 45 (12), 2615–2623*[6]
Candesartan cilexetil	7.53	DrugBank
Eprosartan	3.9	DrugBank
Eprosartan Mesylate	3.8	DrugBank
Fimasartan	4.21	1. J Clin Pharmacol. 2016;56:576[7] 2. DrugBank
Irbesartan	5.40*	J. Med. Chem., *2002, 45 (12), 2615–2623*[6]
Losartan	3.46*	J. Med. Chem., *2002, 45 (12), 2615–2623*[6]
Olmesartan	5.9	DrugBank
Olmesartan Medoxomil	4.46	DrugBank
Telmisartan	6.66	DrugBank
Valsartan	4.44*	J. Med. Chem., *2002, 45 (12), 2615–2623*

**Values are clogP.*

tinuous stirring and pH monitoring until complete dissolution and pH adjustment to a value between 9 and 10 were obtained. The resulting solution at molar ratio of 1:2 was thereafter frozen at –80 ^{0}C and freeze-dried using a Kryodos-50 model Telstar lyophilizer.

Preparation of liposome mixture: DPPC and IRB stock solutions were prepared by dissolving weighed amounts of dry DPPC or mixture of DPPC/cholesterol (*x*=0.15 or 15 mol%) and IRB–2-HP-β-CD powder in chloroform. The DPPC (or DPPC/cholesterol) complex concentration was *x*=0.2 (20 mol%). DPPC (or DPPC/cholesterol) complex IRB–HP-β-CD were then evaporated at room temperature under a gentle stream of nitrogen and thereafter placed under vacuum for 12 hours in order to form a thin lipid film at the bottom of glass vials. The obtained mixtures were then fully hydrated (50% wt/wt water) in order to achieve multilamellar vesicles (MLVs).

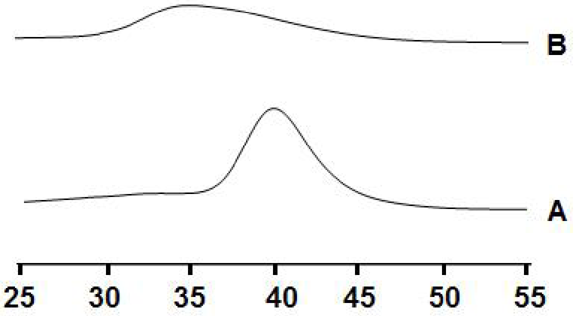

Figure 2: *(A) DPPC bilayers containing the complex [irbesartan/2-HP-β-CD] 80:20, and (B) DPPC:cholesterol bilayers containing the complex [irbesartan/2-HP-β-CD] 80:20.*

Table 2: Enthalpy changes and maxima of the phase transitions observed in the preparations studied.

Samples	**Transition state**	
	ΔH (J/g)	**Tm (ºC)**
DPPC/complex [irbesartan/ 2- HP-β-CD] 80:20	47.67	39.82
[DPPC/cholesterol]/ complex [irbesartan/2-HP-β-CD] 80:20	29.78	34.86

Differential scanning calorimetry: The prepared samples for DSC were transferred to stainless steel capsules obtained from Perkin-Elmer and sealed. Thermal scans were obtained on a TA instrument MDSC Model 2910 (De, USA). All samples were scanned from 10 to 60 °C at least three times until identical thermal scans were obtained using a scanning rate of 2.5 °C/min. The temperature scale of the calorimeter was calibrated using indium (*Tm* = 156.6 °C) and DPPC bilayers (*Tm* = 41.2 °C).

X-ray diffraction experiments: Small angle X-ray scattering (SAXS) measurements were performed with a high flux SAXSess camera (Anton Paar, Graz, Austria) connected to a Debyeflex 3003 X-ray generator (GE-Electric, Germany), operating at 40 kV and 50 mA with a sealed-tube Cu anode. The Goebel-mirror focused and Kratky-slit collimated Xray beam was line shaped (17 mm horizontal dimension at the sample) and scattered radiation was measured in the transmission mode and recorded by a one-dimensional MYTHEN-1k microstrip solid-state detector (Dectris Switzerland), within a q-range (with q being the magnitude of the scattering vector) of 0.01 to 0.5 Å^{-1}. Using Cu Kα radiation of wavelength 1.54 Å and a sample-to-detector

distance of 307 mm, this corresponds to a total 2θ region of 0.14° to 7°, applying the conversion q [A^{-1}] = 4π(sinθ)/λ with 2θ being the scattering angle with respect to the incident beam and λ the wavelength of the X-rays. Samples were filled into a 1 mm (diameter) reusable quartz capillary (wall thickness of 10 μm) with vacuum-tight sealing screw-caps at both ends. All measurements of the samples in the capillary were done in vacuum and at the respective temperatures with an exposure time of 10 min at each temperature step in a heating scan (20 to 50 °C in 5° intervals with 10 min equilibration).

Results and discussion

The DSC scans of DPPC/cholesterol have been extensively analyzed previously[3-5]. In summary, cholesterol caused the abolition of the pretransition temperature even at very low concentrations, a gradual broadening of the phase transition, and a decrease of Δ*H* as its incorporated concentration increased, while it did not affect significantly the *T*m of DPPC bilayers alone.

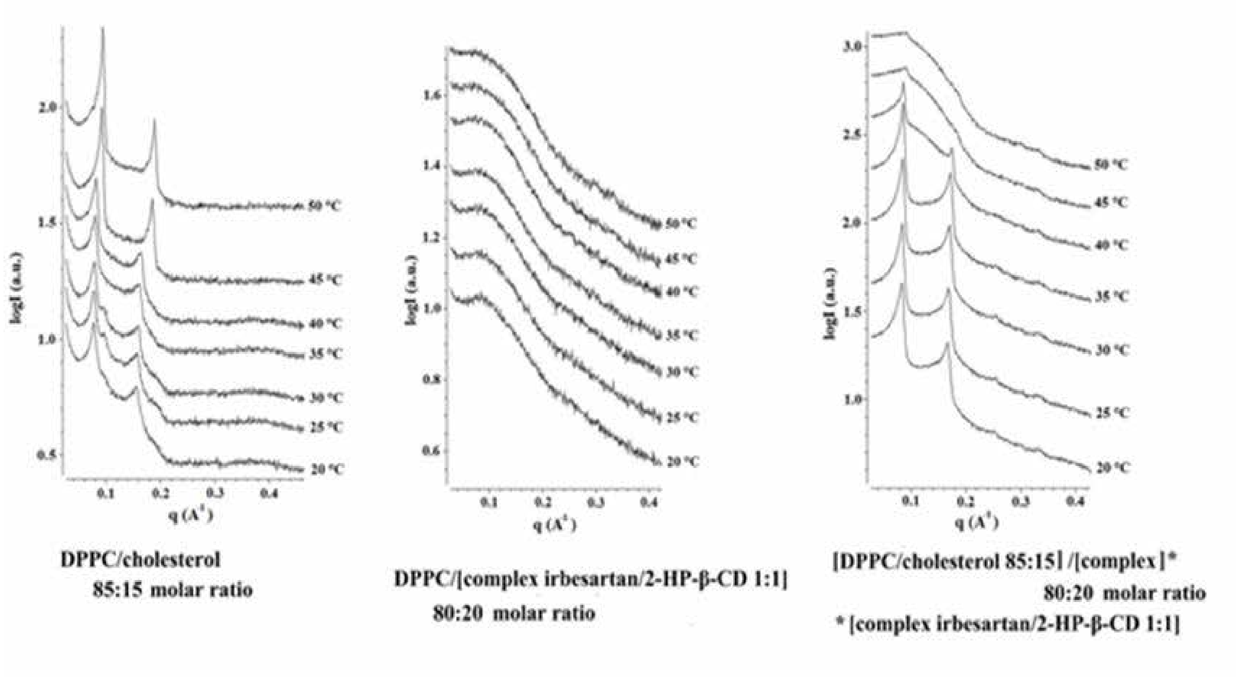

DPPC/cholesterol 85:15 molar ratio

DPPC/[complex irbesartan/2-HP-β-CD 1:1] 80:20 molar ratio

[DPPC/cholesterol 85:15] /[complex]* 80:20 molar ratio
* [complex irbesartan/2-HP-β-CD 1:1]

Figure 3: *SAXS experiments for samples DPPC/cholesterol 85:15 molar ratio (left), DPPC/[irbesartan/2-HP-β-CD 1:1] 80:20 molar ratio (center), and [DPPC/cholesterol 85:15]/[irbesartan/2-HP-β-CD 1:1] 80:20 molar ratio (right).*

This broadening is more effective and a lowering of the *T*m is also observed, signifying that the complex potentiates the perturbation of cholesterol. As shown in **Figure 2** and **Table 2**, the complex alone does not affect significantly the DPPC bilayers as the decrease of *T*m and ΔH is not pronounced.

SAXS experiments show that DPPC: cholesterol samples are characterized by sharp peaks all through the mesomorphic phases (**Figure 3**, left). When the IRB–HP-β-CD complex is added to DPPC bilayers, broad diffraction peaks are apparent in all mesomorphic phases (**Figure 3**, middle). The addition of IRB–HP-β-CD complex in DPPC:cholesterol bilayers resembles that of DPPC: cholesterol x-ray diffraction patterns in the gel phase, but in the liquid crystalline, the peaks become broad and even broader to those of IRB–HP-β-CD complex, in agreement with DSC data (**Figure 3**, right).

Conclusions

When irbesartan is inserted as IRB–HP-β-CD complex in DPPC:cholesterol bilayers, it enhances the effects of cholesterol. This is an intriguing effect and may suggest that a new formulation of irbesartan in such an environment can modify its physicochemical properties and consequently its pharmacological profile in a beneficial matter. ☐

Acknowledgment

This research has been co-financed by the European Union and Greek national funds through the program "Support for Researchers with Emphasis on Young Researchers" (call code: EDBM34) and under the research title: "Preparation and study of innovative forms of administration of pharmaceutical

molecules targeting at improved pharmacological properties".

This work was supported by CERIC funded programme (proposal number 20152002). We are thankful to Prof. H. Iatrou and M. Pitsikalis for providing us the DSC facility and Dr. Manfred Kriechbaum for his help in running the x-ray diffraction experiments.

REFERENCES

1. Liossi A. S., Ntountaniotis D., Kellici T.F., Chatziathanasiadou M.V., Megariotis G., Mania M., Becker-Baldus J., Kriechbaum M., Krajnc A., Christodoulou E., Glaubitz C., Rappolt M., Amenitsch H., Mali G., Theodorou D.N., Valsami G., Pitsikalis M., Iatrou H., Tzakos A., Mavromoustakos T. Exploring the interactions of irbesartan and irbesartan–2-hydroxypropyl-β-cyclodextrin complex with model membranes. *Biochim. Biophys. Acta* 1859, 1089–1098, 2017.
2. Figueiras A., Carvalho R.A., Ribeiro L., Torres-Labandeira J.J., Veiga F.J. Solid-state characterization and dissolution profiles of the inclusion complexes of omeprazole with native and chemically modified beta-cyclodextrin, *Eur. J. Pharm. Biopharm*. 67, 531-539, 2007.
3. Estep T.N, Mountcastle D.B, Biltonen R.L, Thompson T.E. Studies on the anomalous thermotropic behavior of aqueous dispersions of dipalmitoylphosphatidylcholine-cholesterol mixtures. *Biochemistry*, 17, 1984–19893, 1978.
4. Mavromoustakos T., Yang De-Ping, Makriyannis A. Topography of Alphaxalone and Δ16-alphaxalone in Membrane Bilayers containing cholesterol *Biochim. Biophys. Acta* 1194, 69-74, 1994.
5. Kyrikou I., Daliani I., Mavromoustakos T., Maswadeh H., Demetzos, C., Xatziantoniou S., Giatrellis S., Nounesis G. The modulation of thermal and dynamic properties of vinblastine by cholesterol in membrane bilayers *Biochim. Biophys. Acta* 1661, 1-8, 2004.
6. Veber D.F, Johnson S.R. , Cheng, H.-Y., Smith B.R., Ward K.W.,Kopple K.D. Molecular Properties That Influence the Oral Bioavailability of Drug Candidates. J. Med. Chem. 45, 2615-2623, 2002
7. HYPERLINK"https://www.ncbi.nlm.nih.gov/pubmed/?term=Ghim%20JL%5BAuthor%5D&cauthor=true&cauthor_uid=26272450" Ghim J.L., HYPERLINK "https://www.ncbi.nlm.nih.gov/pubmed/?term=Paik%20SH%5BAuthor%5D&cauthor=true&cauthor_uid=26272450" Paik S.H., HYPERLINK "https://www.ncbi.nlm.nih.gov/pubmed/?term=Hasanuzzaman%20M%5BAuthor%5D&cauthor=true&cauthor_uid=26272450" Hasanuzzaman M., HYPERLINK "https://www.ncbi.nlm.nih.gov/pubmed/?term=Chi%20YH%5BAuthor%5D&cauthor=true&cauthor_uid=26272450" Chi Y,H., HYPERLINK "https://www.ncbi.nlm.nih.gov/pubmed/?term=Choi%20HK%5BAuthor%5D&cauthor=true&cauthor_uid=26272450" Choi H.K., HYPERLINK "https://www.ncbi.nlm.nih.gov/pubmed/?term=Kim%20DH%5BAuthor%5D&cauthor=true&cauthor_uid=26272450" Kim D.H., HYPERLINK "https://www.ncbi.nlm.nih.gov/pubmed/?term=Shin%20JG%5BAuthor%5D&cauthor=true&cauthor_uid=26272450" Shin J.G. Absolute bioavailability and pharmacokinetics of the angiotensin II receptor antagonist fimasartan in healthy subjects. J. Clin. Pharmacol. 56,576-80, 2016 .

Comparative Study of the Thermal Effects of Drugs Acting on the RAS System

Dimitrios Ntountaniotis[1], Georgios Leonis[1], Eirini Christodoulou[2], Thomas Mavromoustakos[1*]

[1]National and Kapodistrian University of Athens, Department of Chemistry, Panepistimiopolis Zografou 15771, Athens, Greece.

[2]National and Kapodistrian University of Athens, Department of Pharmacy, Panepistimiopolis Zografou, 15771, Athens, Greece.

KEYWORDS: aliskiren, captopril, candesartan cilexetil, DPPC bilayers, Differential Scanning Calorimetry.

***Corresponding author:** Thomas Mavromoustakos, National and Kapodistrian University of Athens, Department of Chemistry, Athens, Greece;
email: tmavrom@chem.uoa.gr

Introduction

For many years, we investigate the interactions of AT1 antagonists in lipid bilayers as the latter play an important role in drugs mode of action[1-2].

Here, we compare the thermal effects of drugs acting on the RAS system (renin inhibitor aliskiren, ACE inhibitor captopril, and AT1 antagonist candesartan cilexetil) in lipid bilayers to study their similarities and differences in their perturbing effects. The lipophilicity profile of selected molecules (**Figure 1**) to be studied is shown in **Table 1**.

Materials and Methods

Materials: Dipalmitoyl-phosphatidylcholine (DPPC) was purchased from Avanti Polar Lipids (Birmingham, AL) and was used without further purification. Candesartan cilexetil (TCV-116) was kindly provided by Medochemie Hellas A.E. (Pharma Cypria). Captopril was

Table 1. Lipophilicity profile of selected drugs (logP).

Drug	Lipophilicity value
Aliskiren	3.9[1]
Candesartan	4.8[2,3]
Candesartan cilexetil	7.5[1]
Captopril	1.0[1]
Enalapril	0.6[1]
Eprosartan Mesylate	3.8[1]
Irbesartan	5.4[2,3]
Lisinopril	–1.2[1]
Losartan	3.5[1,3]
Olmesartan	5.9[1]
Telmisartan	6.7[1]
Valsartan	4.4[2,3]

Predicted values from
[1]DrugBank, [2]J. Med. Chem., 45, 2615–2623, 2002.[11]
[3]Values are clogP.

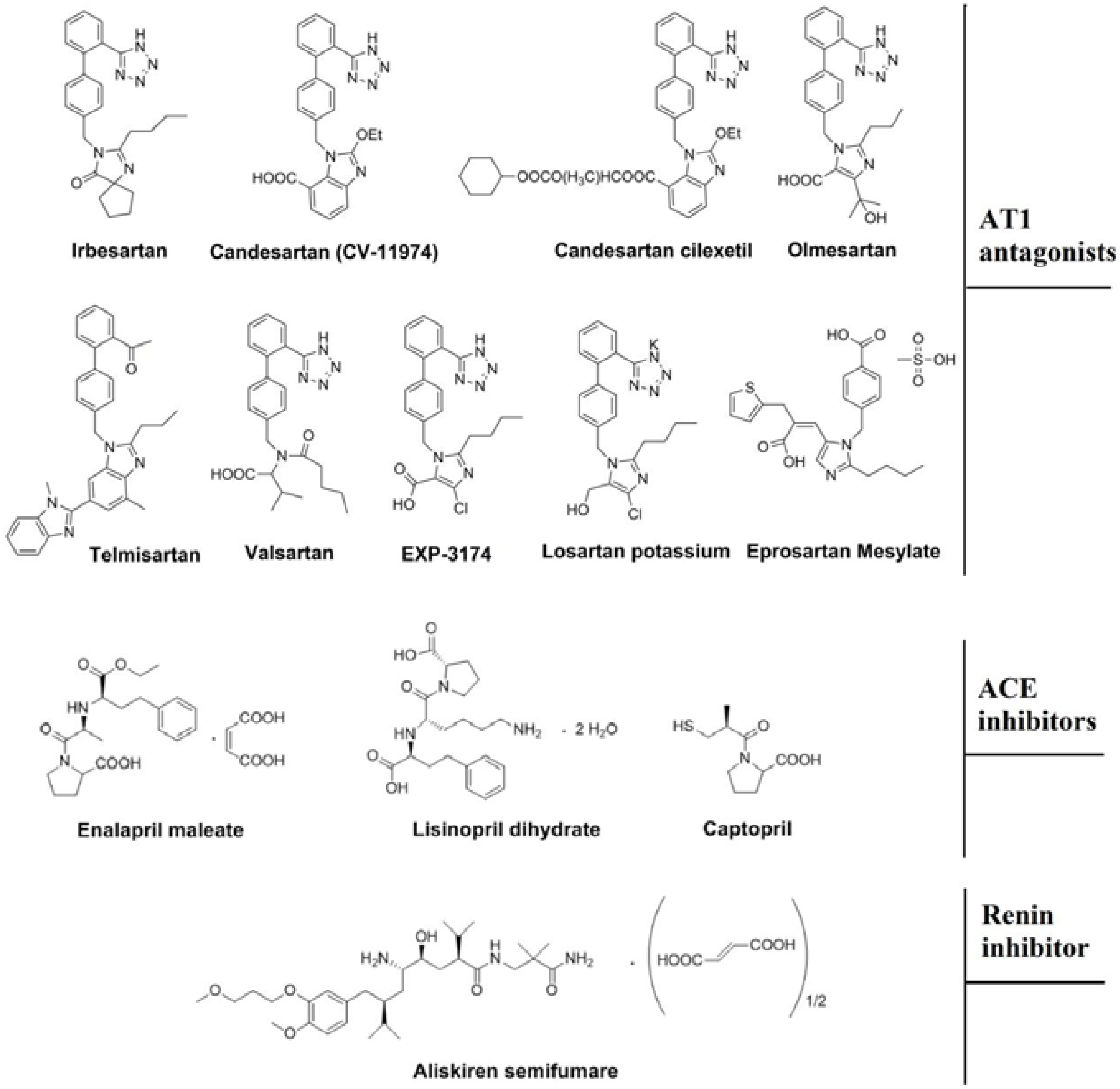

Figure 1. *Drugs acting on the RAS system.*

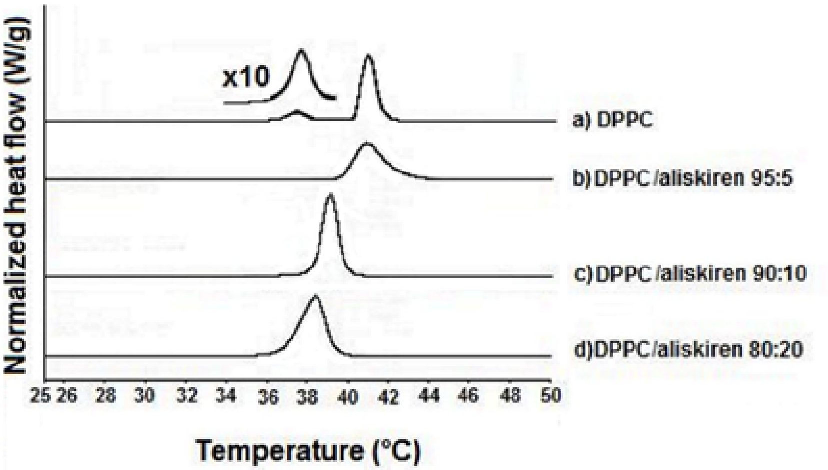

Figure 2. *Thermal effects of aliskiren at x=0.05, 0.10 and 0.20 on DPPC bilayers.*

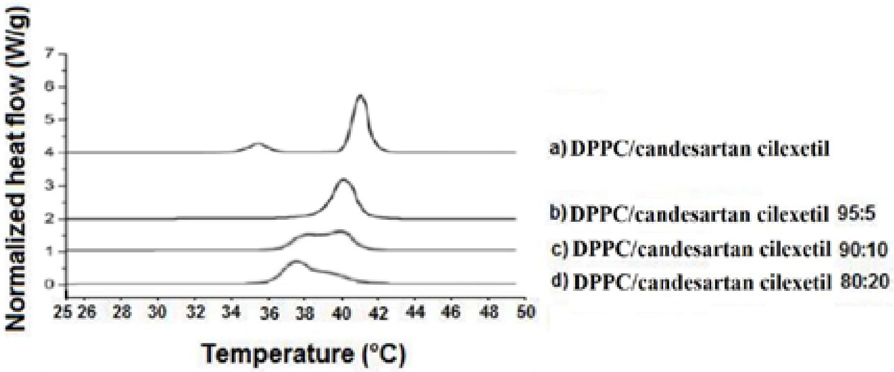

Figure 3. *Thermal effects of candesartan cilexitil at x=0.05, 0.10 and 0.20 on DPPC bilayers.*

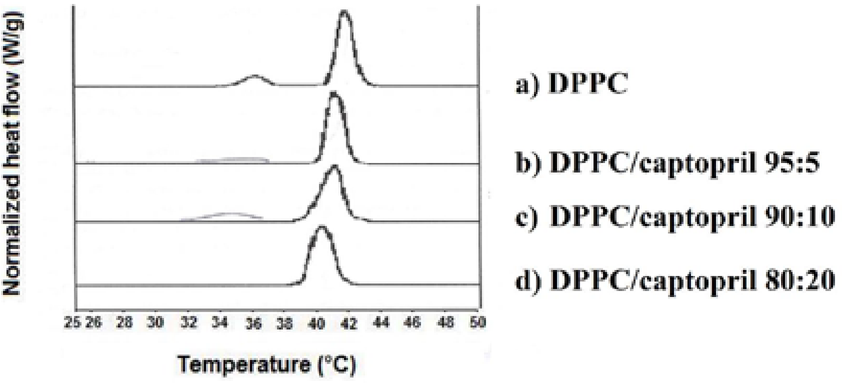

Figure 4. *Thermal effects of captopril at x=0.05, 0.10 and 0.20 at DPPC bilayers.*

Table 2. DSC results for aliskiren, captopril and candesartan cilexetil in DPPC bilayers.

Samples	T_{pre}	$\Delta T_{1/2pre}$	ΔH_{pre} (kcal/mol)	Tm (°C)	ΔTm1/2 (°C)	ΔH_m (kcal/mol)
DPPC	35.50	1.0	1.20	41.20	1.0	7.89
DPPC/aliskiren 95:5	-	-	-	41.04	1.6	7.87
DPPC/aliskiren 90:10	-	-	-	39.19	0.9	*9.47*
DPPC/aliskiren 80:20	-	-	-	38.45	1.5	10.45
DPPC/captopril 95:5	30.09	3.5	0.34	40.39	1.3	7.91
DPPC/captopril 90:10	28.20	2.8	0.16	40.31	1.6	8.23
DPPC/captopril 80:20	-	-	-	39.30	1.7	8.37
DPPC/cand. cilexetil 95:5	-	-	-	40.1	1.3	8.61
DPPC/cand. cilexetil 90:10	-	-	-	38.3 40.1	1.6 1.3	4.53, 4.4 (8.97)
DPPC/cand. cilexetil 80:20	-	-	-	37.5 39.2	1.3	5.44, 4.53 (8.97)

kindly offered by ELPEN A.E. (Greece) and aliskiren by Novartis. Spectroscopic grade $CHCl_3$ was obtained from Sigma Aldrich (St. Louis, MO).

Differential Scanning Calorimetry: For DSC experiments, portions of *ca*. 5 mg from 50% (w/w) liposomal dispersions were used. The drug concentrations used were x=0.005 (5% mol), x=0.10 (10% mol) and x=0.20 (20% mol). The samples were transferred to a Perkin-Elmer DSC-7 instrument (Norwalk, CT). All samples were scanned from 10 to 60 °C at least three times until identical thermal scans were obtained using a scanning rate of 2.5 °C/min. The following diagnostic parameters were used for the study of drug–membrane interactions: *T*m (maximum position of the recorded heat capacity), $\Delta T_{m1/2}$ (the full width at half maximum of the phase transition) and the enthalpy change, Δ*H*.

Results and Discussion

The thermal changes in pure DPPC/water and the influence of aliskiren are shown in **Figure 2, Table 2**. In pure DPPC (**Figure 2**, top curve), two characteristic endothermic peaks are visible referring to the pre- and the main transition, respectively. The DPPC molecules form the well-organized lamellar gel phase, $L_{\beta'}$, below the pretransition, while the fluid lamellar phase, L_a is apparent above the main transition temperature. An intermediate phase, $P_{\beta'}$, is also observed, in which the bilayers are modulated by a periodic ripple (ripple phase). The recorded transition temperatures and enthalpy values are in agreement with literature values[3].

Aliskiren at a low concentration of x=0.05 broadens the main phase transition and abolishes the pretransition without significantly affecting the maximum of the phase transition temperature and ΔH. At higher concentrations, it lowers the main phase transition and causes an increase in ΔH.

Such an increase of ΔH at the same concentration has been observed for the AT1 antagonists losartan, irbesartan, EXP3174, valsartan and candesartan cilexetil, but not for candesartan and telmisartan. In addition, this progressive broadening of the phase transition and abolishment was more eminent to losartan, irbesartan, EXP3174, valsartan and candesartan cilexetil (**Figure 3**), but not for candesartan and telmisartan[4-10].

The ACE inhibitor captopril is also found to progressively broaden the phase transition temperature, to abolish the pretransition at high concentration, and to cause an increase of ΔH (**Figure 4, Table 2**).

Conclusions

Evidently, the three classes of molecules appear to act similarly regarding their thermal effects on lipid bilayers. This is an interesting result, which suggests that possibly all these drugs function with similar modes on membrane bilayers. □

Acknowledgment

This research has been co-financed by the European Union and Greek national funds through the program "Support for Researchers with Emphasis on Young Researchers" (call code: EDBM34) and under the research title: "Preparation and study of innovative forms of administration of pharmaceutical molecules targeting at improved pharmacological properties". We are thankful to Emeritus Professor K. Vyras and G. Roumelioti for performing part of DSC experiments on DPPC:captopril samples.

REFERENCES

1. Kellici T.F., Tzakos A.G., Mavromoustakos T. Rational Design and Synthesis of Molecules Targeting the Angiotensin II Type 1 and Type 2 Receptors. *Molecules,* 20, 3868-3897, 2015.
2. Kellici T.F., Liapakis G., Tzakos A.G., Mavromoustakos T. Pharmaceutical compositions for antihypertensive treatments: a patent review. *Expert Opin. Ther. Patents* 25, 1-12, 2015.
3. Koynova R., Caffrey M. Phases and phase transitions of the phosphatidylcholines, *Biochim. Biophys. Acta* 1376, 91–145, 1998.
4. Ntountaniotis D., Mali G., Grdadolnik S. G., Halabalaki M., Skaltsounis A.L., Potamitis C., Siapi E., Chatzigeorgiou P., Rappolt M., Mavromoustakos T.. Thermal, dynamic and structural properties of drug AT1 antagonist olmesartan in lipid bilayers. *Biochim. Biophys. Acta,* 1808, 2995-3006, 2011.
5. Hodzic A., Zoumpoulakis P., Pabst G., Mavromoustakos T., Rappolt M. Losartan's affinity to fluid bilayers couples to lipid/cholesterol interactions. *Phys. Chem. Chem. Phys.* 14, 4780-4788, 2012.
6. Fotakis C., Megariotis G., Christodouleas D., Kritsi E., Zervou M., Zoumpoulakis P., Ntountaniotis D., Potamitis C., Hodzic A., Pabst G., Rappolt M., Mali G., Baldus J., Glaubitz C., Papadopoulos M. G., Afantitis A., Melagraki G., Mavromoustakos.T. Comparative study of the AT1 receptor prodrug antagonist candesartan cilexetil with other sartans on the interactions with membrane bilayers. *Biochim. Biophys. Acta* 1818, 3107-3120, 2012.

7. Aggelis G., Resvani A., Ntountaniotis D., Chatzigeorgiou P., Koukoulitsa C., Matsoukas J., Čendak T., Codec U., Mali G., Mavromoustakos T. Interactions of the potent synthetic AT1 antagonist analog BV6 with membrane bilayers and mesoporous silicate matrices. *Biochim. Biophys. Acta*, 1828, 1846-1855, 2013.

8. Ntountaniotis D., Kellici T., Tzakos A., Kolokotroni P., Tselios T., Becker-Baldus J., Glaubitz C., Lin S., Makriyannis A., Mavromoustakos T. The application of solid state NMR spectroscopy to study Candesartan Cilexetil (TCV-116) membrane interactions. Comparative study with the AT1 antagonist drug olmesartan. *Biochim. Biophys. Acta*, 1838, 2439-2450, 2014.

9. Sadeghpour A., Rappolt M., Ntountaniotis D., Chatzigeorgiou P., Viras K., Megariotis G., Papadopoulos M., Siapi E., Mali G., Mavromoustakos T. Comparative Study of Interactions of Aliskiren and AT1 Receptor Antagonists with Lipid Bilayers. *Biochim. Biophys. Acta* 1848, 984-994, 2015.

10. Liossi A. S., Ntountaniotis D., Kellici T.F., Chatziathanasiadou M.V., Megariotis G., Mania M., Becker-Baldus J., Kriechbaum M., Krajnc A., Christodoulou E., Glaubitz C., Rappolt M., Amenitsch H., Mali G., Theodorou D.N., Valsami G., Pitsikalis M., Iatrou H., Tzakos A., Mavromoustakos T. Exploring the interactions of irbesartan and irbesartan–2-hydroxypropyl-β-cyclodextrin complex with model membranes. *Biochim. Biophys. Acta* 1859, 1089–1098, 2017.

11. Veber D.F, Johnson S.R. , Cheng, H.-Y., Smith B.R., Ward K.W., Kopple K.D. Molecular Properties That Influence the Oral Bioavailability of Drug Candidates. J. Med. Chem. 45, 2615-2623, 2002.

www.hsmc.gr/en/pharmakeftiki-journal/

DSC: A valuable tool to study drug:membrane interactions

Thomas M. Mavromoustakos

Kapodistrian University of Athens, Chemistry Department, Laboratory of Organic Chemistry, Panepistimiopolis Zografou 11571

KEYWORDS: Differential Scanning Calorimetry; Lipid Bilayers; Bioactive drugs; Membranes; Phospholipids;

Corresponding author: Thomas Mavromoustakos, National and Kapodistrian University of Athens, Department of Chemistry, Athens, Greece; email:tmavrom@chem.uoa.gr

1. Introduction

DSC is a thermodynamic technique suitable for studying the effects of drugs on the phase transitions of membrane bilayers The technique, as its name signifies is based on the differential heat flow between a sample that undergoes a phase transition in the temperature range under study and an inert reference material that lacks such a phase transition in the same temperature range. When a phase transition occurs, the sample undergoes a thermally-induced event. The following parameters in an endothermic or exothermic event are recorded during the phase transition: (a) *Tm* (maximum of the peak) (b) *Tonset* (the starting temperature of the phase transition); (c) $T_{m1/2}$ (the half-height width of the phase transition); (d) the area under the peak which represents the enthalpy change during the transition *(DH)*.

Due to the high complexity of the biological membranes and their instability, the study of their phase transitions is not an easy task. Therefore, lipids and especially phospholipid bilayers which share many of the conformational and dynamic properties of the natural membranes are used as a model membranes.

In this plenary lecture, examples of the effects of bioactive molecules with lipid bilayers will be given and the complementarity information of various other techniques will be mentioned.

2. Materials and Methods

Materials: Lα-dipalmitoyl - phosphatidylcholine (Lα-DPPC, 99+%) was purchased from Avanti Polar Lipid Inc. and $CHCl_3$ from Sigma Aldrich. Valsartan was kindly donated by Novartis.

Methods: Appropriate amounts of DPPC and valsartan were diluted in chloroform and were mixed, dried under a stream of N_2 and then stored under vacuum overnight. After dispersing in water (50% w/w), ca. 5 mg were sealed in stainless steel capsules obtained from Perking-Elmer. The drug concentrations used were x=0.01, x=0.02, x=0.05, x=0.10 and x=0.20.

3. Results and Discussion

Figure 1 shows the calorimetric scan of La dipalmitoyl phosphatidylcholine multilamellar vesicles in the absence and presence of valsartan. These bilayers have been studied extensively since they show two endothermic transitions, a broad low enthalpy pretransition (*Tm*=35.3 °C) and a main phase transition (Tm=41.2 °C). Below the pretransition the phospholipid molecules are arranged in a one-dimensional lamellar gel

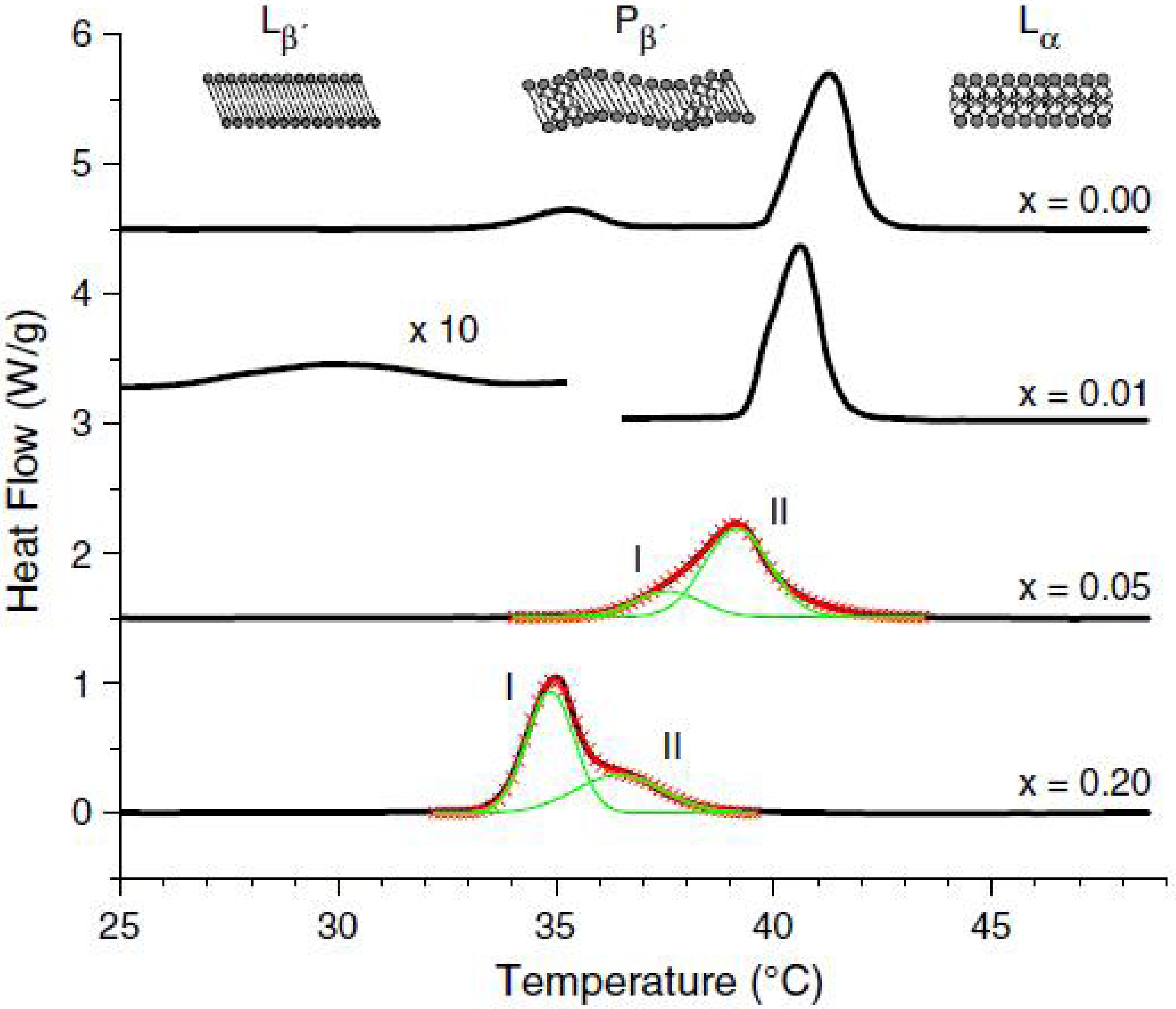

***Figure 1**. DSC scan for DPPC bilayers alone and ascending concentrations of valsartan.*

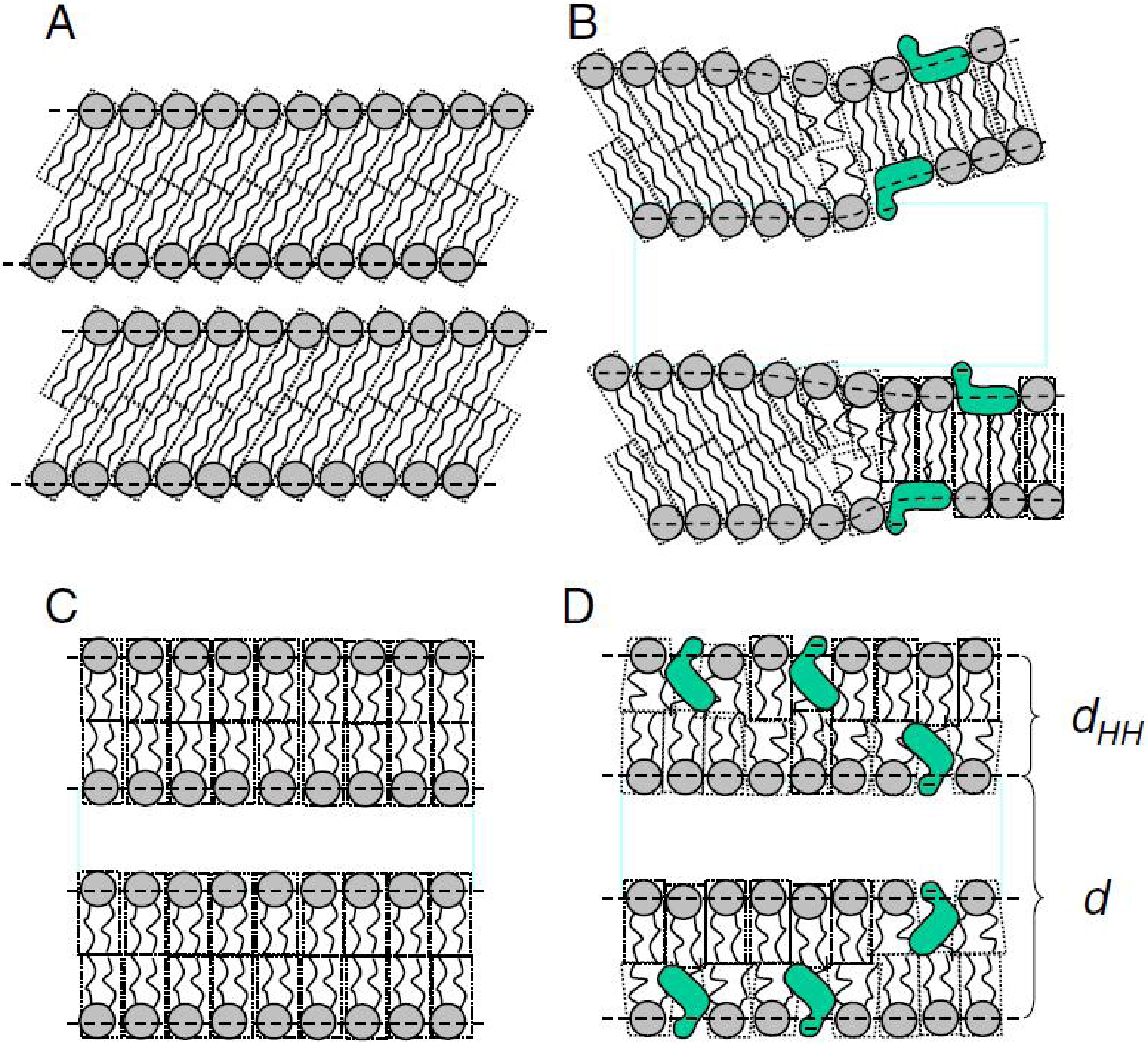

***Figure** 2. Proposed perturbations induced by valsartan when it is incorporated in lipid bilayers. A and C Figures show DPPC bilayers at gel and liquid crystalline phases. B shows the effect of valsartan (20% mol) in the gel phase and D in the liquid crystalline phase. In the gel phase valsartan induces the formation of valsartan rich-domains with chain interdigition ($L_{\beta I}$), This partial interdigitation is also evident in the liquid crystalline phase as depicted by the decrease of the thickness of lipid bilayers[4].*

phase (L_b'), while above the main transition they exist in the liquid crystalline phase (L_a'). At temperatures between the ripple phase (P_b')[1] and main phase transition (La) based on solid-state NMR evidence, the bilayers are composed of coexisting gel and liquid crystalline components.

Below pretransition temperature, the chains are in all-trans conformation[2] and are tilted with respect to membrane normal about 32°[3]. Above the phase transition a trans:gauche isomerization is evident. At only 1 mol% of valsartan, the pretransition is almost suppressed, the enthalpy is lowered by a factor of three and the transition width spans over 7-8 °C. This illustrates the interface activity of the drug molecule. Increased of drug concentration leads to the decrease of the phase transition monotically. From the 5-20% valsartan concentration there is a splitting of the main phase transition into two components (**Table 1**). The total enthalpy increased quite significantly from 7.5 to 9.8 kcal/mol for 1-20 mol%. This enthalpy change as it is confirmed by x-ray diffraction data and Raman spectroscopy is due to the induce of a partial interdigitation of the alkyl chains.

The mechanism of action of valsartan on membrane bilayers in gel and liquid crystalline phase base on a combination o biophysical results is shown in **Figure 2**.

Conclusions

Valsartan is hypothesized that exerts its action probably through the lipid bilayers. DSC in combination with x-ray diffraction and Raman spectroscopy defined its topographical position and its effects on lipid bilayers. It is evident from this study that valsartan is possible to perturb lipid bilayers inducing partial interdigitation. This is not a common feature for the rest seven AT1 commercially available antagonists. This indicates that partial interdigitation is based on subtle structural features. ☐

REFERENCES

1. Koyonova R., Caffery M. Phases and phase transitions of the phosphatidylcholines. *Biochim. Biophys. Acta* 1376, 91-145, 1998.
2. Albon N., Sturtevant J.M. Nature of the gel to liquid crystal transition of synthetic phosphatidylcholines. *Proc. Natl. Acad. Sci. USA*, 75,2258,2260, 1978.
3. Tristan-Nagle S., Zhang R., Suter R.M., Worthington C.R., Sun W.J., Nagle J.F. Measurement of chain tilt angle in fully hydrated bilayers of gel phase lecithins. *Biophys. J.* 64, 1097-1109, 1993.
4. Potamitis C., Zervou M., Katsiaras V., Zoumpoulakis P., Durdagi S., Papadopoulos M., Hayes J., Grdadolnik S., Kyrikou I., Argyropoulos D., Vatougia G., Mavromoustakos T.. Antihypertensive Drug Valsartan in solution and at the AT_1 Receptor: Conformational Analysis, Dynamic NMR Spectroscopy, in silico Docking and Molecular Dynamics Simulations. *J. Chem. Inf. Mod.* 49, 726-739, 2009.

ΕΡΕΥΝΗΤΙΚΗ ΕΡΓΑΣΙΑ

RESEARCH ARTICLE

Kinetic study of the thermodynamic behavior of lipid bilayers in the presence of aminoadamantane drugs

Maria Chountoulesi[1] Athina Konstantinidi[2], Nikolaos Naziris[1] Dimitris Kolokouris[2], Antonios Kolocouris[2*], Costas Demetzos[1*], Thomas Mavromoustakos[3*]

[1]Section of Pharmaceutical Technology, Department of Pharmacy, School of Health Sciences, National and Kapodistrian University of Athens, Panepistimioupolis Zografou, 15771 Athens, Greece

[2]Section of Medicinal Chemistry, Department of Pharmacy, School of Health Sciences, National and Kapodistrian University of Athens, Panepistimioupolis Zografou, 15771 Athens, Greece

[3]Laboratory of Organic Chemistry, Department of Chemistry, School of Natural Sciences, Kapodistrian University of Athens, Panepistimioupolis Zografou, 15771, Athens. Greece

KEYWORDS: Biomembranes; Amantadine; Thermodynamics; Kinetics

***Corresponding Authors:**
Antonios Kolocouris, ankol@pharm.uoa.gr,
Costas Demetzos, demetzos@pharm.uoa.gr,
Thomas Mavromoustakos, tmavrom@chem.uoa.gr

Introduction

Differential scanning calorimetry (DSC) has been proven to be a very useful and fast technique towards the revealing of interactions between drug molecules and lipid biomembranes[1].

The scope of the present study is to assess the interactions of two congener amphiphilic drug molecules, namely amantadine and its synthetic analog spiro[pyrrolidine-2,2′-adamantane] compound (AK13), with 1,2-dimyristoyl-*sn*-glycero-3-phosphocholine (DMPC) model membranes.

Apart from the calorimetric profile of the systems, we attempted to evaluate their thermodynamic properties upon time and monitor their kinetic mode.

Material and Methods

The amantadine drug (Amt) (Merck Schuchardt OHG – Hohenbrunn) and its synthetic analog AK13 (synthesized in the lab of Prof. A. Kolocouris) were mixed with DMPC phospholipid (Avanti Polar Lipids, Inc.) at four drug molar concentrations (5, 8, 20 and 50%) and dissolved in methanol that was evaporated at room temperature under a gentle flow of argon. Subsequently, the samples were placed under vacuum for 24 hours in order to form a thin lipid film. The prepared samples were fully hydrated with phosphate buffer saline (PBS). Samples were hydrated immediately after preparation (indicated as "new"), as well as two weeks later (indicated as "old") and were subjected to DSC scans. Moreover, the DSC measurements of all the samples were repeated after 15 days. An 822e Mettler-Toledo instrument (Schwerzenbach, Switzerland) was used, while all thermal ($T_{onset,m}$, T_m) and thermodynamic (ΔHm) parameters were calculated with the Mettler-Toledo STARe software.

Results and Discussion

Starting from the pure DMPC bilayers (**Figure 1**),

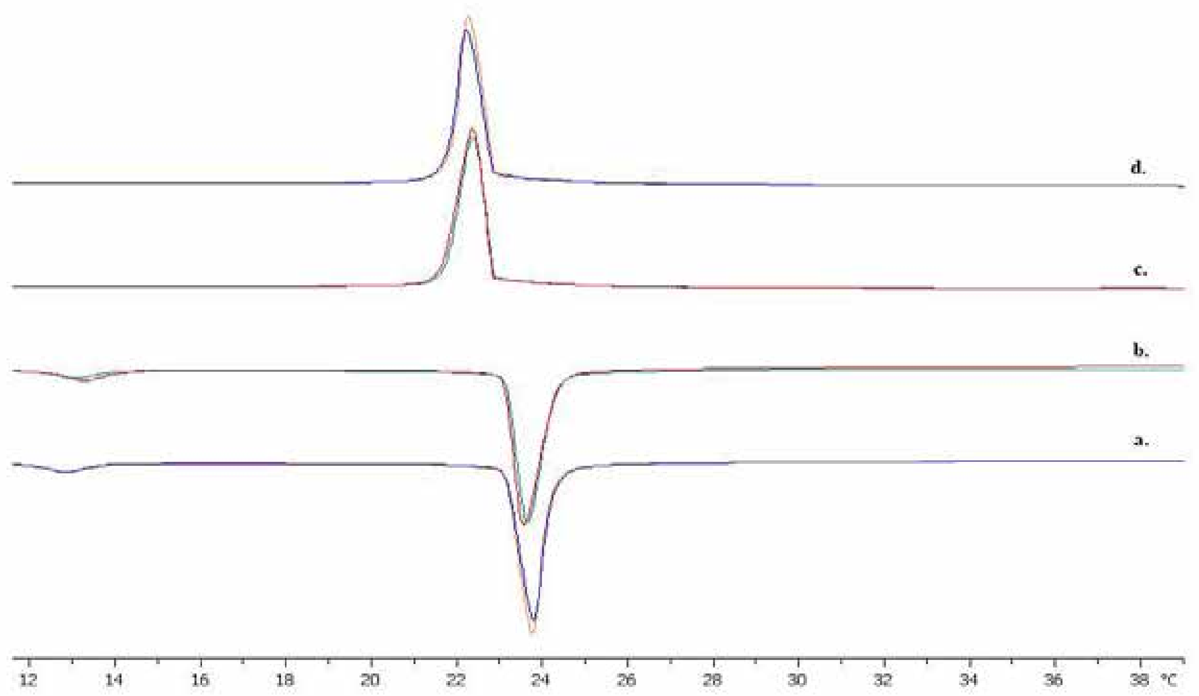

Figure 1: *Thermodynamic stability after 15 days during heating of (a) old DMPC bilayers; (b) new DMPC bilayers; during cooling of (c) new DMPC bilayers; and d) old DMPC bilayers. The DSC measurements were repeated twice.*

some differences between the old and the new samples were observed. This observation implies that the preparation protocol can influence significantly the thermal properties of a sample.

Referred to the DMPC bilayers that were incorporated with the two lipophilic drug molecules, it can be assumed that both molecules affected significantly the calorimetric parameters of the main transition of DMPC bilayers (**Table 1**), while they also caused abolishment of the pretransition, reflecting alterations of the membrane organization[2,3]. The curves of **Figures 2** and **3** suggested a strict dependence of the thermodynamic behavior on the drug concentration.

Moreover, many differences appeared between the old and new samples (**Figure 2**), highlighting that the long interval between sample preparation and hydration affected the thermal behavior. Finally, the changes observed upon the time reflected some kinetic instability of the thermodynamic behavior of all the studied samples, especially for AK13. More specifically, the drug topography, orientation and the formation of various domains depicted in the scans with complex peaks and using high concentrations are very sensitive to the drug preparation and sample equilibration conditions.

Conclusions

This study showed that DSC thermodynamic technique is very sensitive to the sample equilibration conditions. Distinct scans are observed with DMPC

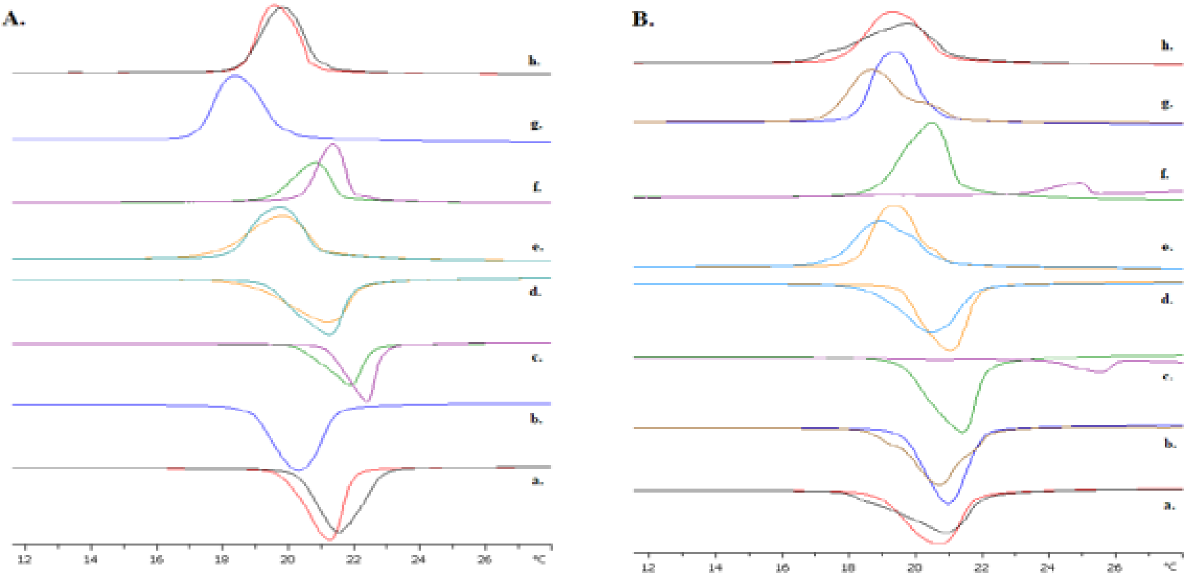

Figure 2: *Thermodynamic stability after 15 days of heating and cooling A) a+h) DMPC:Amt 5% old, b+g) DMPC:Amt 5% new, c+f) DMPC:AK13 5% old, d+e) DMPC:AK13 5% new and B) a+h) DMPC:Amt 8% old, b+g) DMPC:Amt 8% new, c+f) DMPC:AK13 8% old, d+e) DMPC:AK13 8% new. The DSC measurements were repeated twice.*

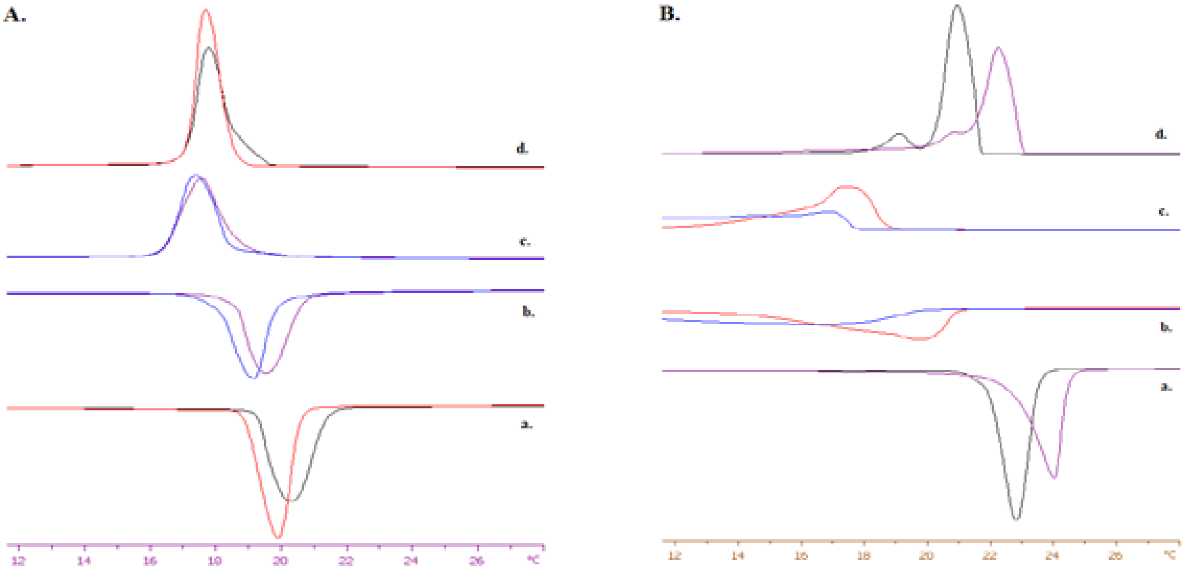

Figure 3: *Thermodynamic stability after 15 days of A) a+d) DMPC:Amt 20%, b+c) DMPC:AK13 20% and B) a+d) DMPC:Amt 50%, b+c) DMPC:AK13 50%. The DSC measurements were repeated twice.*

bilayers containing amantadine or AK13 at different concentrations using different preparation protocols. The consequences of these observations are significant. Kinetic instability modifies the thermodynamic parameters and thermal scans. Thermal scans reflect the topographical position and orientation of drugs incorporated in membrane bilayers. As thermal scans are modified according to protocol preparation is inferred that topographical position and orientation of the drug embedded in lipid bilayers are also modified. ☐

Table 1. Calorimetric profiles of DSC runs and reruns of bilayers (heating cycle).

Sample	Day	Drug Molar%	$T_{onset,m}$ (°C)	T_m (°C)	$\Delta T_{1/2,m}$ (°C)	ΔH_m ($J\ g^{-1}$)
DMPC:Amt	1	5 old	20.21	21.40	1.54	41.23
DMPC:Amt	15	5 old	19.88	21.13	1.21	43.22
DMPC:AK13	1	8 old	19.51	21.36	1.57	*50.34*
DMPC:AK13	15	8 old	23.72	25.57	1.33	24.02
DMPC:AK13	1	8 new	19.48	20.90	1.48	38.35
DMPC:AK13	15	8 new	18.92	20.29	1.82	39.60
DMPC:Amt	1	20	19.20	20.12	1.38	46.97
DMPC:Amt	15	20	18.82	19.69	1.01	48.45
DMPC:AK13	1	20	18.53	19.40	1.34	41.59
DMPC:AK13	15	20	17.98	19.02	1.10	41.50
DMPC:Amt	1	50	21.89	22.60	0.92	52.74
DMPC:Amt	15	50	22.70	23.88	0.96	43.80
DMPC:AK13	1	50	16.27	19.69	3.93	41.98
DMPC:AK13	15	50	10.63	16.67	6.53	26.30

REFERENCES

1. Naziris N., Pippa N., Pispas S., Demetzos C. (2017) The Thermal Analysis of Liposomal Formulations as an Element to Evaluate their Effectiveness as Drug and Vaccine Delivery Systems, In: Pearson, B.R. ed. *Liposomes: Historical, Clinical and Molecular Perspectives*. New York, Nova Science Publishers, vol. 1, p.p. 265-318.
2. Koynova R., Caffrey M. Phases and phase transitions of the phosphatidylcholines. *Biochim. Biophys. Acta*. 1376, 91-145, 1998.
3. Matsingou C., Hatziantoniou S., Georgopoulos A., Dimas K., Terzis A., Demetzos C. Labdane-type diterpenes: thermal effects on phospholipid bilayers, incorporation into liposomes and biological activity. *Chem. Phys. Lipids*, 138, 1-11, 2005.

ZITA MEDICAL MANAGEMENT

www.hsmc.gr/en/pharmakeftiki-journal/

ΕΡΕΥΝΗΤΙΚΗ ΕΡΓΑΣΙΑ

RESEARCH ARTICLE

Linear Thermodynamic Behavior in Complex Chimeric Nanosystems[#]

Nikolaos Naziris[1], Athanasios Skandalis[2], Stergios Pispas[2], Costas Demetzos[1,*]

[1]*Section of Pharmaceutical Technology, Department of Pharmacy, School of Health Sciences, National and Kapodistrian University of Athens, Panepistimioupolis Zografou 15771, Athens, Greece*

[2]*Theoretical and Physical Chemistry Institute, National Hellenic Research Foundation, Vassileos Constantinou Avenue 11635, Athens, Greece*

[#]The paper has received the 1st award in the Conference Therma2018, Athens 12-13 October 2018

KEYWORDS: Chimeric lyotropic nanosystems; Complexity; Information/entropy balance; Linearity; Biofunctionality

***Corresponding Authors:** Costas Demetzos, demetzos@pharm.uoa.gr

Introduction

Complexity and variability of bio-systems are encoded elements of natural processes that govern their functionality and adaptability. Drug delivery nanosystems that are characterized as biomimetics should be designed following the natural concept of complexity and variability[1]. Initial conditions, including biomaterial concentration in lyotropic biosystems and their dynamics, give birth to complexity, which in turn leads to non-linearity and stochasticity. Non-linearity itself is the cause of chaos and self-organization/assembly, the most typical example being the cell membrane and its artificial models, *e.g.* liposomes. Morphogenesis of deviant structures has been repeatedly linked to concentration and molar ratio of molecules in a binary or of higher complexity nanosystem[2]. Herein, we attempt to evaluate the observed linear thermodynamic behavior in certain ranges of thermoresponsive chimeric biomimetic lyotropic self-assembled nanosystems, which could be utilized to predict the biofunctionality of drug delivery nanosystems. A similar approach has been proposed in a previous study, regarding pH-responsive chimeric nanosystems[3].

Materials and Methods

The saturated phospholipid 1,2-dipalmitoyl-sn-glycero-3-phosphocholine (DPPC) was purchased from Avanti Polar Lipids Inc. (Alabaster, AL, USA) (**Figure 1A**). The thermoresponsive ampliphilic diblock copolymers poly(N-isopropylacrylamide)-b-poly(lauryl acrylate) (PNIPAM-b-PLA) 1/2 (66-34/50-50 molar compositions and 18,000/6,500 molecular weights) were synthesized through RAFT polymerization (**Figure 1B**). Pure lipid and chimeric bilayers were prepared by mixing the appropriate amounts of DPPC:PNIPAM-b-PLMA 1/2 (9:0.02, 9:0.05, 9:0.1, 9:0.2, 9:0.5 and 9:1 molar ratios) in chloroform solutions and subsequently evaporating the solvents. Those were fully hydrated with phosphate buffer saline (PBS, pH = 7.4) and subjected to differential scanning calorimetry (DSC), by utilization of a DSC822^e Mettler-Toledo (Schwerzenbach, Switzerland) calorimeter, calibrated with pure indium (T_m = 156.6°C). Two heating-cooling cycles and a heating scan were performed, in order to ensure good reproducibility of the data.

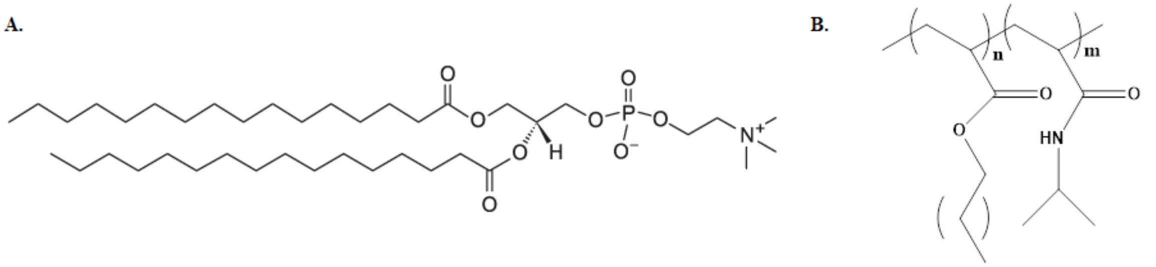

***Figure 1:** Molecular structures of A) DPPC and B) PNIPAM-b-PLA.*

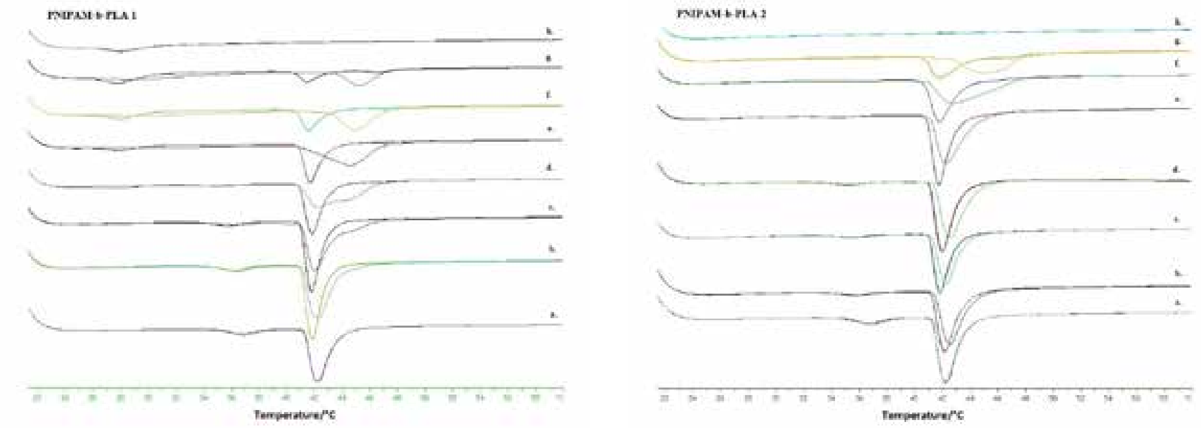

***Figure 2:** DSC heating scans of a) DPPC, DPPC:PNIPAM-b-PLA 1/2 b) 0.02 c) 0.05 d) 0.1 e) 0.2 f) 0.5 g) 1 and h) PNIPAM-b-PLA 1/2.*

Results and Discussion

The DSC heating scans of DPPC:PNIPAM-b-PLMA 1/2 in various molar concentrations are presented in **Figure 2.** The most obvious phenomenon is that, in both cases, by increasing the polymer content inside the phospholipid bilayers, the main transition during the 1st heating process is shifted to higher temperatures, in a concentration-dependent way. This phenomenon inside a complex lyotropic liquid crystalline system is important for two reasons. First, the thermoresponsiveness of the constructed chimeric nanosystems is a dynamic and irreversible behavior and occurs at a temperature value that is determined by the polymer-membrane interactions. Second, the incorporation of the polymers inside the bilayer creates a phase that is organized in a way that is defined by the polymer intramembrane conformation, which changes as the polymer chains become overcrowded and defines the information/entropy balance of the system[4]. The dynamics of the creation of such phases is non-predictable in a complex system that leads to morphologies, behaviors and kinetics that are also non-predictable and always based on the probabilities arising from the various interactions. In this case however, as described below, it is evident that certain thermodynamic parameters may be predicted based on the polymer concentration and in certain ranges, something that has up until now been considered as highly unlikely for lyotropic systems.

Concerning the systems containing PNIPAM-b-PLA, we observed that there is a polymer concentration range in which the alteration of some thermodynamic parameters exhibits a linear trend, found through regression analysis between the system polymer content and each parameter separately. Specifically for PNIPAM-b-PLA 1, in the range between 0.1 and 1 polymer molar ratios, the 1st cycle transition enthalpy (ΔH_m) decreases in a slightly linear way ($R^2 = 0.9352$), which also applies for the 2nd cycle ΔH_m ($R^2 = 0.9069$). The ΔH_m of the bilayers incorporating PNIPAM-b-PLA 2 presented an even stronger linear dependence on the concentration of the polymer in the aforementioned range, for both the 1st ($R^2 = 0.9973$) and 2nd cycle ($R^2 = 0.9972$). In addition, for this polymer, the 1st cycle transition temperature (T_m) increases in a slightly linear way ($R^2 = 0.9188$). These facts indicate that certain thermodynamic phenomena in complex systems, such as artificial membranes with more than one components, may be governed by linearity, at least in specific ranges, which may also apply for biological membranes. Linear behavior in certain ranges of complex systems that are highly and variably affected by the initial conditions, e.g. concentration, potentiates that the information/entropy balance is constant or constantly altered, representing the system characteristics and determining the system process kinetics, such as aggregation, stability and drug release. Previous works have shown that factors such as the shape and morphology of nanosystems affect these properties in similar ways[5].

Conclusions

Initial conditions of a complex system, such as concentration of biomolecules, create variability and through non-linear processes, lead to self-assembly of morphologies that are chaotically or stochastically determined. The discovery of functions, linear or other, that connect the initial conditions with the outcome of self-assembly or with behaviors that occur after that, despite all the intermediate dynamic processes, could be the next step in controlling the functional properties of such systems, including biofunctionality and biological stability. Prediction over probability of traits of drug delivery nanosystems, like stability and drug release kinetics, is the next step towards the development of quality new products, as well as towards the determination of specifications required by the regulatory authorities for building nanosimilars. □

Acknowledgments

The research work was supported by the Hellenic Foundation for Research and Innovation (HFRI) and the General Secretariat for Research and Technology (GSRT), under the HFRI PhD Fellowship grant (GA. no. 392).

REFERENCES

1. Naziris N., Pippa N., Pispas S., Demetzos C. The Formation of Chimeric Nanomorphologies, as a Reflection of Naturally Occurring Thermodynamic Processes. *J. Phys. Conf.* 931, 2017.
2. Naziris N., Pippa N., Chrysostomou V., Pispas S., Demetzos C., Libera M., Trzebicka B. Morphological Diversity of Block Copolymer/Lipid Chimeric Nanostructures. *J. Nanopart. Res.* 19, 347-357, 2017.
3. Naziris N., Pippa N., Stellas D., Chrysostomou V., Pispas S., Demetzos C., Libera M., Trzebicka B. Development and evaluation of stimuli-responsive chimeric nanostructures. *AAPS PharmSciTech.* 2018 [Epub ahead of print].
4. Naziris N., Pippa N., Pispas S., Demetzos C. The Role of the Information/Entropy Balance in Self-assembly. The Structural Hierarchy of Chimeric Drug Delivery Nanosystems. *Pharmakeftiki*. 29, 77-82, 2017.
5. Pippa N., Psarommati F., Pispas S., Demetzos C. The Shape/Morphology Balance: A Study of Stealth Liposomes via Fractal Analysis and Drug Encapsulation. *Pharm. Res.* 30, 2385-2395, 2013.

www.hsmc.gr/en/pharmakeftiki-journal/

ΦΑΡΜΑΚΕΥΤΙΚΗ, 30, 4 (2018) ΕΡΕΥΝΗΤΙΚΗ ΕΡΓΑΣΙΑ

PHARMAKEFTIKI, 30, 4 (2018) RESEARCH ARTICLE

Effect of Thermal Shock Cycling on the Dynamic Mechanical Properties of Epoxy Matrix Composites Reinforced with Natural Fiber Fabric

A. Kollia[1], George C. Papanicolaou[2], Stefanos Zaoutsos[1]

[1]*Laboratory of Advanced Materials and Constructions, Department of Mechanical Engineering, TEI of Thessaly, 41110, Larissa, Hellas*
[2]*Composite Materials Group, Department of Mechanical and Aeronautical Engineering, University of Patras, Rion 26500, Hellas*

KEYWORDS:
dynamic mechanical analysis, viscoelastic material, flax composite, thermal shock

Corresponding Author:
S.P. Zaoutsos
szaoutsos@teilar.gr

ABSTRACT

Abstract: The aim of the present work is to investigate the influence of thermal shock cycling on the dynamic properties of epoxy matrix composites reinforced with natural fibers. Polymer composites reinforced with flax fiber fabric were manufactured. The samples have been exposed to a certain number of thermal shock cycles (50, 100, 200, 300, 400), at a temperature range from -40^{o}C to +28^{o}C. Dynamic mechanical analysis tests were performed in pristine and thermally shocked specimens in order to determine the viscoelastic response of the material. Storage and loss modulus values were decreased on the order of 50 % due to thermal fatigue, up to a certain number of thermal cycles. After 100 cycles, no further degradation of dynamic properties was observed. On the contrary, glass transition temperature and damping factor values showed minor variation as the thermal shock increased. The time-temperature superposition principle (TTSP) was successfully applied, confirming the fact that the flax composite is a thermo-rheologically simple material. Likewise, three-point bending tests were executed and a decrease of 20% was observed for a maximum number of cycles 400.

Introduction

In recent years, natural composites are used in industrial fields due to an increasing requirement for developing sustainable materials. Flax fibers are a type of natural reinforcement combining low environmental impact with a relatively low cost offering specific mechanical properties comparable to those of glass fibers. Likewise, alike most natural fibers, they have low density, which reduces the weight of the final structure or product.

As the use of composites expands into fields like automotive, aeronautics and aircraft, their components may be subjected to thermal shock or moisture environments. Thus, it is critical to understand how bio-sourced composite materials behave to

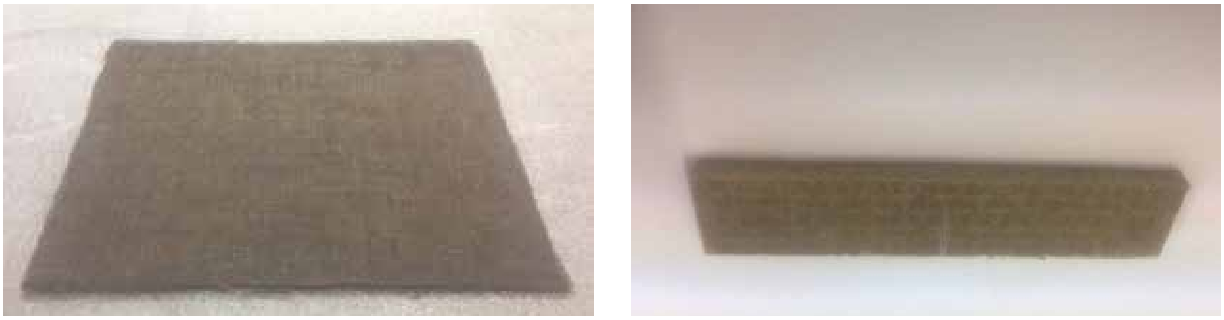

Fig. 1. *(a) flax fabric composite plate after polymerization, (b) flax fabric composite specimen for three-point bending test*

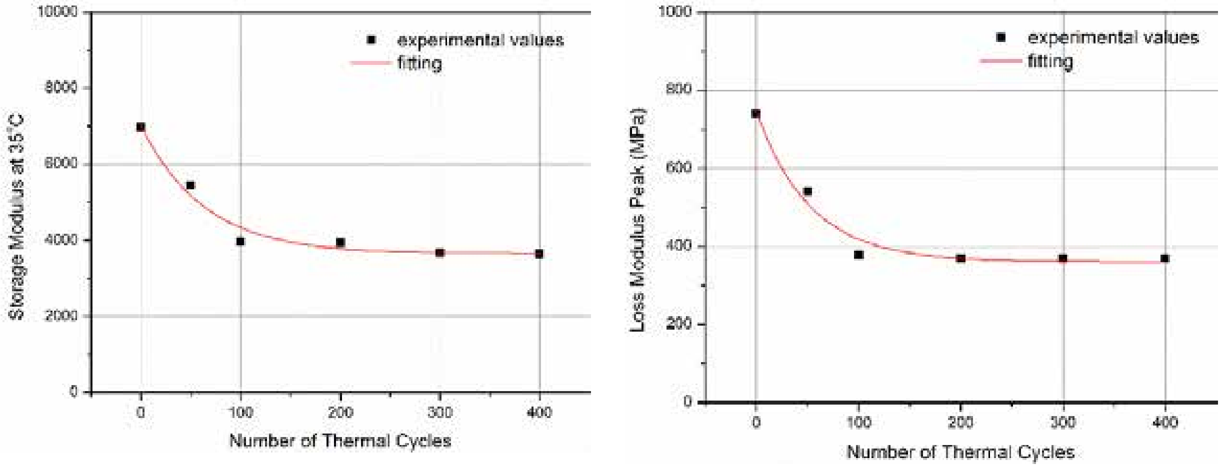

Fig. 2. *Variation of (a) storage modulus, (b) loss modulus versus number of thermal cycles.*

such extreme conditions in order to produce a well-designed, cost effective and energy efficient product. During thermal shock cycling, damage typically appears in the form of macroscopic cracks as a result of cyclic thermal stresses and strains due to temperature changes, under constrained thermal deformation[1]. The thermal shock process is rather complex because of the structural heterogeneity of composite materials[2]. Radical effects like matrix cracking or fibre–matrix interface degradation may occur, under extreme temperatures[3]. Additionally, voids and cracks in the microstructure of a material can further lead to an increase of moisture or water absorption which can cause matrix plasticization or delamination and eventually leading to failure[4].

1. Materials and Experimental Procedure

1.1 Materials and Manufacture Process

The epoxy system used as matrix material was the resin Renlam CY219 combined with a curing agent Renlam HY 219 at a ratio 2:1, by weight. Four plies of flax fabric in plain weave were used as reinforce-

Table 1. Variation of glass transition temperature, for different thermal shock cycles

Thermal Fatigue	Tg (^{o}C)	Tan Delta	Tg (^{o}C)	Tan Delta	Tg (^{o}C)	Tan Delta
0 cycles	69.99084	0.31068	79.99960	0.30342	84.99976	0.36542
50 cycles	69.99213	0.28221	79.99960	0.30342	85.00055	0.31293
100cycles	69.99124	0.29459	79.99907	0.31362	85.00016	*0.32631*
200 cycles	69.99074	0.28105	79.99938	0.29645	84.99999	0.30921
300cycles	69.99222	0.29251	80.00028	0.30925	84.99991	0.32276
400 cycles	69.99203	0.27945	79.99968	0.30053	85.00031	0.31444

ment, having 0/90o orientation. The manufacturing method used to produce the composite is a well-known technique, called resin vacuum infusion. It is an advanced technique, which is widely used for high-performance, defect-free, composite materials. Specimens were cut from the primary composite plates (**Fig. 1a**) in dimensions 58 x 12 x 2.5 mm (Fig. 1b).

1.2 Static Mechanical Test

Static three-point bending tests were performed in a UTM Instron 3382 of 100 kN loading capacity, at a room temperature. A constant crosshead speed 0.5 mm/min was applied and samples had a total length of 58 mm and a gauge length of 45 mm.

1.3 Dynamic Mechanical Analysis

Dynamic mechanical analysis tests were executed on a DMA Q800 system of TA Instruments, in three-point bending mode and dual cantilever. Multi-frequency isothermal tests were performed within the range of 1 to 100 Hz with the temperature being in the range 35oC to 150oC while the heating rate in all cases was set at dT/dt =5oC/min. Thus, stepwise isothermal frequency sweeps were obtained.

1.4 Thermal Shock Cycling

The flax composite specimens were induced in thermal shock cycling and the effect on their viscoelastic characteristics was investigated. The specimens were exposed to 28oC for 10 min and then they were immediately placed in a freezer at -40oC temperature, for the same period of time. During this process, the samples were removed regularly at 50, 100, 200, 300 and 400 cycles in order to evaluate their dynamic properties as a function of the number of thermal shock cycles.

2 Results and Discussion

The storage and loss modulus measured, are plotted against the number of thermal cycles (at 1 Hz) in **Fig.1**. For the pristine specimens, the storage modulus at 35^{o}C (approx. 7500 MPa) is clearly higher from the corresponding modulus values for the thermal shocked samples (**Fig. 2a**), indicating the influence of thermal cycling on the stiffness at lower temper-

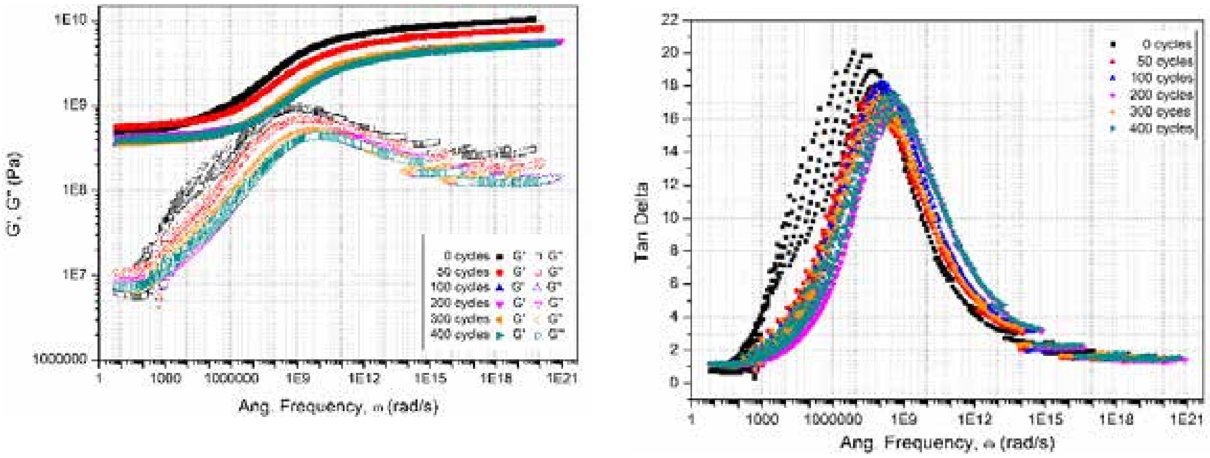

Fig. 3. *(a) master curve of storage and loss modulus, (b) master curve of tan delta with angular frequency at a reference temperature of 150oC after different thermal shock cycles*

atures (T<Tg). The storage modulus curves, in all cases, exhibit a less significant drop as the testing temperature rises, approaching the rubbery state and reach a rubbery plateau at higher temperatures (T>Tg)[5]. A higher peak of loss modulus is also observed for the non-thermal shocked samples (Fig. 2b), which shows a regular decrease with the increase of thermal cycles.

A reduction in storage and loss values on the order of ~48% and ~50%, respectively, is observed. The degradation of the dynamic properties seems to take place up to a certain number of thermal cycles, which is 100 cycles, where the saturation of microdamage is attained.

The reduction of the dynamic properties due to the thermal cycling can be attributed to a combination of several factors. During the thermal shock process the localized stress concentration arises because of the heterogeneity of composites and the different coefficients of thermal expansion of their components. The cycling temperature changes can result to the initiation and the propagation of cracks which finally may lead to changes in geometry and the physical characteristics of composites[6-8].

Glass transition temperatures were measured from the peak's location of the damping factor curves. Their values remained unaffected from the thermal shock cycling duration since Tg is an inherent property.

2.1 Application of the time-temperature superposition principle (TTSP)

The master curves of storage modulus, loss modulus and damping factor obtained from the application of the TTSP, are displayed in **Fig. 3.** They have been constructed by the automatic shift program, at a reference temperature of 150°C. The values can be obtained for an otherwise not measurable wide range of frequencies.

At high frequencies, a reduction of both storage and loss modulus values is observed (**Fig. 3a**), up to 100 thermal cycles, while a less significant drop is noticed for the damping factor values. The peaks of the tan delta corresponding to these frequencies suggest a high frequency vibration damping capability of the composite.

The horizontal shift coefficient is given from the

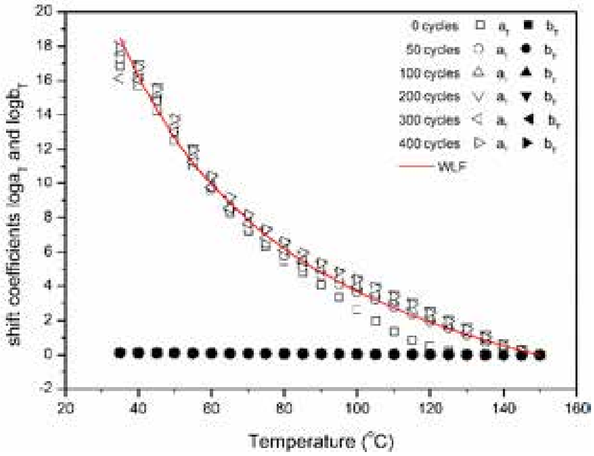

Fig. 4. Horizontal and vertical shift coefficients versus temperature

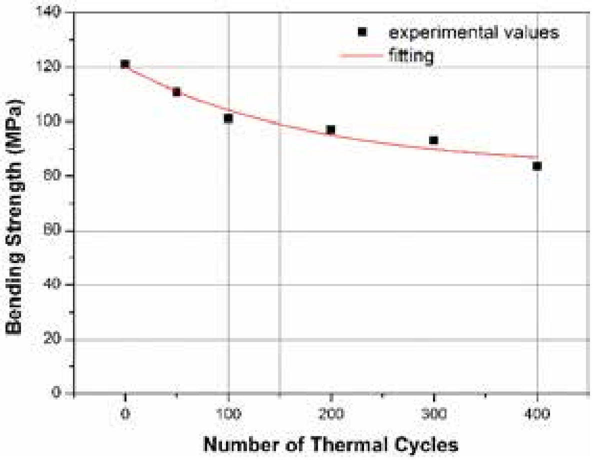

Fig. 5. Variation of bending strength versus number of thermal cycles

application of TTSP which is empirically determined and is a function of temperature. The data of horizontal shift factor have been extrapolated using Wiliams-Landel-Ferry equation (eq. 1), with 150°C as reference temperature, where C_1 and C_2 treated as fitting parameters (**Fig.4**).

$$\ln(a(T)) = -C1(T - Tref) / (C2 + (T - Tref)) \quad (1)$$

Predicted values were found in relativity good agreement with respective experimental results. However, there are some points of divergence. Likewise, the vertical shift coefficient is almost zero at all cases, which indicates that the effect of thermal expansion may be omitted.

From the **Fig. 5**, a decrease in bending modulus was observed due to the increase of the number of thermal cycles. A maximum decrease of ~20% was achieved at 400 thermal cycles due to the structural deterioration of the material increasing the loading cycles.

3. Conclusions

In the current study the influence of thermal shock cycling on the dynamic mechanical behavior of polymer composite reinforced with flax fabric is investigated. The samples were mechanically tested and characterized after having subjected to thermal shock conditions in a temperature range from -40oC to 28oC, at testing frequencies 1-100 Hz. The main conclusions are as follows:

1. The thermal shock process decreases the values of storage and loss modulus. Up to 100 cycles a decrease on the order of ~ 50 % is achieved.

2. After 100 thermal cycles, no significant further reduction of the dynamic mechanical properties is observed. There is seems to be a certain point at which saturation of damage is attained.

3. The damping factor (tanδ) and the glass transition temperature (Tg) do not get affected by the thermal shock cycling.

4. The results of the application of TTSP principle meet the assumption of a thermo-rheologically simple material that can be used for damping high-frequency vibrations.

5. A decrease in bending strength with the increase of thermal shock process is observed. A maximum decrease of ~ 20% is achieved at 400 cycles. □

REFERENCES

1. Xin Q. Thermal Fatigue Durability and Reliability in Diesel Engine System Design, 2013
2. Nayfeh A.H. Thermomechanically induced interfacial stresses in fibrous composites, *Fiber Sci. Technol.* 10, 195-209, 1977.
3. Jang, B. Z. (1994) Advanced Polymer Composites: Principles and Applications, ASM International, Materials Park, CRC Press.
4. Mohanty A.K., Misra M., Drazal L.T. (2005) Natural Fibers, Biopolymers and Biocomposites, CRC Press, Boca Raton
5. Pascault J.P., Sautereau H., Verdu J., Williams R.J.J. (2002) Thermosetting Polymers, Marcel Dekker.
6. Hancox N. L. Thermal effects on polymer matrix composites: Part 1. Thermal cycling *Mater. Design* 19, 85-91, 1998,.
7. Parlevliet P. P., Bersee H. E. N., Beukers A. Residual stresses in thermoplastic composites – a study of the literature. Part III: Effects of thermal residual stresses *Compos. Part A: Appl. Sci. Manuf*. 38, 1581 -1596, 2007..
8. Chung K., Seferis J. C., Nam J. D. Investigation of thermal degradation behavior of polymeric composites: prediction of thermal cycling effect from isothermal data *Compos. Part A: Appl. Sci. Manuf.* 31, 945-957,2000.

www.hsmc.gr/en/pharmakeftiki-journal/

ΦΑΡΜΑΚΕΥΤΙΚΗ, 30, 4 (2018) ΕΡΕΥΝΗΤΙΚΗ ΕΡΓΑΣΙΑ

PHARMAKEFTIKI, 30, 4 (2018) RESEARCH ARTICLE

Products obtained from the catalytic pyrolysis of polymeric materials found in WEEE.

Aristea Rousi, Evangelia Vouvoudi*, Dimitris Achilias

Laboratory of Chemistry and Technology of Polymers and Dyes, Department of Chemistry, Aristotle University of Thessaloniki, Thessaloniki, PC. 54124, Macedonia, Hellas

KEYWORDS: Polymer recycling; catalytic degradation; polymeric waste

***Corresponding author's:**
email evouvoud@chem.auth.gr

1. Introduction

The recent trend towards shorter lifespan of Electrical and Electronic Equipment (EEE) has changed the electronics industry over the last decade as more demand is generated. Great demand has created an expansion of technology, along with short innovation cycles that have produced different versions of similar electronic products. Thus, the percentage of obsolete EEE has increased and has generated a huge volume of waste electrical and electronic equipment (WEEE)[1]. In order to specifically manage this waste, the European Commission has implemented Directive 2002/96/EC by setting targets for the recovery of useful materials from WEEE between 70% and 80%[2]. WEEE contains about 20-30% polymeric materials and therefore it is imperative to include these polymers in material recovery or recycling systems. Recycling of WEEE is a major challenge, mainly for two reasons. Firstly, inert WEEE contains more than 10 different types of polymers such as (acrylonitrile-butadiene-styrene) copolymer (ABS), high impact polystyrene (HIPS), polypropylene (PP), polystyrene (PS), (styrene-acrylonitrile) copolymer (SAN), polyesters, polyurethane (PU), polyamides (PA), PC/ABS blends and HIPS/*p*-phenylene oxide (PPO), thus the economy of any kind of recycling is put into question[3,4]. Secondly, polymeric WEEE may contain organic and inorganic hazardous compounds[3]. Advanced thermochemical methods for the treatment of WEEE provide a viable and promising recovery solution, as reported extensively in the literature, where not only the largest proportion of monomers could be recovered (up to 60%), but it was also possible to produce compounds of commercial and research interest such as gases (low MW hydrocarbons), tar (waxes and liquids too high in flavourings) and carbon (elemental and/or activated carbon)[5].

The pyrolysis process appears to be a promising alternative for the degradation of WEEE as it can, under controlled conditions, act on a large number of organic macromolecules and degrade them into useful products (some of which are of high commercial value). Allowing the recovery of high added value products such as precious metals, fuels and chemicals (usually the polymers' monomers and other organic ingredients)[5,6]. Thermal cracking requires high temperatures due to the low thermal conductivity of the polymers, furthermore it is not very selective and a possible solution for reducing these reaction conditions is the application of catalytic cracking. Catalytic cracking is another alternative to recycling clean or mixed plastic waste[7]. Catalysts reduce the temperature and reaction time and allow the production of hydrocarbons with a higher added value, such as fuel oils and petrochemical feedstocks. That is, the usage

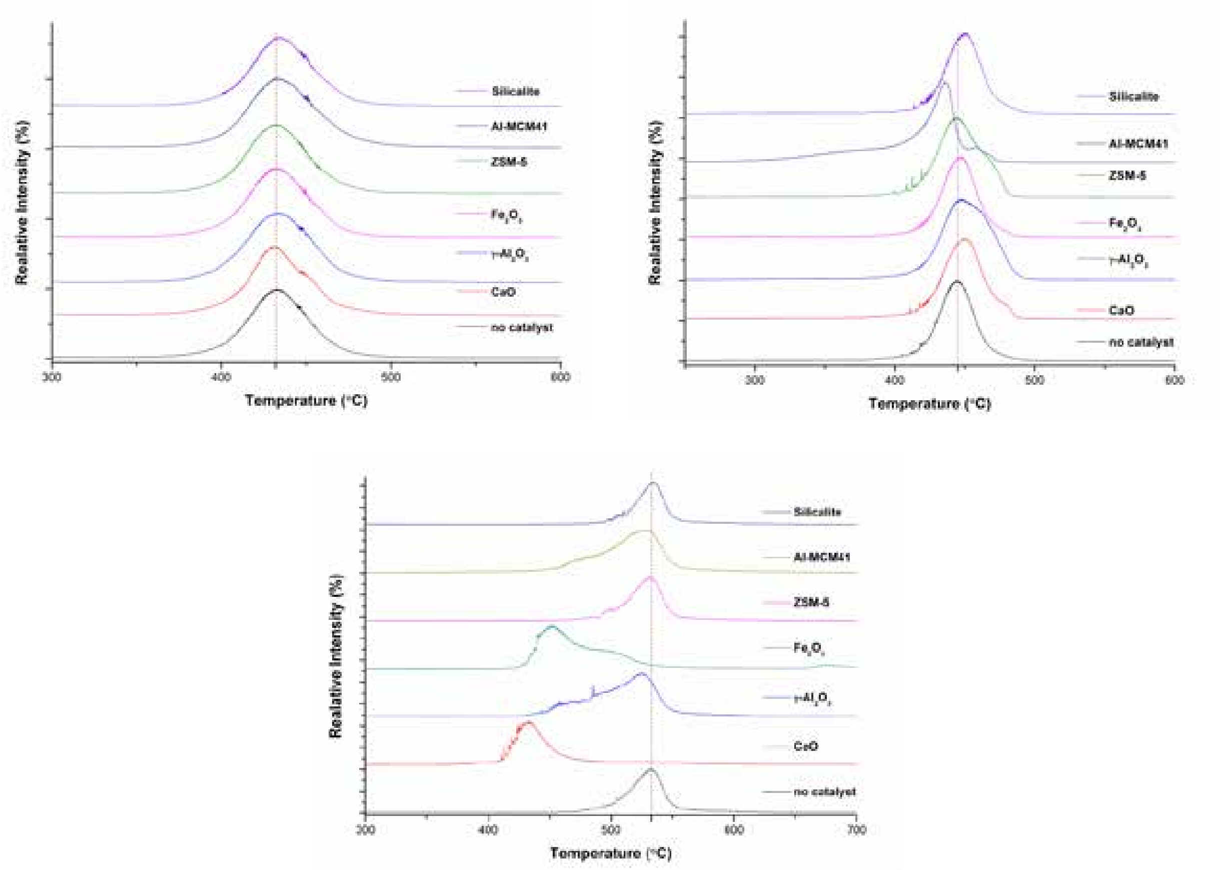

Figure 1. *EGA thermograms of (a) ABS, (b) HIPS, (c) PC.*

of catalysts gives an added value to the pyrolysis and cracking efficiency of these catalysts depending both on its chemical and physical characteristics[7].

2. Materials and Methods

2.1. Polymers and Catalysts

In the present study, the standard materials chosen for the pyrolytic experiments are the poly(acrylonitrile-butadiene-styrene) (ABS), poly(styrene-butadiene) (HIPS) and poly(bis-phenol A carbonate) (PC) which are mainly present in the polymeric parts of WEEE. The polymers were supplied by Sigma-Aldrich USA. A mill was used to grind the ABS, HIPS, PC pellets to a size of less than 2 mm. The catalysts that were used in the pyrolysis of the polymers were behaving as Lewis' acids or bases. The acidic catalysts were represented by zeolites (ZSM-5, silicalite), a mesoporous MCM-41 alumino-silicate, *γ*-alumina (γ-Al_2O_3), iron(III) oxide (Fe_2O_3), while the basic catalyst was calcium oxide (CaO). They were all dry.

2.2. Experiment procedures

The pyrolysis of ABS, HIPS and PC were conducted in a Py-GC/MS (EGA/PY-3030D by Frontier Lab coupled with QP-2010 Ultra Plus GC/MS by Shimadzu,

Table 1. EGA curves maxima and selected temperatures for SS pyrolysis.

	No catalyst	CaO	γ-Al_2O_3	Fe_2O_3	Silicalite	ZSM-5	Al-MCM-41
ABS Tpeak (°C)	430	430	435	430	435	430	430
HIPS Tpeak (°C)	445	450	445	445	450	445	435
PC Tpeak (°C)	530	435	525	450	535	530	*530*

Japan), where products were separated chromatographically and identified spectroscopically. The EGA thermogram was obtained after heating the polymer from 100-700 °C at a rate of 20 °C/min and an interface temperature of 300 °C. From the thermogram, we can get information about the thermal behaviour of the material, our interest is focused on the peak temperature. The SS programs, later, are generated by flash pyrolysis of the polymers at the selected temperatures for 0.5 min. The evolved gases are separated into the Ultra Alloy (5% diphenyl- 95% dimethyl)polysiloxane (30m x 0.25mm x 0.25μm) capillary column following a temperature program of 45 min. the column flow was set at 1 mL/min, the He flow at 3 mL/min, the split ratio at 100 and the MW range 10-500. The database libraries NIST and Frontier are equipped for analyzing the results on a LabSolutions ver. 2.71 software. The sample:catalyst ratio was 2:1.

3. Results and discussion

The results evolved by the pyrolyzer and EGA process showed wide curves (**Figure 1**) with their characteristic peak values included in **Table 1**. At ABS thermograms in the absence of catalysts, a peak of decomposition at 430 °C is exhibited. Although there is almost no difference in the decomposition temperature, by using a catalyst there is a large increase in product peaks, new compounds are detected as well as the number of hybrid compounds (consisting of acrylonitrile and styrene) significantly increase. The maximum temperatures at the peaks of HIPS decomposition is at 430 °C. When CaO, γ-$Al_2O_{3,}$ Fe_2O_3 catalysts are used the pyrograms result with fewer compounds. The maximum temperatures at the top of the decomposition area of PC is at 530°C. Although when using catalysts CaO and Fe_2O_3 the temperature at the maximum of the PC decomposition area is significantly lower than without the use of a catalyst, however, there is no advantage in terms of the products produced, on the contrary less products are detected .Same results observed by catalyst ZSM-5 too. The bold letters for temperatures in **Table 1** show the most effective catalyst choice.

At **Table 2**, we can see the compounds identified after the pyrolysis of ABS copolymer. Pyrolysis of ABS results in the production of the styrene and acrylonitrile monomers, together with styrenic dimer and trimer and along with hybrid dimers and trimers of styrene and acrylonitrile. By using a catalyst there is a large increase in product peaks as we can see in **Figure 2a**, new compounds are detected, as well as the number of hybrid compounds (the trimers particularly from 8 in the non-catalytic pyrogram reach about 30 for the

Table 2. Identified compounds found after the SS pyrolysis of ABS.

t (min)	Compound	MW	% Similarity
0.50	acetonitrile	57	80
0.59	acetonitrile	57	80
1.85	acrylonitrile	53	80
3.95	styrene	104	72
4.12	styrene	104	89
4.18	styrene	104	85
4.64	styrene	104	97
11.40	2-methylene-4-phenylbutanenitrile - hybrid	157	94
12.53	4-phenylpent-4-enenitrile - hybrid	157	69
15.34	1,3-diphenyl-propane	196	96
16.12	3-butene-1,3-diyldibenzene - styrenic	208	96
17.17	2-methylene-4-phenethylpentanedinitrile - hybrid	210	88
17.57	2-methylene-4phenylheptanedinitrile - hybrid	210	95
17.76	2-(2-phenylallyl)pentanedinitrile - hybrid	210	71
20.15	2-methylene-4,6-dipenylhexanenitrile - hybrid	261	98
20.57	4,6-diphenylhept-6-enenitrile - hybrid	261	95
20.81	2-phenethyl-4-phenylpent-4-enenitrile - hybrid	261	93
23.07	5-hexene-1,3,5-triyltribenzene - styrenic	312	95

catalysts CaO, γ-Al_2O_3, Fe_2O_3, at 26 for Al-MCM-41, while for Silicalite, ZSM-5 only 12 peaks). The Al-MCM-41 catalyst is the only catalyst that hybrid trimers are observed from retention time 10min and on, whereas in all the other catalysts after 16 min. Aliphatic nitriles of up to 18 C atoms are present, but aromatic too. With Silicalite, ZSM-5, Al-MCM-41 catalysts applied no products are observed after 26 min of elution, while with CaO, γ-Al_2O_3, products are observed up to 32 min and for Fe_2O_3 catalyst up to 33 min. With these latter 3 catalysts at 32 min elution area the 1-tetratriacontene compound appers. Some compounds are common to all catalysts, others common to some of them, while there are compounds found in a specific catalytic experiment. Generally, in all catalytic pyrolysis most of the compounds are aromatic. Using Fe_2O_3 on ABS, has produced even around

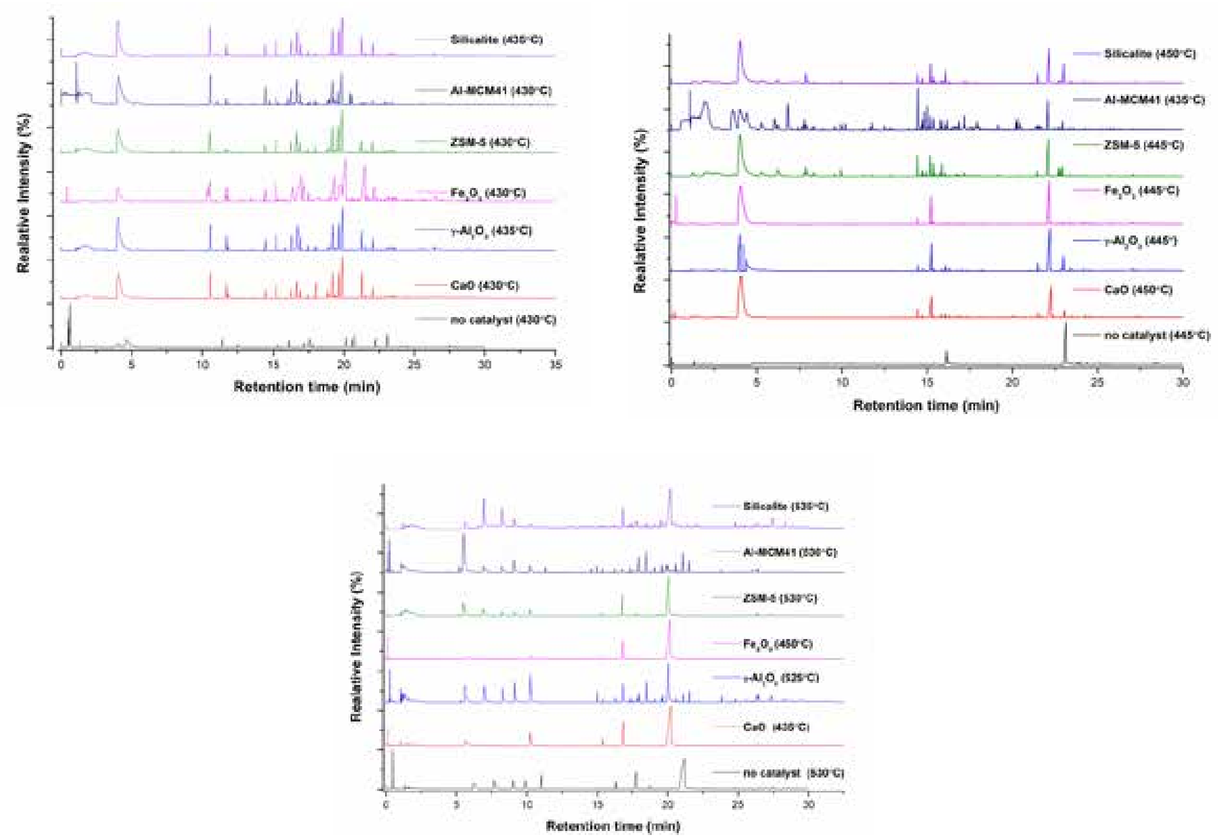

Figure 2. *Pyrograms produced after SS pyrolysis of (a) ABS, (b) HIPS, (c) PC.*

80 compounds, the highest number followed by γ-Al_2O_3, Al-MCM-41, CaO experiments, while the fewer are with the Silicalite and ZSM-5 catalysts. When Fe_2O_3 is applied as catalyst, besides most compounds being identified, there is also a great variety of products, like *p*-tert-butylphenol or 2-ethylhexyl-2-cyano-3,3-diphenylacrylate.

The pyrogram of HIPS in **Figure 2b** is rather simple and the main compounds identified are the styrenic dimmer and trimmer. With much smaller intensity, some aromatic compounds with 2-3 phenyl rings are also identified as shown in **Table 3**. By comparing the decomposition products in all chromatograms, we observe that the styrenic trimer of 5-hexene-1,3,5-triyltribenzene is found in more peaks with CaO pyrolysis and fewer with Al-MCM-41. With CaO, γ-Al_2O_3, Fe_2O_3 catalysts, the pyrograms with the fewer compounds are obtained. With the exception of 5-hexene-1,3,5-triyltribenzene and triphenylbenzene, most products bear two benzene rings, while for the ZSM-5 and Al-MCM-41 catalysts there are compounds with more than two benzene rings such as 5,6-dihydrochrysene, 7,12-dimethyl-1,2-benzanthracene, 1,2-dihydro-1-phenylnaphthalene or 1,3-diphenylpyrene. Caution should be given to the CaO

Table 3. Identified compounds found after the SS pyrolysis of HIPS.

t (min)	Compound	MW	% Similarity
1.35	ethane	30	75
15.36	1,3-diphenylpropane	196	92
16.13	3-butene-1,3-diyldibenzene - styrenic	208	97
17.27	benzene,1,1’-(1-butene-1,4-diyl)bis	208	85
23.14	5-hexene-1,3,5-triyltribenzene - styrenic	312	96
24.66	benzene,1,1'[3-(2-phenylethylidene)1,5-pentanediyl]bis	326	69
25.15	benzene,1,1'-(3-methyl-1-propene-1,3-diyl)bis	208	66
26.73	triphenylbenzene	306	92
28.31	benzene,1,1'[3-(2-phenylethylidene)1,5-pentanediyl]bis	326	69
28.49	ethylene,tetrabenzyl	388	68

catalyst, as the formation of bisphenol A is then observed. By using the catalyst Fe_2O_3, more compounds than non-catalytic pyrolysis are observed, however fewer than the rest of catalysts (the catalyst with most degradation products is Al-MCM-41). Aliphatic products are only detected with γ-Al_2O_3 and Al-MCM-41 effect. When Al-MCM-41 is added compounds with lower MW such as ethylbenzene, styrene, *p*-ethyltoluene, α-methylstyrene, are observed too.

Likewise, as for the pyrogram of PC, in **Fig. 2c**, the compounds identified were several phenols with one or two aromatic rings, with main products the monomer bisphenol A, the *p*-hydroxy-2,2-diphenylpropane and *p*-isopropenylphenol. All the compounds that were identified in the 30min elution are shown in **Table 4**. Using the CaO catalyst as shown in the pyrogram **Figure 2c**, the chromatogram with fewer products is yield, fewer even from when it’s absent. Although the temperature at the maximum of the decomposition area is significantly lower than without the use of a catalyst, there is no advantage in terms of the products produced. Similar findings exist for the Fe_2O_3 catalyst, the temperature at maximum decomposition decreases greatly to 450 °C, the products however are again less than without catalytic presences. At 500 °C in the shoulder of the main stage the products are more, the number similar to that without the usage of catalyst and only two new compounds are detected: α-methylstyrene and 2,4-bis[2-(4’-hydroxyphenyl)-2-propyl]phenol. The ZSM-5 catalyst does not reduce the decomposition temperature and the products are in a lower ratio at 530 °C pyrolysis relatively to the non-catalytic cracking. Some non-catalytic cracking compounds do not appear here, but there is the presence of α-methylstyrene, *o*-cresol, 2,4-bis[2-(4’-hydroxyphenyl)-2-propyl]phenol, while the products identified overall are still less than non-catalytic case.

The most interesting pyrograms for PC have

Table 4. Identified compounds found after the SS pyrolysis of PC.

t (min)	Compound	MW	% Similarity
1.77	carbon dioxide	44	89
5.20	carbon monoxide	28	73
6.20	phenol	94	97
6.42	phenol	94	97
7.68	*p*-cresol	108	98
7.84	*p*-cresol	108	97
9.03	*p*-ethylphenol	122	98
9.18	*p*-ethylphenol	122	97
9.84	*p*-vinylphenol	120	94
9.90	*p*-isopropylphenol	136	95
10.07	*p*-vinylphenol	120	83
10.36	*p*-ethyl phenol	122	14
11.04	*p*-isopropenylphenol	134	98
11.12	*p*-isopropenylphenol	134	85
15.52	*p*-hydroxy-2,2-diphenylpropane	212	82
15.86	diphenylcarbonate	214	92
16.31	4-isopropenyldiphenylether	210	97
17.72	p-hydroxy-2,2-diphenylpropane	212	97
18.71	p-hydroxy-3-methyl-2,2-diphenylpropane	226	85
20.43	4,4′-ethylidenediphenol	214	87
20.53	4,4′-ethylidenediphenol	214	89
21.14	bisphenol A	228	94
21.19	bisphenol A	228	94

occurred by using the catalysts γ-Al_2O_3 and Al-MCM-41 or Silicalite, regarding the diversity and the number of products as well as the intensity displayed in relation to non-catalytic cracking.

With γ-Al_2O_3 catalyst applied, almost all the compounds appeared here are further aromatic with -OH, C=O or O=C-O groups. With Silicalite catalyst on the other hand, the *p*-cresol, *p*-ethylphenol compounds are in higher proportion than without a catalyst, while the different compounds are almost twice as high. It is the only catalyst that most aromatic oxygen-free compounds are detected, such as fluorene or anthracene. Interest is also shown in the appearance of the 5-hexene-1,3,5-triyltribenzene compound, ie the styrenic trimer that appears also at the pyrograms of ABS and HIPS. When Al-MCM-41 catalyst applies, there are also more compounds yield than non-catalytic cracking. There is an interesting difference in the percentage corresponding to phenol and bisphenol A without catalyst; the first compound is at about 20% and the second at 80% in the presence of catalyst, phenol reaches 100% intensity while bisphenol A at 20%. Herein all the new aromatic compounds that appear also have oxygen bonds. No aliphatic compounds are found in any pyrograms. From these catalysts, in terms of product intensity at the pyrograms, the highest is detected by using γ-Al2O3 catalyst, followed by Al-MCM-41 and finally by Silicalite. While using Silicalite catalyst many products are presented, their intensity is not quite large at the highest decomposition rate.

4. Conclusions

Over the years the consumption of EEE products has increased, generating big amounts of WEEE and environmental concern has generated too. Pyrolysis has been effective compared to other disposal methods, because it can (re)use the energy and the raw materials contained in those waste, reducing thereby the environmental impacts. The pyrolysis process may be simple or catalytic. Thermal degradation is an endothermic process and due to the low thermal conductivity of polymers, there is a need for high temperatures. Due to that, there is a high demand of energy. In order to decrease this temperature, catalysts may be used. Using a catalyst will favour the pyrolysis process, both by selectiveness in the production of selected compounds and by the reduction of energy requirements due to the reduction of reactive activation energy. Moreover with the catalytic pyrolysis, the catalytic reaction decreases the degradation time. The composition and amount of the obtained products depend on the catalyst used.

Thermal pyrolysis of ABS, HIPS generates mainly their monomers, but also styrenic dimer and trimer for ABS, HIPS and hybrid dimer and trimer for ABS. As far as PC is concerned, the main products after its pyrolysis are the monomer bisphenol A, the *p*-hydroxy-2,2-diphenylpropane and *p*-isopropenylphenol.

When using catalysts the number of products obtained as well as the diversity of them increases exceptionally with most catalysts. After using six different catalysts for the catalytic pyrolysis of these polymers based on the rise of the diversity and number of products obtained, taking also into account the intensity of the peaks comparing all the catalytic pyrograms with each other and the programs, we could extract an assumption on the best option of catalyst for each polymer.

Regarding ABS, the catalyst Fe_2O_3 has some advantages over the rest catalysts which are the number of hybrid compounds, namely trimers, pyrolytic products are observed up to 33 min of elution, the pyrogram with the most compounds (about 80) are observed, demonstrating the greatest variety of products and interest.

When using Al-MCM-41 as catalyst for HIPS the relative intensity of most product peaks is at 20% or more, indenes, naphthalenes and their derivatives, as well as derivatives of anthracene appear, compounds with more than two benzene rings occur, since it is the catalyst with the most breakdown products while the decomposition temperature decreases. And finally for PC polymer, when compared to all the other catalysts the one that stands out is γ-Al_2O_3 and that is because the compounds that are yield are almost twice as high as in non-catalytic pyrolysis, the intensity of the products peaks is greater, the decomposition temperature decreases significantly and the number of products increases, showing variety of products. ☐

REFERENCES

1. Debnath B., Roychowdhury P., Kundu R. Electronic Components (EC) Reuse and Recycling – A New Approach towards WEEE Management. *Procedia Environmental Sciences* 35, 656-668, 2016.
2. Maris E., Botané P., Wavrer P., Froelich D. Characterizing plastics originating from WEEE: A case study in France*. Minerals Engineering* 76, 28-37, 2015.
3. Schlummer M., Gruber L., Mäurer A., Wolz G., van Eldik R. Characterisation of polymer fractions from waste electrical and electronic equipment (WEEE) and implications for waste management. *Chemosphere* 67, 1866-1876, 2007.
4. Martinho G., Pires A., Saraiva L., & Ribeiro R. Composition of plastics from waste electrical and electronic equipment (WEEE) by direct sampling. *Waste Management* 32(, 1213-1217, 2012.
5. Antonakou E. (2014) Development of advanced thermochemical polymer recycling techniques. Doctorate Thesis. Aristotle University of Thessaloniki.
6. Luda M. (2012) Pyrolysis of WEEE plastics. In V. Goodship & A. Stevels, Waste electrical and electronic equipment (WEEE) Handbook. Cambridge: Woodhead Publishing Limited.
7. Almeida D., Marques M. Thermal and catalytic pyrolysis of plastic waste. *Polímeros*, *26*, 44-51, 2016.

Catalytic pyrolysis of polymeric materials used for packaging via TGA and Py-GC/MS.

Evangelia Vouvoudi*, Dimitris Achilias

Laboratory of Chemistry and Technology of Polymers and Dyes, Department of Chemistry, Aristotle University of Thessaloniki, Thessaloniki, PC. 54124, Macedonia, Hellas

KEYWORDS: Polymer recycling; catalytic degradation; packaging waste

***Corresponding author's:**
email evouvoud@chem.auth.gr

1. Introduction

The necessity of packaging for all products and services is profound, since it protects the product, gives identity and information for the content, ensures the safe storage and carriage even makes it attractive. Packaging material may be wood, paper, glass, metal or polymeric, known for this case as "plastics". The main advantages of polymer packaging are the low cost, light density, easy shaping, safety for consumers[1]. The statistics say that more than 50% of the packaging materials are plastics while for 2016 year 335 mil. tones of polymers were produced worldwide, 60 of them corresponding to Europe[2]. Out of these, first application sector is packaging. As it is expected therefore, the large consumption of goods for developed societies and economies generates great amounts of waste, reaching the limits of pollution for both waters and soil. From all polymer waste gathered in Europe in 2015, the 60% of it came from packaging, due to their short life[3]. European Union acts towards pollution caused by plastics, through awaking public concern on the matter or publishing councils' guidances and committees' reports/studies proposing the countermeasures[3]. It should be emphasized that polymers are not toxic for the environment because of their ingredients but because of their vast volume and non biodegrability.

One of the main problems to be faced by the industry of plastic materials today is the development of methods and processes for recycling, in order to produce raw materials or valuable secondary materials, without additional burden on the environment. The environment-friendly techniques are not always the most profitable or economically beneficial, but they are helpful for the earth climate. Greece for example, distributed the plastic post-consuming waste as follows: 21% in recycling, 77% in landfill disposal and 2% for energy recovery[4]. In this context, the thermochemical recycling methods, using a small amount of energy, lead not only to recycling (and therefore potentially disappearing) of polymers but also to the creation of petrochemical products with commercially-added value. The main problems for pyrolysis of plastics, though, are the variety/mixing of the polymers found, the inconsistency in the feeding for the facilities, the presence of additives and the contamination by exterior factors[5].

A variety of polymers utilized as packaging materials, are pyrolytically studied in this work. The objective of the study is the determination of the decomposition behaviour of the polymeric structures via TGA and identification of smaller molecules or parts of the macromolecular chains produced, when the materials are subject to simple or catalytic pyrolysis.

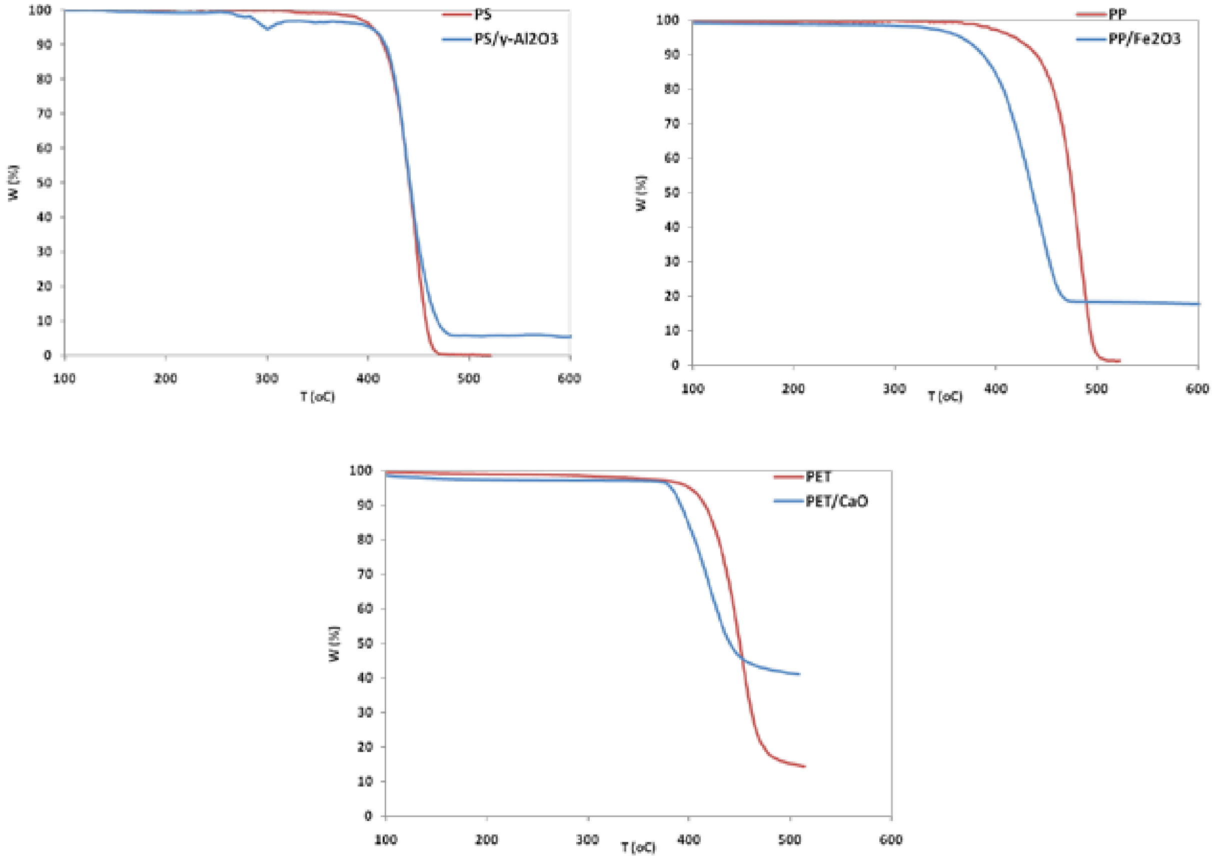

***Figure. 1**. TGA curves of (a) PS, (b) PP, (c) PET with various catalysts.*

2. Materials and Methods

2.1. Polymers and Catalysts

In the present study, the standard materials chosen for the pyrolytic experiments are the poly(ethylene terephthalate) (PET), polystyrene (PS) polypropylene (PP), polyethylene (HDPE or LDPE) which constitute the plastic packaging waste. The polymers were supplied by Sigma-Aldrich USA. A mill was used to grind the pellets to a size of less than 2 mm. The catalysts that were used in the pyrolysis of the polymers were behaving as Lewis' acids or bases. The acidic catalysts were represented by γ-alumina

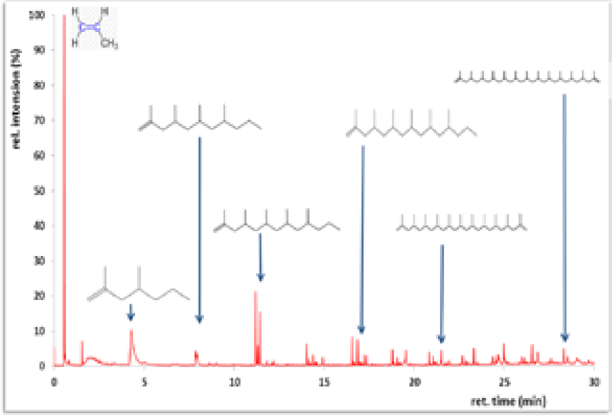

***Figure 2.** The chromatogram after 460 oC PP pyrolysis, the main decomposition products are also shown.*

Table 1. Identified compounds found after the SS pyrolysis of HDPE.

t (min)	Matching compound	MW	Similarity (%)
14.83	n-heptadecane	240	92
15.91	n-octadecane	254	98
16.85	p-hydroxy-2,2-diphenylpropane	212	77
16.94	n-nonadecane	268	97
17.93	n-eicosane	282	97
18.88	heneicosane	296	94
19.78	docosane	310	94
20.66	tricosane	324	94
21.27	benzyl butyl phthalate	312	88
21.49	tetracosane	338	96
22.31	1-pentacosene	350	64
23.08	hexacosane	366	97
23.85	heptacosane	380	97
24.55	octacosane	394	96
25.24	nonacosane	408	96
25.91	1-triaconetene	420	76
26.59	hentriacontane	436	94
27.32	1-dotriacontene	448	80
28.16	1-tritriacontene	462	85
29.13	1-tetratriacontene	476	89
30.29	pentatriacontane	492	96
31.69	pentatriacontane	492	91
31.98	tetratriacontene	476	94
33.37	pentatriacontane	492	95
34.81	1-tetratriacontene	560	66

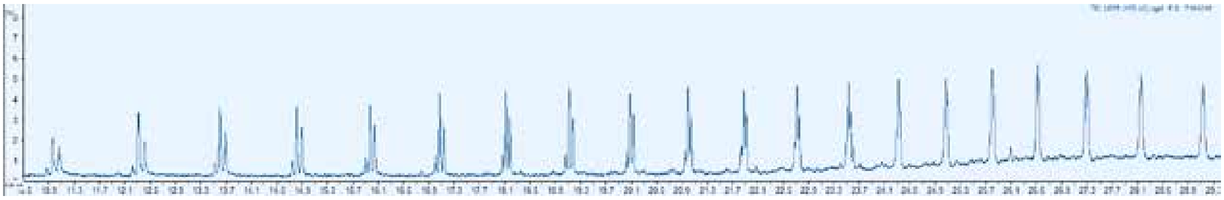

Figure 3. *Pyrogram produced after SS pyrolysis of LDPE/Fe2O3 at 440 oC.*

(γ-Al$_2$O$_{3),}$ iron(III) oxide (Fe$_2$O$_{3),}$ while the basic catalyst was calcium and magnesium oxide (CaO, MgO). They were all dry.

2.2. Experiment procedures

The pyrolysis of PET, PE, PP, PS was conducted on a Pyris 1 TGA balance (Perkin Elmer, USA) under 20 ^{o}C/min heating rate and 20 mL/min N2 flow. Later, the flash pyrolysis were executed in a Py-GC/MS (EGA/PY-3030D by Frontier Lab coupled with QP-2010 Ultra Plus GC/MS by Shimadzu, Japan), where products were separated chromatographically and identified spectroscopically. From the TGA thermogram we can get information about the thermal behaviour of the material, our interest is focused on the dTG curve peak temperature. The SS programs, thus, are generated by flash pyrolysis of the polymers at the selected temperatures for 0.5 min. The evolved gases are separated into the Mega 5HT (Italy) (5% diphenyl- 95% dimethyl)polysiloxane (30m x 0.25mm x 0.25μm) capillary column following a temperature program of 30 or 90 min. The column flow was set at 1 mL/min, the He flow at 3 mL/min, the split ratio at 100 and the MW range 10-500. The database libraries NIST and Frontier are equipped for analyzing the results on a LabSolutions ver. 2.71 software. The sample:catalyst ratio was 2:1[6].

3. Results and discussion

Some of the results gained by TGA experiments are shown in **Figure 1**, where a comparison of the simple polymer degradations is held along with a catalytic one. As it seems, for PS the effect of γ-Al$_2$O$_3$ is absent, on the contrary both PP and PET are affected by Fe$_2$O$_3$ and CaO correspondingly as catalysts. That reveals that each polymer may be facilitated for its decomposition by a certain kind of inorganic compounds as catalyst. It can also be observed in **Figure 1** that the ratio for sample to catalyst may influence the results (it was applied various proportions, like 10, 20, 25%). The evaluation of dTG curves leads to the determination of maximum degradation rate temperatures, which are used later for the Py-GC/MS experiments. Those are 480 for HDPE, 470 for LDPE, 460 for PP, 420 for PS and 435 ^{o}C for PET.

In PP thermogram in the absence of catalysts, a peak of decomposition at 460 °C is exhibited. Although there are slight differences in the decomposition temperatures by using catalysts, there is a large increase in product peaks. In **Figure 2**, PP demonstrates olefinic derivatives as pyrolysis products. The highest peak corresponding to the monomer C_3H_6, is given soon, less than 1min of elution, then the MW rises. Trimmer is eluted at 5 min, C15 to C20 compounds are yield between 5-20 min of recording, C30 molecules and more are given away till the end of the elution. As we can see, the pyrolates structures follow the monomer repetition, we may assume that the breakdown of the PP chain progresses by radical reactions, the unsaturated ending bond (or bonds) indicates that.

At **Table 1**, the main decomposition products of HDPE pyrolysis at 445 ^{o}C in the presence of Fe$_2$O$_3$ are seen. The notable comment on PE pyrolysis in general is the elution of pyrolyzates in a way that the chromatogram peaks shape a "crown" on the plot area. The absence of peak for 10 or 15 min of elution is followed by dense peak area of 15 to 35 min of elution. The degradation products are H/C of high MW in the range of 240 to 500, compounds from C16 to C34. In some cases, rather few, a double bond for the first C is shown.

Moving on to LDPE and **Figure 3**, working likewise, we may see a part of the recording got, regarding 10 to 30 min of elution, where the repetitive peak shape is well-shown (three sharp peaks of different heights going to one large).

Looking in PS thermal behaviour, we would recommend Fe_2O_3 as the best catalytic choice for its pyrolysis. PS does generate its monomer and oligomers as pyrolysis products, which makes the procedure worth. Apart from that, other aromatics are α-methylstyrene, toluenes and xylenes, diphenylpropane, propenylbenzene or diphenylbenzene isomers[7,8]. Fully aromatic derivatives are noticed for greater elution times in recordings. The contribution of the catalyst is the variation of products found. Those compounds are known as raw materials for solvents/diluents in industry.

As for PET, it is the only polymer that contains O atoms in its structure, meaning that the decomposition of it produces aromatic compounds with –OH or -O- groups. Catalysts facilitate its pyrolysis significantly, by lowering the peak temperature for 10 or 15 ^{o}C, and most importantly by releasing a greater variety of molecules. The catalyst with the greater influence on PET is γ-Al_2O_3. The compounds repeatedly found are *p*-cresol, *p*-ethylphenol, *p*-isopropylphenol, *p*-hydroxy-2,2-diphenylpropane or heavier isomers of benzophenones, ethylbenzophenones, diphenyls etc.

4. Conclusions

For last decades the consumption of packaging polymer materials, known as "plastics" has increased, generating big amounts of packaging waste and environmental concern has risen. Pyrolysis, simple or catalytic, has been effective compared to other disposal methods, because it can earn energy and the raw materials contained in those waste, reducing thus the environmental impacts. Thermal pyrolysis of PS, PP generates mainly their monomers, but also oligomers which are valuable for reproducing the material. As far as PET is concerned, the main products after its pyrolysis are the hydroxy-diphenylpropane and isopropenylphenol isomers. When using catalysts the number of products obtained as well as the diversity of them increases in some cases (taking also into account the intensity/shape of the peaks). The PE pyrolysis products are olefins of great MW, with C16-C38 range, indicating liquid H/C derivatives. Regarding PS, the catalyst Fe_2O_3 has some advantages over the rest catalysts, while when using γ-Al_2O_3 as catalyst for PET the intensity of the products peaks is greater, the decomposition temperature decreases significantly and the number of products rises, showing variety of products. ☐

Acknowledgement

The research was conducted under the funding of IKY Foundation Post-Doctoral Research Scholarships 2017-2019 (MIS: 5001552).

REFERENCES

1. Achilias D.S., Andriotis L., Koutsidis I.A., Louka D.A., Nianias N.P., Siafaka P., Tsagkalias I., Georgia Tsintzou G. (2012) Recent Advances in the Chemical Recycling of Polymers (PP, PS, LDPE, HDPE, PVC, PC, Nylon, PMMA), Material Recycling – Trends and Perspectives, pp 1-63
2. Association of plastic manufactures. (2017) Plastics – the Facts 2017, An analysis of European plastics production, demand and waste data.
3. European Commission (2013) Communication from the commission to the European Parliament, the Council, the European Economic and Social Committee and the Committee of the Regions.
4. European Commission (2018) A European Strategy for Plastics in a Circular Economy.
5. Achilias D.S., Giannoulis A., Papageorgiou G.Z. Recycling of polymers from plastic packaging materials using the dissolution/ reprecipitation technique. *Polymer Bulletin* 63,449-465, 2009
6. Shimadzu and Frontier Lab. (2010) Instrumental manuals and sheets
7. Chrissafis K., Pavlidou E., Vouvoudi E., Bikiaris E. D. Decomposition kinetic and mechanism of syndiotactic polystyrene nanocomposites with MWCNTs and nanodiamonds studied by TGA and Py-GC/MS, *Thermochimica Acta* 583, 15–24, 2014).
8. Vouvoudi E.C., Rousi, A.T. & Achilias, D.S. Thermal degradation characteristics and products obtained after pyrolysis of specific polymers found in Waste Electrical and Electronic Equipment. Front. Environ. Sci. Eng. (2017) 11: 9.

Preparation of graphitic carbon nitride (g-C_3N_4) from urea. Study with Thermal Analysis.

Feidias Bairamis, Ioannis Konstantinou, Dimitrios Petrakis, Tiverios Vaimakis*

Department of Chemistry, University of Ioannina, 45110, Ioannina, Greece

Keywords:
Urea; Graphitic Carbon Nitride; Thermal Analysis

***Corresponding author**
Tel: +30-2651008352;
E-mail: tvaimak@cc.uoi.gr

ABSTRACT

Graphitic carbon nitride (g-C_3N_4) is a hotspot emerging material widely used in different applications including pharmaceutical residues treatment and biomedical imaging due to its unique physicochemical properties. In the present study, g-C_3N_4 polymeric material was prepared by thermal condensation process using urea as a precursor compound. The physicochemical characterization was conducted by several techniques such as X-ray diffraction (XRD), scanning electron microscopy (SEM), Fourrier-transformed infrared spectroscopy (FT-IR) and thermal analysis (TA).The results confirmed the successful synthesis of g-C_3N_4 at the temperature range examined bearing mesoporous and packed layered structure. Thermal analysis revealed the transformation of the precursor material to g-C_3N_4 through several steps. The most effective for both the polymerization step and the produced quantity of g-C_3N_4 are the Al crucibles.

1. Introduction

Graphitic carbon nitride (g-C_3N_4), a metal-free semiconductor with a band gap (2.7eV) corresponding to an optical wavelength of 460 nm has been investigated in various applications like sensors, organic synthesis, photocatalysis, lithium-ion batteries etc. G-C_3N_4 with two dimensional (2D) nanostructure has high thermal (up to 600°C in air) and chemical stability, which credited to the s-triazine ring structure. Also, shows high resistance in acidic and basic solutions and is insoluble in common solvents as ethanol and water.[1-3]

Pharmaceuticals have been frequently detected in various surface waters, posing potential threat to human health and environment. G-C_3N_4 has been previously used for the photocatalytic treatment and degradation of pharmaceutical residues. Recently, g-C_3N_4/ZnO/$ZnFe_2O_4$ composite photocatalyst have been used for the enhanced degradation of ibuprofen (IBF) and sulfadiazine (SDZ)[4]. WO_3/TiO_2/g-C_3N_4 composite has been used for photocatalytic degradation of aspirin (acetylsalicylate) and caffeine (methyl-theobromine)[5], while iodine and potassium co-doped g-C_3N_4[6], BiOCl/g-C_3N_4/Cu_2O/Fe_3O_4 composite[7] and WO_3–g-C_3N_4 compos-

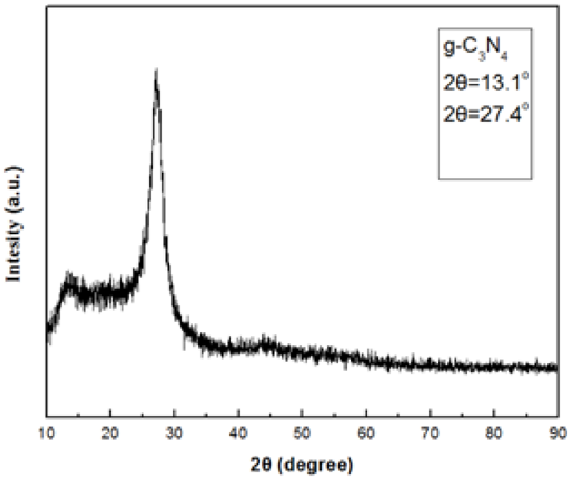

Figure 1. *XRD pattern of g-C3N4.*

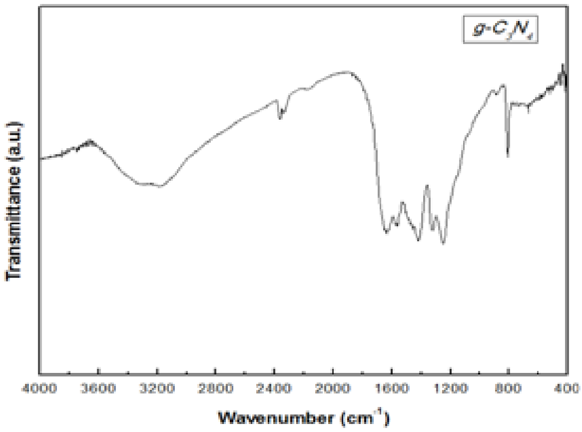

Figure 2. *The FT-IR spectrum of g-C3N4.*

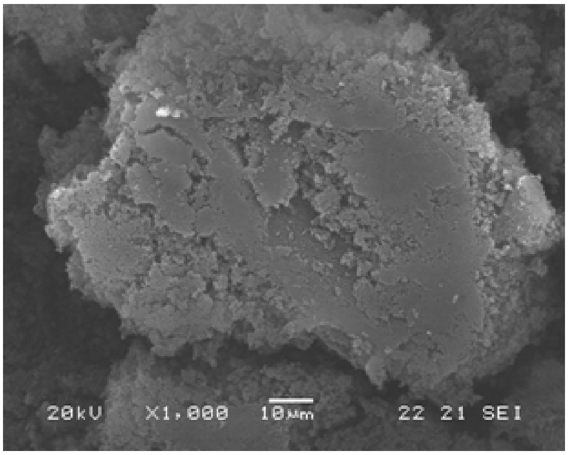

Figure 3. *SEM image of g-C3N4.*

ite photocatalyst[8] have been used for sulfamethoxazole degradation. Finally, properties such as inherent blue light photoluminescence, high stability and good biocompatibility, suggested g-C$_3$N$_4$ materials to be studied as a platform for bio-related applications, and more specifically, an important candidate for bioimaging applications.[9]

Several methods have been investigated for the preparation of g-C$_3$N$_4$ with different architectures and electronic properties. However, thermal condensation of nitrogen-rich precursors such as urea, melamine, cyanamide, thiourea, trithiocyanucic acid, triazoles etc. has been the most attractive method for preparation of g-C$_3$N$_4$ because of the simplicity and use of cheap and readily available precursors.

In this work the effect of the used crucible in the g-C$_3$N$_4$ synthesis from urea was studied using thermogravimetry (TGA) and differential scanning calorimetry (DSC) techniques.

2. Materials and methods

The g-C$_3$N$_4$ powder was synthesized by thermal condensation process using urea (99.5%, Acrōs Organics) as a precursor compound. In a typical synthesis, 30g of urea powder was dried out at 90^{o}C for 24h and then was put into an aluminum foil coated ceramic crucible and was treated in air at 500^{o}C for 4h at the heating rate of 100C/min. The X–ray diffraction (XRD) patterns of the prepared g-C$_3$N$_4$ was determined using a Bruker Advance D8 XRD instrument generating monochromatic Cu –Ka (λ= 1.5418 Å) radiation with a continuous

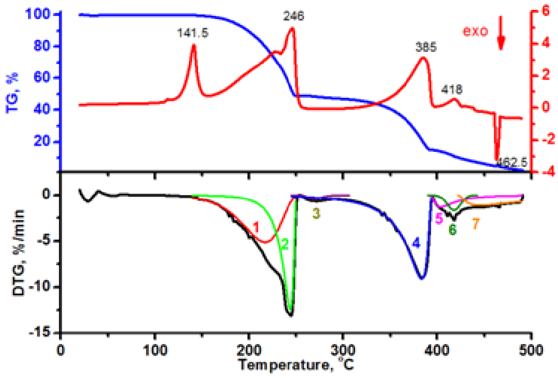

***Figure 4.** Thermal analysis curves for thermal treatment of urea in Al open crucible.*

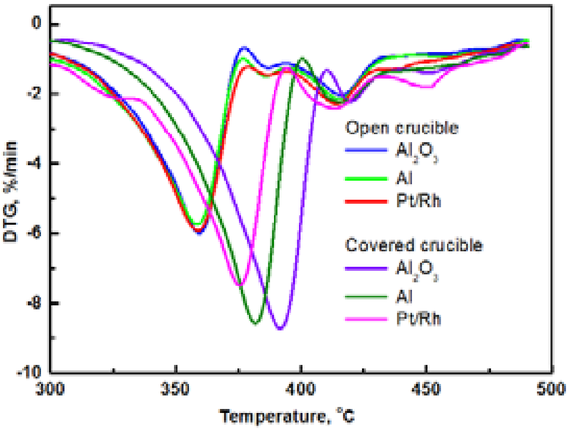

***Figure 5.** DTG curves, at selected temperature ranges, in open/covered Al2O3, Al and Pt/Rh crucibles.*

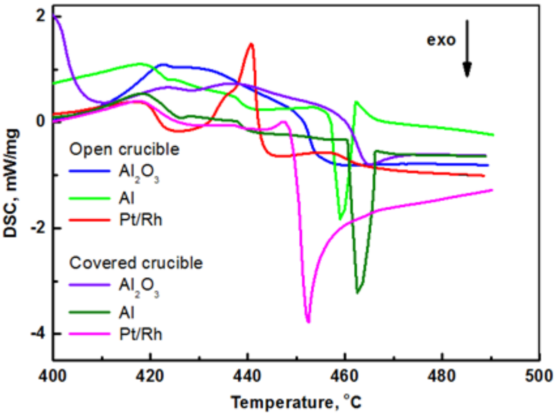

***Figure 6.** DSC curves, at selected temperature ranges, in open/covered Al2O3, Al and Pt/Rh crucibles.*

scanning rate in the range of 10°≤ 2θ ≤ 90° in steps of 0.02° and rate 0.01 °θ/sec. The patterns were assigned with the use of the International Center for Diffraction Data (ICCD). Fourier transform infrared spectroscopic (FT – IR) analysis was carried out by a Perkin Elmer Spectrum BX instrument. Spectral grade KBr (≥ 99%, Acrōs Organics) was used as a reference. G-C_3N_4 was ground with KBr in 1:5 ratio and made into pellets using a hydraulic press. The pellet was scanned in the range 4000-400 cm^{-1}. The morphology of the prepared g-C_3N_4 was studied using a Jeol JSM 5600 scanning electron microscopy (SEM) instrument. Thermogravimetric analysis (TGA) was performed by STA 449C Netzsch instrument with a heating rate of 10°C/min from 25 to 800°C. The covered and uncovered crucibles used were Al, Al_2O_3 and Pt/Rh.

3. Results and Discussion

Figure 1 is shown the XRD pattern of g-C_3N_4. Two characteristic intense peaks of g-C_3N_4 at $13.1^0$and 27.4^0 were detected. The peak at 2θ=13.1^0corresponds to the (100) plane of g-C_3N_4 and it is attributed to the in-plane repetitive and continuous heptazine network. The peak that located at 27.4^0 corresponds to the (002) plane of g-C_3N_4 and is assigned to the stacking of the conjugated aromatic system.[10-13]

The chemical composition and bonding information of g-C_3N_4 powder was also studied by FT-IR spectroscopy (**Figure 2**). Several peaks of g-C_3N_4 can be observed at 1573, 1465, 1403, 1319 and 1241 cm^{-1} confirming the stretching vibration of C–N(–C)–C or C–NH–C heterocycles. The peaks between 3300 and 3000 cm^{-1} related to the stretching vibration of N-H and the peak at 1637 cm^{-1} corresponding to the C=N bending vibration. The peak at 810 cm^{-1} is the most characteristic for g-C_3N_4 attributed to the out-of-plane bending vibration characteristic of heptazine rings. The morphology of the prepared g-C_3N_4 was studied by SEM. The SEM image (**Figure 3**) reveals a structure of packed nanosheets of g-C_3N_4 via π-π stacking.

The thermal analysis of urea, using uncovered Al crucible is given in **Fig. 4**. The thermal decomposition of urea takes place in three main steps. The DTG curve deconvolution reveals that the first step it consisits from two stages, in which mainly melamine is produced. In the second and third steps, which consist of several stages, the decomposition of melamine leads to the formation of triazine rings and polymerization. An exothermic peak at 462.5 ^{o}C, without significant weight loss, is attributed to a further polymerization process.

Figures 5 and **6** illustrate τhe DTG and DSC curves in the temperature range where melamine is decomposed / polymerized for various open or covered crucibles. The DTG curves indicate that with open crucibles the curves are similar regardless of the crucible material. With covered crucibles, this stage is 30% greater in weight loss and occurs at a higher temperature range with increasing value for crucibles: Pt/Rh <Al <Al_2O_3. The DSC curves indicate that an exothermic polymerization step gives the open and covered crucible Al, as well as the covered Pt/Rh crucible. From the above results, we conclude that the most effective for both the polymerization step and the produced quantity of g-C_3N_4 are the Al crucibles. ☐

Σύνθεση Γραφιτικού Νιτριδίου g-C_3N_4 από ουρία. Μελέτη με Θερμική Ανάλυση.

Φειδίας Μπαϊράμης, Ιωάννης Κωνσταντίνου, Δημήτριος Πετράκης, Τιβέριος Βαϊμάκης
Τμήμα Χημείας, Πανεπιστήμιο Ιωαννίνων, Πανεπιστημιούπολη Ιωαννίνων, Τ.Θ. 1186, 45110 Ιωάννινα

KEYWORDS:
Ουρία,
γραφιτικό νιτρίδιο,
θερμική ανάλυση

ABSTRACT

Το γραφιτικό νιτρίδιο του άνθρακα είναι ένα αναδυόμενο και πολλά υποσχόμενο υλικό το οποίο ερευνάται σε διάφορες εφαρμογές συμπεριλαμβανομένων της φωτοκαταλυτικής διάσπασης υπολειμμάτων φαρμακευτικών ενώσεων και των βιο-ιατρικών απεικονίσεων. Στην εργασία παρασκευάσθηκε το πολυμερικό γραφιτικό νιτρίδιο του άνθρακα με θερμική συμπύκνωση της ουρίας ως πρόδρομης ένωσης. Πραγματοποιήθηκε φυσικοχημικός χαρακτηρισμός του υλικού με διάφορες τεχνικές όπως περίθλαση ακτίνων Χ, ηλεκτρονική μικροσκοπία σάρωσης, φασματοσκοπία υπερύθρου και θερμική ανάλυση. Τα αποτελέσματα των τεχνικών έδειξαν την επιτυχή σύνθεση γραφιτικού νιτριδίου με μεσοπορώδη δομή των συσσωρευμένων (πακεταρισμένων) νάνο-φύλλων. Η θερμική ανάλυση έδειξε ότι η μετατροπή της ουρίας λαμβάνει χώρα σε τρία διαδοχικά βήματα. Τα πλέον αποτελεσματικά, τόσο για το στάδιο πολυμερισμού όσο και για την παραγόμενη ποσότητα g-C_3N_4 είναι τα χωνευτήρια Al.

ΒΙΒΛΙΟΓΡΑΦΙΑ

1. Mamba G., Mishra A.K. Graphitic carbon nitride (g-C3N4) nanocomposites: A new and exciting generation of visible light driven photocatalysts for environmental pollution remediation. *Appl. Catal. B: Environ.* 198, 347-377, 2016.
2. Wang Y., Wang X., Antonietti M. Polymeric graphitic carbon nitride as a Heterogeneous organocatalyst: From photochemistry to multipurpose catalysis to sustainable chemistry. *Angew. Chem. Int. Ed.* 51, 68-89, 2012.
3. Zhao Z., Sun Y., Dong F. Graphitic carbon nitride based nanocomposites: A review. *Nanoscale* 7, 15-37, 2015.
4. Di G., Zhu Z., Huang Q., Zhang H., Zhu J., Qiu Y., Yin D., Zhao J. Targeted modulation of g-C_3N_4 photocatalytic performance for pharmaceutical pollutants in water using ZnFe-LDH derived mixed metal oxides: Structure-activity and mechanism. *Sci. Total Environ*. 650, 1112–1121, 2019.
5. Tahir M.B., Sagir M., Shahzad K., Removal of acetylsalicylate and methyl-theobromine from aqueous environment using nano-photocatalyst WO3-TiO2 @g-C_3N_4 composite. *J. Hazard. Mater.* 363, 205–213, 2019.
6. Kriselle L., Paragas B., Daniel M., de Luna G., Doong R-A., Rapid removal of sulfamethoxazole from simulated water matrix by visible-light responsive iodine and potassium co-doped graphitic carbon nitride photocatalysts. *Chemosphere* 210, 1099-1107, 2018.
7. Kumar A., Kumar A., Sharma G., Al-Muhtaseb A.H., Naushad M., Ghfar A.A., Stadler F.J. Quaternary magnetic BiOCl/g-C_3N_4/Cu_2O/Fe_3O_4nano-junction for visible light and solar powered degradation of sulfamethoxazole from aqueous environment. *Chem. Eng. J.* 334, 462–478, 2018.
8. Zhu W., Sun F., Goei R., Zhou Y. Construction of WO_3–g-C_3N_4 composites as efficient photocatalysts for pharmaceutical degradation under visible light Catal. *Sci. Technol.* 7, 2591-2600, 2017.
9. Liu J., Wang H., Antonietti M. Graphitic carbon nitride “reloaded”: emerging applications beyond (photo) catalysis, *Chem. Soc. Rev.* 45, 2308-2326, 2016.
10. Zhang G., Zhang T., Li B., Jiang S., Zhang X., Hai L., Chen X., W. Wu. An ingenious strategy of preparing TiO2/g-C3N4 heterojunction photocatalyst: In situ growth of TiO2 nanocrystals on g-C3N4nanosheets via impregnation-calcination method. *Appl. Surf. Sci*. 433, 963-974, 2018.
11. Wang C., Hu L., Chai B., Yan J., Li J. Enhanced photocatalytic activity of electrospun nanofibrous TiO2/g-C_3N_4 heterojunction photocatalyst under simulated solar light. *Appl. Surf. Sci*. 430, 243-252, 2018.
12. Tong Z.W., Yang D., Xian T.X., Tian Y., Jiang Z.Y. Biomimetic fabrication of g-C_3N_4/TiO_2 nanosheets with enhanced photocatalytic activity towards organic pollutant degradation. *Chem. Eng. J.* 260, 117-125, 2015.
13. Hao R.R., Wang G.H., Jiang C.J., Tang H., Xu Q.C. In situ hydrothermal synthesis of g-C_3N_4/TiO_2 heterojunction photocatalysts with high specific surface area for Rhodamine B degradation. *Appl. Surf. Sci.* 411, 400-410, 2017.

ΕΚΔΗΛΩΣΕΙΣ - MEETINGS

- **2 - 3 ΦΕΒΡΟΥΑΡΙΟΥ 2019, ΑΘΗΝΑ, ΜΕΓΑΡΟ ΔΙΕΘΝΕΣ ΣΥΝΕΔΡΙΑΚΟ ΚΕΝΤΡΟ ΑΘΗΝΩΝ**

3ο ΕΠΙΣΤΗΜΟΝΙΚΟ ΣΥΝΕΔΡΙΟ ΦΑΡΜΑΚΕΥΤΙΚΗΣ ΦΡΟΝΤΙΔΑΣ της Ελληνικής Φαρμακευτικής Εταιρείας
https://www.pharmamanage.gr/images/10th/10h-Programma.pdf#page=8

- **4-6 MARCH 2019, PARIS, FRANCE**

"International Conference on PharmScience Research & Development" (Pharma R&D-2019)
https://pharmaconference.com

- **6-8 MARCH 2019, FRANKFURT, GERMANY**

EUFEPS Annual Conference 2019: Personalized Medicines, Targeted Therapies,
Precision Drug Delivery

- **15 - 16 ΜΑΡΤΙΟΥ 2019, ΑΘΗΝΑ, ΖΑΠΠΕΙΟ ΜΕΓΑΡΟ**

5ο Δ|Υ|Ο FORUM 2019
www.dyoforum.gr

- **15-17 MAY, 2019, AMSTERDAM, NETHERLANDS**

2nd EUROPEAN CHEMISTRY CONFERENCE , ECC-2019
http://europeanchemistry.madridge.com

- **10-13 JUNE 2019, KRAKOW, POLAND**

EFMC-ACSMEDI: Medicinal Chemistry Frontiers 2019

- **23-27, JUNE 2019, IOANNINA, GREECE**

CMTPI-2019: 10th International Symposium on Computational Methods in Toxicology
and Pharmacology Integrating Internet Resources
http://cmtpi.net/

- **27−30 JUNE, 2019, PRAGUE, CZECH REPUBLIC.**

11th Joint Meeting on Medicinal Chemistry 2019
https://www.jmmc2019.cz/

- **1 - 5 SEPTEMBER 2019, ATHENS, GREECE**

EFMC-ASMC'19 - EFMC International Symposium on Advances in Synthetic and Medicinal Chemistry
http://www.rsc.org/events/detail/35235/efmc-asmc19-efmc-international-symposium-on-advancesin-synthetic-and-medicinal-chemistry

- **08-11 SEPTEMBER, 2019, ISTANBUL, TURKEY**

12th AFMC / AIMECS 2019
Asian Federation for Medicinal Chemistry (AFMC) 12th International Symposium
"New Avenues for Design and Development of Translational Medicine"
http://www.aimecs2019.org/